

M.Sc. Kishore Natte

**Synthesis of novel polymeric  
hybrid nanoparticles with enhanced  
interfacial and colloidal properties  
for biomedical studies**

Die vorliegende Arbeit entstand an der BAM Bundesanstalt für Materialforschung und -prüfung.

Impressum

**Synthesis of novel polymeric hybrid nanoparticles  
with enhanced interfacial and colloidal properties  
for biomedical studies**

2013

Herausgeber:

BAM Bundesanstalt für Materialforschung und -prüfung  
Unter den Eichen 87

12205 Berlin

Telefon: +49 30 8104-0

Telefax: +49 30 8112029

E-Mail: [info@bam.de](mailto:info@bam.de)

Internet: [www.bam.de](http://www.bam.de)

Copyright © 2013 by

BAM Bundesanstalt für Materialforschung und -prüfung

Layout: BAM-Referat Z.8

ISSN 1613-4249

ISBN 978-3-9815360-7-2

# **Synthesis of novel polymeric hybrid nanoparticles with enhanced interfacial and colloidal properties for biomedical studies**

vorgelegt von

Master of Science in Chemistry

**Kishore Natte**

aus Warangal, Indien

von der Fakultät II – Mathematik und Naturwissenschaften  
an der Technischen Universität Berlin  
zur Erlangung des akademischen Grades

Doktor der Naturwissenschaften

Dr. rer. nat.

genehmigte Dissertation

Promotionsausschuss:

Vorsitzender: Prof. Dr. rer. nat. Reinhard Schomäcker (TU Berlin)

1. Bericht: Prof. Dr. rer. nat. Regine von Klitzing (TU Berlin)

2. Bericht: Prof. Dr. rer. nat. Rainer Haag (FU Berlin)

3. Bericht: Prof. Dr. rer. nat. Jörg F. Friedrich (BAM Berlin)

Tag der wissenschaftlichen Aussprache: 19. Dezember 2012

Berlin 2013

D83



*Dedicated to my Family*

*..... for being “Mentors” of my Life*



# Acknowledgments

---

It has been my privilege to meet and work with a lot of nice and talented people over the course of my PhD at Bundesanstalt für Materialforschung und –prüfung (BAM) and Technical University of Berlin, Germany. So I would like to thank each and every person. Special thanks to some of the important persons.

Firstly, I would like to express my deep gratitude to my supervisor Prof. Dr. Regine von Klitzing at Technical University Berlin for her valuable suggestions, discussions, continued encouragement and inspiration. Her understanding and patience helped instil confidence and courage to develop myself as a Research Scientist.

I am extremely grateful to Prof. Dr. Jörg Friedrich, for believing and providing me an opportunity to work in BAM, Berlin. His constant guidance and mentoring helped me overcome many hurdles throughout my PhD research and also gave me lot of opportunities to present my work at conferences (MACRO 2010 and 2012, ISOS-XV1).

I wish to express my sincere thanks to Prof. Dr. Rainer Haag from Freie University Berlin for being external professor in my PhD dissertation.

I want to thank Prof. Dr. Reinhard Schomäcker from Technical University Berlin for accepting to be the "Vorsitzender" in my PhD defence.

I am sincerely grateful to Dr. Werner Österle for his outstanding assistance, numerous scientific discussions and mentoring. He encouraged me a lot and gave me opportunities to present my work at many conferences.

I am truly thankful to Dr. Guillermo Orts-Gil, for his constant engagement with my work, providing motivation and enthusiasm. I appreciate all his contributions of time, ideas for my success. I am thankful to him for guiding me and teaching the research skills. This thesis would not have been completed successfully without his supervision, guidance, generosity towards sparing time during the course of the work and compilation of this dissertation.

I would like to acknowledge to Dr. Sebastian Wohlrab and Dr. Narayana Kalevaru for giving me an opportunity to pursue my PhD in BAM, Germany. Special thanks to Dr. Behnke, Dr. Ute and Würth for their valuable discussions during fluorescence experiments.

I would like to show gratitude to Prof. Dr. Ravinder Vadde (Kakatiya University, India) for his constant interest in my research and his care for my personal life.

Besides, within the BAM, I would like to further address sincere thanks to Marianne Haske, Schulz Brigitte and all the staff of the group 6.10 and also administration staff for helping me in all ways possible. I would like to further address sincere thanks to Frank Milczewski for making me to talk in German and at times also coffee breaks.

In addition, I would like to thank Jana Lutzki for measuring AFM samples and to all those friends in the Stanski laboratory are acknowledged.

Last but not least, I would like to thank my fellow colleagues and friends Maalolan, Purv, Thomas, Sven, Huajie, Sanjeev, Kirti and Joshi for explaining patiently each and every even a small doubt and also enjoyable discussions between work.

I am extremely grateful to my family: To my parents, Narasamma and Narayana for their continuous support and encouragement they have provided me during these years, to my siblings, Kavitha and Rajesh and ofcourse to my brother-in-law Srikanth and sweet niece Sahasra for always being there for me. Without my family, I would not have been able to preserve and accomplish this work. I would like to dedicate this thesis to my Family. Finally, I would like to thank Samatha, for her patience, encouragement and steadfast support. I love you sam!



# Abstract

---

The reduced size of nanoparticles (diameter < 100 nm) confers them high specific surface areas and permeability through many biological pathways resulting in high interaction with biological systems. Therefore, in the recent years, nanoparticles (NPs) have increasingly found many applications in biomedical research. Herein, silica-based NPs are among the most promising candidates for biomedical studies due to their relative low toxicity and the possibility of functional variability. The main focus of this thesis work has been the synthesis and characterisation of novel hybrid NPs with enhanced properties for biomedical studies. More specifically, suppression of protein adsorption and achievement of highly fluorescent NPs in serum-rich media are well focused.

First, a chemical strategy for the preparation of highly fluorescent silica nanoparticles by covalent attachment of Alexa dyes and subsequent shielding by an additional pure silica shell is well presented. These nanoparticles were investigated by Dynamic light scattering (DLS), Transmission electron microscopy (TEM) and fluorescence spectroscopy, the latter includes determination of absolute fluorescence quantum yields of such scattering suspensions with an integrating sphere setup and the assignment of fluorescence intensity values. At low shelling extension core-shell fluorescent silica nanoparticles show smooth surfaces and high quantum yields, even comparable to those for free dyes. However, by increasing the amount of shell precursor, nanoparticle surfaces show raspberry morphologies and decay of the quantum yields.

Secondly, two different types of novel silica-poly(ethylene glycol) hybrid nanoparticles (H-SiO<sub>2</sub>-PEG and G-SiO<sub>2</sub>@PEG) have been synthesized by use of the same polymer precursor: Here the influence of concentration of the polymer precursor poly(ethylene glycol) methyl ether-3-(triethoxysilyl) propyl urethane (mPEG-IPTES) on the particle properties was scrutinised. For polymer grafted NPs, the concentration of polymer precursor increases the PEG density and the hydrophobicity of the NPs surface. On the other hand, for condensated NPs, the polymer precursor influences the size, but not the density of polymer chains on the NPs surface, which indicates that PEG on the surface of the NPs effectively reduces the adsorption of Bovine serum albumin (BSA).

Finally, the influence of polymer length on the ability to repel BSA adsorption onto nanoparticles is reported. SNPs@PEG with different molecular weights (mPEG: 350, 2000 and 5000 g/mol) were synthesized by nucleophilic substitution of tosylated mPEG to

aminated silica nanoparticles (chemical grafting). The resulted hybrid nanoparticles were consistently characterized by DLS, TEM, Fourier transform infrared spectroscopy (FTIR), Thermogravimetric analysis (TGA) and X-ray photoelectron spectroscopy (XPS). BSA at different concentrations were used as a model protein to study the protein-corona formation after adsorption onto the pristine and modified nanoparticles (SNPs@PEG). For pristine SNPs and SNPs@PEG (MW = 350 g/mol), zeta potential at different incubation times (0, 24 and 48 h) show a dynamic evolution of the nanoparticle-protein corona. Conversely, for SNPs@PEG with MW  $\geq$  2000 g/mol, a significant suppression of corona formation and time evolution was observed. In resume, protein corona is strongly influenced by the adsorption inhibition of PEG surfaces.

# Zusammenfassung

---

Die geringe Größe von Nanopartikeln (Durchmesser  $< 100$  nm) gewährleistet sowohl eine hohe spezifische Oberfläche sowie Permeabilität durch eine Vielzahl biologischer Systeme. Als Folge weisen Nanopartikel (NP) eine starke Wechselwirkung mit biologischen Systemen auf, wodurch diese in den letzten Jahren zunehmend in der biomedizinischen Forschung Anwendung fanden. Aufgrund der relativ geringen Toxizität sowie der Möglichkeit zur Einführung unterschiedlicher funktioneller Gruppen eignen sich besonders auf Siliziumdioxid (Silica)basierende Nanopartikel für biomedizinische Studien. Der Schwerpunkt dieser Doktorarbeit lag in der Synthese und Charakterisierung von neuartigen Hybrid-NP mit verbesserten Eigenschaften für biologische Studien. Insbesondere soll eine Unterdrückung der Proteinadsorption erlangt werden sowie stark fluoreszierende NP in Gegenwart serumreicher Medien erhalten werden.

Zu Beginn wird der Syntheseweg zur Darstellung hoch fluoreszierender Silica-Nanopartikel präsentiert, durch kovalente Anbindung des Alexa Farbstoffs und nachfolgender Ummantelung durch eine zusätzliche Silicahülle. Diese Nanopartikel wurden mittels dynamischer Lichtstreuung (DLS), Transmissionselektronenmikroskopie (TEM) und Fluoreszenzspektroskopie untersucht. Letztgenannte Methode beinhaltet die Bestimmung der absoluten Quantenausbeute solcher streuenden Suspensionen mit einer integrierenden Kugelkonfiguration sowie die Zuordnung von Helligkeitswerten. Bei geringer Ausdehnung der Hülle zeigen Silica NP mit Kern-Schale Architektur eine glatte Oberfläche und hohe Quantenausbeuten, in Größenordnung der freien Farbstoffe. Eine Erhöhung der Menge an Hüllen-Precursor führt zu einer himbeerartigen Morphologie der Oberfläche und einer Verminderung der Quantenausbeute.

Es folgt die Darstellung zweier unterschiedlicher Typen neuartiger Silica-Polyethylenglykolhybride NP (H-SiO<sub>2</sub>-PEG und G-SiO<sub>2</sub>@PEG) unter Verwendung desselben Polymerprecursors oder desselben Polymerprecursors: Der Einfluß der Konzentration des Polymerprecursors Poly(ethylen glykol) methylether-3-(triethoxysilyl) propyl urethan (mPEG-IPTES) auf die Partikeleigenschaften wurde ausführlich untersucht. Bei polymergepfropften NP bestimmt die Konzentration des Polymerprecursors die Dichte des angekoppelten PEGs und folglich die Hydrophobie der NP Oberfläche. Dagegen beeinflusst bei kondensierten NP der Precursor die Partikelgröße, aber nicht die Dichte der Polymerketten auf der Oberfläche.

Abschließend wird der Einfluss der Polymerlänge auf die Verminderung der BSA Adsorption beschrieben. SNPs@PEG mit verschiedenen Molekulargewichten des mPEG ( $M_w = 350, 2000$  und  $5000$  g/mol) wurden an die NP Oberfläche durch nucleophile Substitution von tosyliertem mPEG an aminierte Silica NP kovalent angebunden (hemisches Pfropfen). Die resultierenden Hybrid-NP wurden einheitlich mittels DLS, TEM, Fourier-Transformations-Infrarotspektroskopie (FTIR), thermogravimetrischer Analyse (TGA) und Photoelektronenspektroskopie (PES) charakterisiert. Bovine Serum Albumin (BSA) wurde in verschiedenen Konzentrationen als Modellprotein verwendet, um die Ausbildung der protein corona durch Adsorption an ursprünglichen sowie an modifizierten NP oder modifizierten NPs (SNPs@PEG) zu untersuchen. Das Zeta-Potenzial der ursprünglichen Silica NP sowie SNPs@PEG ( $M_w = 350$  g/mol) zeigen eine dynamische Entwicklung der Nanopartikel-protein corona in Abhängigkeit von der Inkubationsdauer (0, 24, 48 h). Im Gegensatz hierzu konnte bei SNPs@PEG mit  $M_w \approx 2000$  g/mol eine signifikante Minderung der Ausbildung der protein corona sowie der zeitlichen Entwicklung beobachtet werden. Insgesamt wird die protein corona stark von den adsorptionshindernden Eigenschaften des PEGs beeinflusst.

# Table of contents

---

<b>Acknowledgments</b>	
<b>Abstract</b>	
<b>Zusammenfassung</b>	
<b>1 Introduction and Motivation</b>	<b>1</b>
<b>2 Scientific background</b>	<b>3</b>
2.1 Physico-chemical properties of colloidal silica.....	3
2.2 Applications of colloidal silica.....	5
2.3 Synthesis and functionalisation of silica nanoparticles (SNPs).....	6
2.3.1 Stöber synthesis of silica and its modifications.....	6
2.3.2 Silanization and Amination of SNPs.....	10
2.3.3 Poly(ethylene glycol) (PEG) and Bovine Serum Albumin (BSA).....	12
2.3.4 PEGylation chemistry (covalent attachment of tosyl mPEG to aminated SNPs).....	15
2.3.5 Hybrid nanoparticles.....	16
2.4 Non-specific protein adsorption onto nanoparticle surfaces.....	17
2.4.1 Nanoparticle-protein corona.....	18
2.4.2 Nanoparticle-protein interactions.....	20
2.4.3 Surface modification of nanoparticles to reduce non-specific protein adsorption.....	22
2.5 Open questions.....	25
<b>3 Experimental Methods</b>	<b>27</b>
3.1 Chemicals.....	27
3.2 Methods.....	28
3.2.1 Dynamic light scattering (DLS).....	28
3.2.2 Transmission electron microscopy (TEM).....	31
3.2.3 Fourier transformation-Infrared spectroscopy (FTIR).....	31
3.2.4 X-ray photoelectron spectroscopy (XPS) measurements.....	32
3.2.5 Thermo gravimetric analysis (TGA).....	32
3.2.6 Atomic force microscopy (AFM).....	32

3.2.7	Absorption and fluorescence spectroscopy.....	32
3.2.7.1	Absorption measurements.....	33
3.2.7.2	Fluorescence measurements.....	33
3.2.7.3	Absolute fluorescence quantum yield.....	33
3.2.7.4	Determination of the amount of SNP-coupled dye and calculation of particle intensity.....	34
<b>4</b>	<b>Synthesis and characterisation of highly fluorescent core-shell nanoparticles based on Alexa dyes</b>	<b>36</b>
4.1	Introduction.....	36
4.2	Preparation of materials.....	38
4.2.1	Preparation of silica nanoparticles (SNPs).....	38
4.2.2	Preparation of amino-functionalised silica particles (SNPs-NH <sub>2</sub> ).....	38
4.2.3	Covalent attachment of Alexa dyes to aminated SNPs.....	38
4.2.4	Formation of a protective pure silica shell.....	39
4.3	Results and Discussions.....	40
4.3.1	Physicochemical characterisation.....	40
4.3.2	Spectroscopic characterisation.....	43
4.4	Conclusions.....	46
<b>5</b>	<b>Tuning interfacial properties and colloidal behavior of hybrid nanoparticles by controlling the polymer precursor</b>	<b>47</b>
5.1	Introduction.....	47
5.2	Preparation of materials.....	48
5.2.1	Synthesis of mPEG-IPTES precursor.....	48
5.2.2	Synthesis of condensated silica-PEG hybrids (H-SiO <sub>2</sub> -PEG).....	49
5.2.3	Synthesis of silica-PEG grafted NPs (G-SiO <sub>2</sub> @PEG).....	49
5.2.4	BSA adsorption onto nanoparticles.....	50
5.3	Results and Discussions.....	50
5.3.1	Morphology of prepared nanoparticles and degree of functionalisation.....	50
5.3.2	Particle size, colloidal stability and interfacial properties.....	54
5.3.2.1	Condensated hybrid nanoparticles.....	54
5.3.2.2	Grafted hybrid nanoparticles.....	57
5.3.2.3	Discussion of BSA adsorption.....	58

5.4	Conclusions.....	60
<b>6</b>	<b>Impact of polymer shell on the formation and time evolution of nanoparticle–protein corona</b>	<b>62</b>
6.1	Introduction.....	62
6.2	Preparation of materials.....	64
6.2.1	Tosylation of poly(ethylene glycol) monomethylether (mPEG-OTS).....	64
6.2.2	PEGylation of aminated silica particles (SNPs@PEG).....	64
6.2.3	Nanoparticles/BSA mixtures and purifications.....	65
6.3	Results and Discussions.....	66
6.3.1	Particles characterisation.....	66
6.3.2	Protein corona formation onto pristine and SNPs@PEG nanoparticles.....	68
6.3.3	AFM study of BSA/polymer surfaces.....	72
6.4	Conclusions.....	75
<b>7</b>	<b>Summary and Outlook</b>	<b>77</b>
<b>8</b>	<b>Bibliography</b>	<b>79</b>
	<b>Appendix</b>	<b>88</b>
	<b>Appendix to chapter 4</b>	<b>88</b>
A.4.1	Solid-state <sup>13</sup> C NMR of amino-functionalized silica particles (SNPs-NH <sub>2</sub> ).....	88
A.4.2	Fourier transform infrared spectroscopy (FTIR) of SNPs and SNPs-NH <sub>2</sub> .....	88
A.4.3	X-ray photoelectron spectroscopy (XPS) of SNPs and SNPs-NH <sub>2</sub> .....	89
	<b>Appendix to chapter 5</b>	<b>90</b>
A.5.1	<sup>1</sup> H NMR of mPEG-IPTES precursor.....	90
	<b>Appendix to chapter 6</b>	<b>90</b>
A.6.1	XPS.....	90
A.6.2	TGA.....	90
A.6.3	Focused ion beam (FIB).....	92
A.6.4	Reaction scheme and <sup>1</sup> H NMR for tosylation of poly(ethylene glycol) monomethylether (mPEG) (mPEG-OTS).....	93
A.6.5	Cleaning of silicon surfaces.....	93
A.6.5.1	Preparation of amino functionalized silicon wafer (SNPs-NH <sub>2</sub> ).....	93

A.6.5.2 PEGylation of aminated silica wafers (SNPs-NH-PEG).....	94
A.6.5.3 PEGylated silicon wafer /BSA mixtures and purification.....	94
<b>List of symbols, Abbreviations, Publications &amp; Cirriculum vitae</b>	<b>95</b>



# Chapter 1

## Introduction and Motivation

---

Nanoscience and nanotechnology has become a versatile and promising subject for creating new materials with enhanced properties and potential applications. In this regard, nanoparticles have received growing attention in every sector of science and technology. The size, shape, structure and chemical properties of engineered nanoparticles open a vast range of technical applications and novel approaches in basic research science <sup>[1]</sup>. The enormous interest in synthetic nanoparticles (NPs) for a variety of applications has led to the development of methods in order to evaluate their potential impact on biomedical applications. Thus, *in vitro* studies have been proposed as a rapid and facile approach to distinguish between low and high toxicity nanomaterials <sup>[2, 3]</sup>. While characterization of particle's properties like surface area, surface charge and crystallinity has been successively taken into consideration <sup>[4]</sup>. Besides, a better understanding of the basic mechanisms concerning nanoparticle-protein interactions and their colloidal behaviour in different physiological media is needed <sup>[5]</sup>.

In the course of this thesis, only amorphous silica nanoparticles (SNPs) have been used due to less-toxic <sup>[6]</sup>, exhibit various advantages (e.g. possible surface modifications, easy to dialyze, labelling systems, etc.) and show great promise in colloidal, synthetic and pharmaceutical chemistry.

SNPs possess a remarkable colloidal stability in water and in salt solution due to the large negative surface charge under neutral and basic conditions <sup>[7, 8]</sup>. In previous works the colloidal stability of SNPs in the presence of BSA and fetal calf serum (FCS) has been studied and also several studies dealing with the stabilization of SNPs in the presence of serum were published <sup>[9-13]</sup>. These investigations showed the necessity of surface modification in order to prevent non-specific protein adsorption and consequent partial agglomeration of SNPs in serum-rich media. Although the surface modification of SNPs with short functional groups like amine and thiol has been widely used for immobilization of various organic groups, dyes, enzymes, proteins and DNA <sup>[14-17]</sup>, the question how to control the protein adsorption onto nanoparticles has been mainly addressed to the modification with polymers <sup>[7, 18-20]</sup>. For this reason, new functionalisation routes are developed in order to avoid protein adsorption. This is exactly the aim of this thesis: the synthesis of highly monodisperse silica nanoparticles with well-defined sizes and their subsequent surface modification with polymers in order to avoid the adsorption of serum proteins.

The presented dissertation is challenged to answer the surface modification of SNPs by introducing different chemical strategies in order to suppress BSA adsorption. In chapter 4, the synthesis of bright near infrared (NIR)-emissive nanoparticles based on the grafting of SNPs with 3-aminopropyl triethoxysilane (APTES) followed by covalent attachment of Alexa dyes and their subsequent shielding by an additional pure silica shell are consistently characterized and deeply investigated. In Chapter 5, an efficient synthetic strategy is introduced to produce two novel silica-poly(ethylene glycol) hybrid nanoparticles (H-SiO<sub>2</sub>-PEG and G-SiO<sub>2</sub>@PEG) by use of the same polymer precursor poly(ethylene glycol) methyl ether-3-(triethoxysilyl) propyl urethane (mPEG-IPTES). In addition, this chapter also reports the influence of NPs properties on the colloidal stability and BSA adsorption. Chapter 6, describes a systematic study on the adsorption and orientation (side-chain or perpendicular confirmation) of BSA onto pristine and different molecular weights of PEGylated silica (SNPs@PEG) surfaces, where the emphasis is placed on surface functionalization of SNPs (novel synthetic route for SNPs@PEG was designed) and its related interaction with BSA in physiological media.

## Chapter 2

### Scientific background

---

This chapter deals with the fundamental understanding of silica nanoparticle (SNPs) and its surface functionalisation with silanes and polymers in order to suppress the BSA adsorption. Moreover, a brief description about silica and its synthesis, PEG, Hybrid particles, protein corona, non-specific protein adsorption and surface modification of polymers to avoid protein adsorption is given by highlighten and some important literature is also described.

#### 2.1 Physico-Chemical properties of colloidal silica

Colloidal silica is often used to refer to concentrated dispersion and stable dispersions or "sols" made of discrete and dense amorphous silica nanoparticles in a liquid. If the liquid is organic it is called an organosol but the most commonly used is water and then it is referred to as an aquasol or hydrosol <sup>[21]</sup>. The particles of amorphous silica are built up by a random packing of  $[\text{SiO}_4]^{4-}$  units, which results in a non-periodic structure with the general molecular formula  $\text{SiO}_2$  <sup>[21]</sup>. The bulk structure terminates at the surface in two different ways; oxygen on the surface through siloxane groups ( $\equiv\text{Si-O-Si}\equiv$ ) or silanol groups ( $\equiv\text{Si-OH}$ ). Different forms of silanols are presented in Figure 1. The concentration of silanol groups on a maximum-hydroxylated silica surface is approximately  $8\mu\text{mol}/\text{m}^2$  <sup>[22, 23]</sup>.

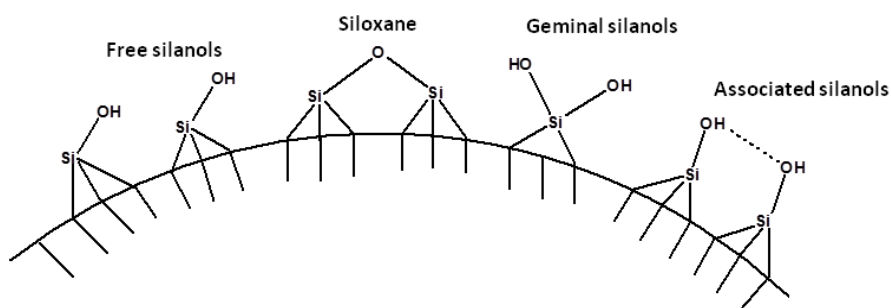


Figure 1: Silica particle showing various silanol groups

Commercial colloidal silica's are commonly available in the form of sols or powders. They are usually synthesized from sodium silicate ( $\text{Na}_2\text{O}_3\text{Si}$ ) solutions neutralized by an acid. The

synthesis starts by the formation of a sol of silica nuclei via removal of sodium ion through dialysis/ion-exchange. The alkaline condition of this process prevents the sol from flocculation by keeping the surfaces negatively charged <sup>[22]</sup>.

Another process used to prepare colloidal silica is the well known Stöber method <sup>[24]</sup>, which provides controlled growth of well-defined silica spheres with a narrow size distribution. In this method the silica particles are produced by base-catalyzed hydrolysis and condensation of tetra alkyl orthosilic acid in an aqueous mixture of alcohol and ammonia.

#### *Stability and Aggregation of colloidal silica*

Small particles dispersed in solution will take long time to settle if only the gravity and viscous drag force are considered. But the Brownian motion caused by natural kinetic energy, will cause the particles to move randomly in the solution. This leads to collision and depending on the forces between the particles they either attract or repel each other <sup>[25]</sup>.

The repulsive forces between two particles in a colloidal suspension need to be larger than the attractive forces to keep the particles from aggregating. The stability of a colloidal silica sol is dependent of attractive van der Waals forces and the opposite repulsive electrostatic forces. There are also effects such as pH and ionic strength contributing from the medium in which the silica particles are dispersed <sup>[26]</sup>.

The famous DLVO theory (Derjaguin, Landau, Verwey and Overbeek) represents the classical framework to describe the stability by the ionic double layer for colloidal particles (also refer section 2.4.2 Nanoparticle-protein interactions). This theory is valid only in the presence of alkali and for larger silica particles. At pH 2 the silica particles has no charge and should according to the DLVO theory therefore be in the least stable region. This is not the case and could be because of steric stabilization from a monolayer of water molecules bonded to the hydroxyl groups on the surface by hydrogen bonding <sup>[21, 27, 28]</sup>.

A silica sol is said to be stable if the particles do not settle and do not aggregate at a significant rate. An aggregate in colloidal science is a group of particles held together in any possible way. The term aggregate is used to describe the structure formed by the cohesion of colloidal particles. Silica sols lose their stability by aggregation of colloidal particles. Colloidal silica particles can be linked together or aggregate by gelation, coagulation, flocculation and coacervation <sup>[21]</sup>.

Gelling is where the particles are linked together in branched chains resulting in increased viscosity and later on forming a solid network which retains the liquid. The silica concentration is same for all macroscopic regions. Coagulation is where the particles come together into relatively close-packed clumps. Flocculation is where the particles are linked

together by bridges of the flocculating agent. The formation of precipitation is common for both the cases. Coacervation is the fourth type of aggregation, in which the silica particles are surrounded by an adsorbed layer of makes the particles less hydrophilic (the present section 2.1 is modified and rewritten from ref. <sup>[21,29]</sup>).

## **2.2 Applications of colloidal silica**

Silica is the common name for silicon dioxide ( $\text{SiO}_2$ ), one of the most abundant component on the earth's crust except carbon found in nature which occurs in crystalline and amorphous forms (non-crystalline). Crystalline silica is known to cause adverse effects like silicosis <sup>[30]</sup>, whereas amorphous silica is considered to be less toxic <sup>[6]</sup>.

The ability to effectively modify the properties of SNPs by controlling their structure at nanoscale level makes them extremely attractive candidates for many applications, from fundamental scientific studies to commercially realizable technologies.

SNPs are having various applications in biomedical fields like targeted drug delivery and controlled drug release for genes and proteins <sup>[31-34]</sup> due to the unique way in which they interact with matter.

Besides biomedical applications, SNPs are used commercially in products such as electronic components, scratch-free paint, sports equipment, mechanical polishing, cosmetics, food color additives, and surface coatings <sup>[35,36]</sup>.

A simple flowchart for applications of silica is shown in Figure 2.

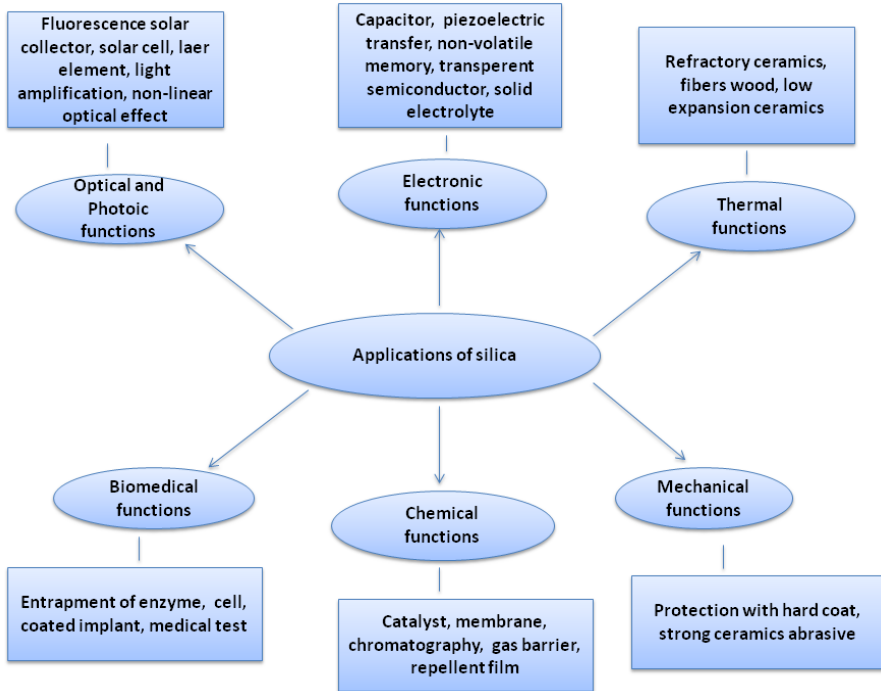


Figure 2: Applications of silica according to S. Sakka <sup>[37]</sup>.

## 2.3 Synthesis and Functionalisation of silica nanoparticles

### 2.3.1 Stöber synthesis of silica and its modifications

One of the widely used methods for silica synthesis (irrespective of product properties) is sol-gel processing and it is used in this study. Figure 3, shows schematically the most used variant of the sol-gel process.

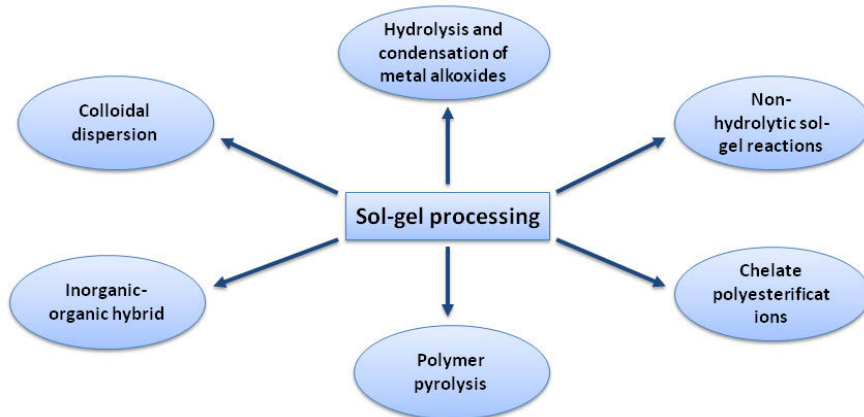
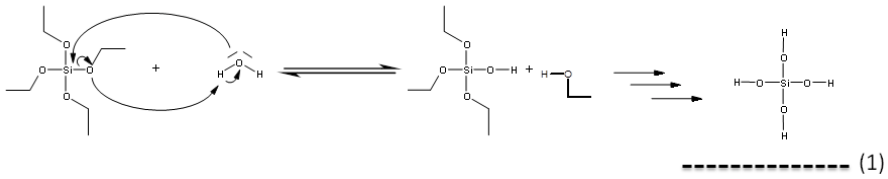


Figure 3: Different routes of the sol-gel processing.

Colloidal silica is of a particular interest due to its ease of synthesis and precise controlling of size and distribution of the particles. Stöber and co-workers [24] reported a pioneering method for the synthesis of fairly monodisperse spherical silica particles and different sizes of silica NPs were prepared in the range of 30 nm to 2  $\mu\text{m}$  with a narrow size distribution. The synthesis proceeds with the hydrolysis and condensation of tetraethyl orthosilicate or tetraethoxy silane (TEOS) in a mixture of alcohol, water and ammonia (catalyst). Since the hydrolysis of TEOS with water is very slow, either an acid or ammonia is used to serve as a catalyst. The former enables the growth of gel structures, while the latter is a morphological catalyst producing spherical particles. In general, the hydrolysis reaction gives the slightly hydrolyzed TEOS monomer Figure 4-1 (Hydrolysis reaction). This hydrolyzed intermediate undergoes condensation to form silica eventually according to Figure 4-2 (condensation reaction).

### 1) Hydrolysis reaction



### 2) Condensation reaction

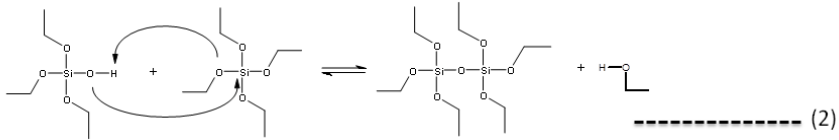


Figure 4: Synthesis of Stöber spherical silica particles.

Polymerization of silicic acid may occur in two ways. In acidic solutions (with salts), chain-like or open-branched polymers are initially produced by the condensation of silane groups. Polymerization in alkaline solutions (base that dissolves in water, eg. ammonium hydroxide, without salts) take place by internal condensation and cross-linking to give particles in which consists of four silicon-oxygen bonds and the hydroxyl groups are attached to the surface of the particles only <sup>[38, 39]</sup> (Figure 5).



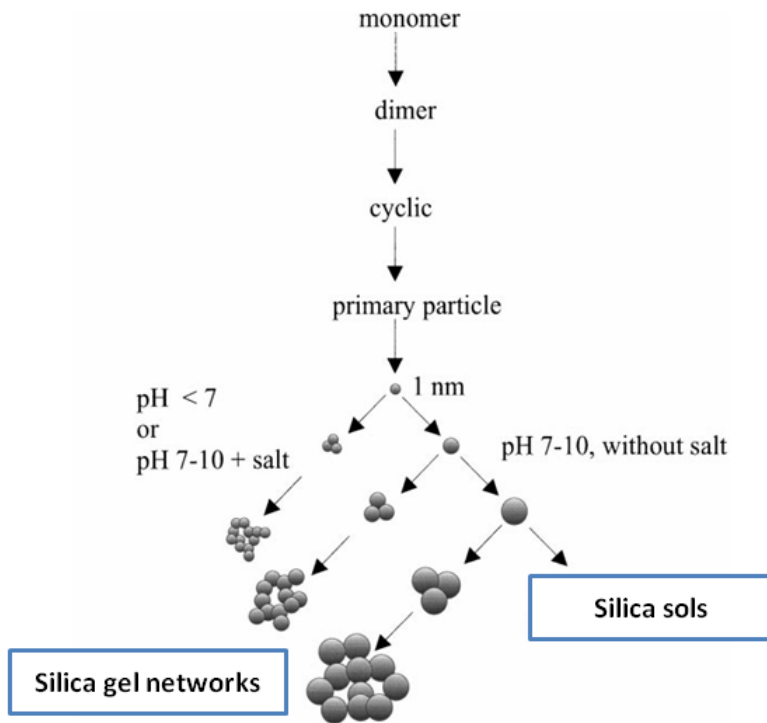


Figure 5 : Polymerization behavior of silica describing the sol-gel process (modified and redrawn from Iler<sup>[28]</sup>).

The reason behind pursuing the sol-gel processing route for the silica synthesis will be apparent from the following important advantages:

- The sol-gel reaction can be carried out at room temperature, one of the key factors in this study, thus avoiding the degradation of reactants and products.
- The flexibility of the sol-gel processing allows the doping or encapsulation of reactants, which in turn alters the product properties significantly.
- The reaction kinetics of the process can be controlled by varying the composition of the reaction mixture.

In spite of the above mentioned advantages, there is also need to overcome the following problems in sol-gel processing.

- Precursors need to be highly pure, which increases the cost. In addition, they (precursors) are highly sensitive to moisture and require careful storage.

- Evaporation of solvent/s and product drying induces significant shrinkage and cracking in the material.

The size of the silica particles depends on the type of silicon alkoxide and alcohol. Silica particles prepared in the methanol solutions are the smallest (diameter >30 nm) with broader distributions, and are not highly monodisperse. To overcome these limitations, Davis and other groups <sup>[40-44]</sup> has introduced a method for synthesizing small, monodisperse silica nanoparticles in an aqueous environment in the presence of lysine (Figure 6) or other basic amino acids. This method allowed tuning the particle size with no aggregation. The size of obtained silica particle sols successfully resulted in the range of < 20 nm with a narrow size distribution. This method is analogous to the so-called "Stöber method", but basic amino acid monomer have been used in place of NH<sub>3</sub>; the hydrolysis and condensation reactions of tetraethyl orthosilicate (TEOS) as a silica source were carried out in the presence of L-lysine monohydrate. This kind of approach allows for the fine tuning the particle size resulting in silica-nanoparticle sols which are stable for months.

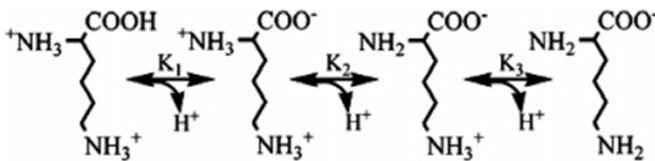


Figure 6: Lysine Equilibrium Relations (adapted from ref. <sup>[45]</sup> ).

The chemical properties of the silica surface are mainly determined by the various silanol and siloxane groups that are present on the external as well as the internal structure. The hydroxyl groups on the surface of silica particles can be easily tailored with organic compounds or polymers. Silanol groups can be easily functionalised by different chemical procedures.

### 2.3.2 Silanization and Amination of SNPs

The most convenient technique for silica surface functionalisation is the use of the reaction of silanol groups with suitable silane reagents. Surface modification by a silanization reaction (using trialkoxysilanes) is used in numerous fields of nanotechnology <sup>[46-51]</sup>. The functionalisation of silica particle surface can be used to enhance and control the overall properties of the particles for the desired applications. The nature of the functional groups on

the particle surface plays a crucial role in the surface properties of particles like hydrophobicity and chemical reactivity [52, 53]. In this regard, aminopropylalkoxysilanes (APTES) are widely used as coupling agents for silica based materials because of their bifunctional (alkoxy and amino groups) nature and low cost (Figure 7). Their applications have been developed enormously because of the increasing relevance of surface chemistry and to life sciences and environmental sciences [54-59]. This reaction is very attractive because it provides a chemical link between the labile group (-NH<sub>2</sub>) containing silane and the silica surface, which can be further reacted with polymers containing easy leaving functional groups like tosyl, bromo, chloro, etc. The advantage of aminated silica is that the amine group can also catalyze inter or intramolecularly the reaction between silane molecules and surface silanol groups with formation of form siloxane bonds [60-62]. The amine group can also be used as a host for bio-organic compounds where some promising applications in biomedical research area have been reported [54].

Two methods have generally been modified for the fabrication of surface modified SNPs: Post modification (or grafting) and in situ modification (or co-condensation) [62, 63]. In general, grafting of APTES molecules onto silica are conducted in the presence of non-polar (benzene, toluene, xylene etc.) media in order to prevent uncontrollable hydrolysis and polycondensation reactions. Nevertheless, during the post-modification the organosilanes (APTES) can lead to a non-homogenous distribution. Two stepped reaction, time and energy consuming are the main limiting factors, so that is why post-modification is not suitable for large scale industries/production.

Another alternative method, the in situ modification is used in order to reduce the limitations in post-modification. The organosilane (APTES) is directly incorporated into the reaction media of silica dispersion. The organic units which are present in APTES can be homogeneously distributed.

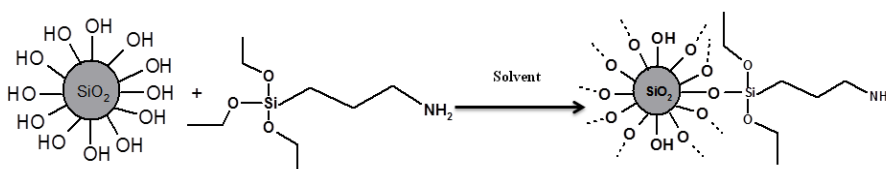


Figure 7: Amination of SNPs

The surface functionalization of APTES onto the silica particles affects the size and the zeta potential. When APTES was added to the silica surface, nanoparticle agglomeration was very high in aqueous suspension and the zeta potential becomes very low <sup>[64, 65]</sup>. Dispersion of aminated silica particles in methanol had shown less agglomeration <sup>[61]</sup>. In this thesis, the further reactions of aminated silica nanoparticles (e.g. chemical grafting with dyes and polymers) are executed in the presence of methanol to avoid agglomeration.

### 2.3.3 Poly(ethylene glycol) (PEG)

Poly(ethylene glycol) (PEG) (Figure 8-a) is a synthetic non-toxic polymer with stealth behaviour and has been approved by the FDA for internal consumption (i.e. makes it suitable for applications in the field of biomedical devices). It is linear and is available in variety of molecular weights, and soluble in water and most organic solvents. It is neutral (uncharged) and possesses no acidic groups (excluding the hydroxyl end-group chain which acts a weak hydrogen-bond acid) and has weakly basic ether linkages.

PEG is mainly soluble in water by virtue of hydrogen bonding between the ether oxygen atoms of PEG and hydrogen atoms of the water molecules <sup>[66]</sup>. Figure 8-b explains two water molecules are bonded to each PEG group (two water molecules/EG monomer). Large number of water molecules leads to large repulsive forces with proteins, hence promoting protein resistance with high molecular weight polymers. This behavior is known as "excluded volume". It means a hydration layer decreases as PEG grafting density increases <sup>[67]</sup>.

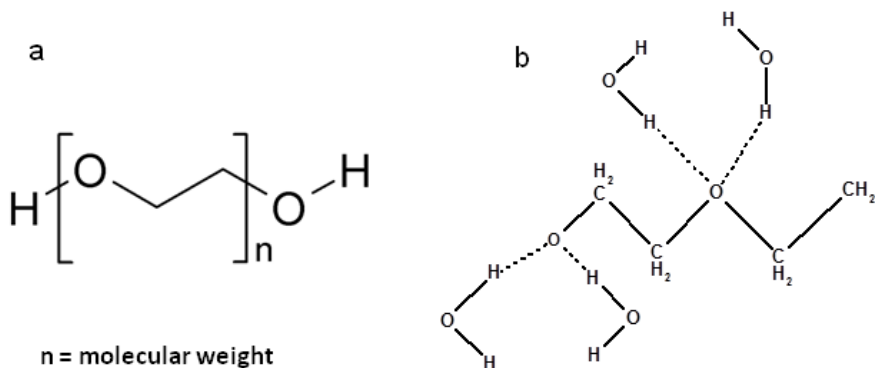


Figure 8: a) Poly(ethylene glycol) b) Water molecules H-bonded to PEG ether group

The terminal hydroxyl group (-OH) is available for coupling/further modification reactions. PEGs possess a variety of properties pertinent to biological applications and an enormous amount of work has been done to explore these properties for different applications, which can be found in literature [68]. Despite of its apparent simplicity, PEG has been found to be highly effective synthetic polymer in reducing non-specific protein adsorption.[68]. Monofunctional PEG molecules coupled to proteins are known to prolong the particle circulation time in blood and reduce immunogenicity [69, 70].

Whitesides and co-workers [71] evaluated four characteristic points, which surface bound polymers must possess to avoid/inhibit protein adsorption: (1) they are hydrophilic (2) they are hydrogen bonded acceptors (3) they are hydrogen bonded donors (4) the electric charge should be neutral. PEG has met all above requirements to inhibit non-specific protein adsorption.

The following key early works (during 1960 `s) have found a platform for the application of PEG as protein resistant material, which are [68]:

- The observation that PEG can be used to drive proteins and nucleic acid from a solution for purification and crystal growth [72, 73].
- Albertsson et al. [74] reported that PEG and dextran, when mixed with a buffer, form an aqueous polymer two-phase system, which are hospitable to biological materials and are extremely useful for the purification of these biological materials.
- Abuchowski et al. [75] observed that covalent attachment of PEG to protein gives active conjugates that are non-immunogenic and non-antigenic, and have greatly increased serum lifetime.
- Mori et al. [76] reported that covalent attachment of PEG to surfaces greatly retards protein adsorption to these surfaces

This early research has led to several active areas of deep investigation, and with progress in the field of toxicology, biotechnology and biomedical science, use of PEG has increased greatly over the years in diverse applications.

## Bovine serum albumin (BSA)

Bovine Serum Albumin is used as a model protein in this work as shown in Figure 9. Albumin is the most abundant protein in the circulatory system which is responsible for the blood pressure and pH<sup>[77, 78]</sup>, having a molecular weight of 66 KDa and dimensions 14×4 nm. BSA is a large protein containing 14% basic groups and 18% acidic groups, with a pI (isoelectric point) of 4.8. It is therefore negatively charged at pH 7.2 and positively charged at pH 4.7<sup>[79]</sup>.

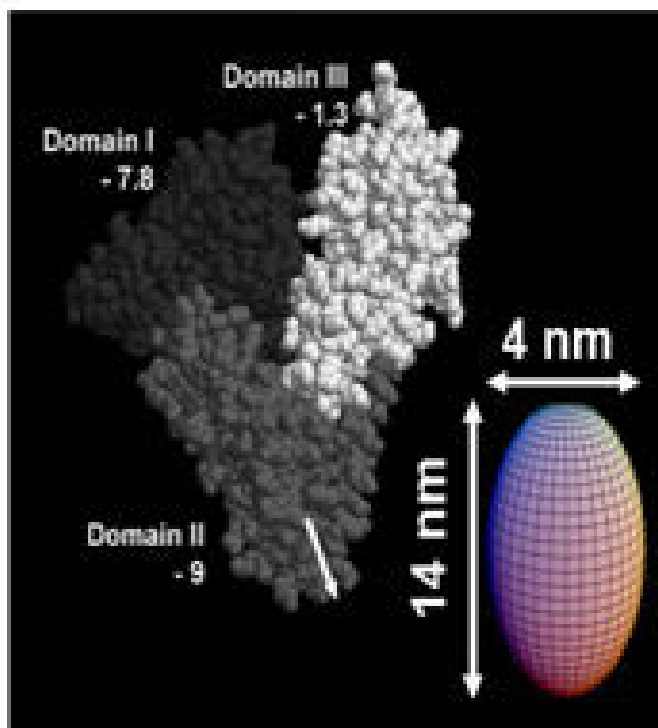


Figure 9: BSA showing the three domains in a N-Form conformation (adapted and redrawn from Rezwan et al.<sup>[80]</sup>).

### 2.3.4 PEGylation chemistry (covalent attachment of tosyl mPEG to aminated SNPs)

A range of techniques have been employed for immobilization/grafting of PEG onto SNPs surfaces and these can broadly be divided as physisorptive or chemisorptive. Physisorption is a very simple and easy method, which relies on relatively weak van der Waals and hydrophobic forces to tether polymers to a nanoparticle surface. Furthermore, the polymers are not irreversibly bound to the surface and proteins may be exchanged with the polymer on the surface [81, 82].

The chemisorptive method is one of the most effective methods for creating permanent grafted polymer (PEG) surfaces [81]. These methods require that functional groups should be introduced onto the substrate or may be onto PEG hydroxyl groups. Apparently, these chemisorption processes are time-consuming, complex processes and have purification problems.

However, PEGylation (chemical grafting) (Figure 10) presents a simpler approach, where PEGs attach directly to the silica surface or labile group (amino, thiol, halo, etc.) containing grafted silica through a strong chemical bond. Molecules with terminal amino functionalities have been employed for the surface modification of polymers, because amines are more nucleophilic and generally do not require the addition of catalysts. In this work, for PEGylation mPEG was pursued with different molecular weights and further tosylated to couple with aminated SNPs (will be discussed in more detail of the section in chapter 6). Among all leaving groups (tosyl, bromo, chloro etc.), tosyl was found to be the best leaving group to form a covalent bond with aminated SNPs and tosylated mPEG.

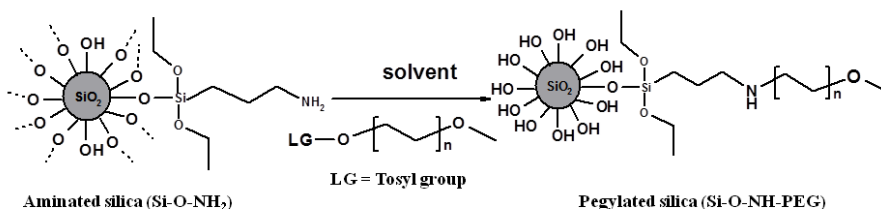


Figure10: PEGylation of aminated silica particles

### 2.3.5 Hybrid nanoparticles

In general, the term "hybrid" is more often used if the inorganic units are *in situ* by using sol-gel chemistry. According to this approach both organic and inorganic phases are formed together through the simultaneous polymerization of organic monomer and sol-gel precursors of the inorganic domains<sup>[83]</sup>.

Depending on the strength or level of interactions, two types of hybrid materials can be classified. Type-I "non-covalent" hybrid materials are characterized by weak interactions between the two phases (organic and inorganic phases consists of non-bonded interactions due to van der Waals, electrostatic and hydrogen bonding forces). This type of non-covalent hybrid material formation mainly focuses on the use of organically modified silica that contain similar to those on polymer backbone to increase the compatibility<sup>[84-86]</sup>. Whereas, Type-II hybrid materials evidence strong chemical interactions between the two phases to increase the phase coupling<sup>[87]</sup>.

Today the organic-inorganic hybrid materials had engrossed a great interest in nanotechnology and material fields. To improve the interactions between silica and organic functional groups, covalent linking is needed. It means there is a need to introduce active inorganic groups like, amines, thiols, isocyanates and vinyl groups on to the colloidal silica. There are two prominent methods, post-modification (grafting) and direct modification (co-condensation), which can be employed to modify silica particles/colloids. Post-modification is a two-step method for covalently linking the alkoxy-silanes with surface silanol groups and has been widely used in the modification of silica colloids<sup>[88-91]</sup>. The drawback of this method is, due to different chemical moieties and the reactivity of the surface hydroxyl groups, only a part of these hydroxyl groups can be used for modification. On the other side the direct-modification method is co-polymerizing the alkoxy-silanes with silica precursors (TEOS). This method enables more homogenous surface coverage of functional groups<sup>[92-94]</sup>. Various studies have been reported in literature to form hybrid silica particles by using the co-condensation method. For instance, in 2003 Xu et al.<sup>[94]</sup> reported a very simple and efficient method about the preparation of hybrid particles with the size range of 50-200 nm, which are useful in biomedical applications. The advantages of this method are to be a one-pot synthetic route and the size selectivity is controlled by the concentration of the catalyst, the main limitation is a very poor monodispersity.

There are many other attempts on the synthesis of hybrid silica nanoparticles by using direct synthesis<sup>[95, 96]</sup>. Click chemistry is also one of the method to synthesize hybrid nanoparticles,



where 1,3-dipolar cyclo-addition of azides and alkynes takes place that was familiarized by Sharpless and co-workers [97].

Lu et al. [98] and Radhakrishnan et al. [99] reported on size control of hybrid particles by using non-polymeric precursors. Interestingly, in these systems the particle size decreased by increasing precursor concentration. Oh et al. [100, 101] and Hwang et al. [102] reported the synthesis of hybrid silica-PEG by using a polymeric precursor but without tuning particle size. Their strategy was to modify silica by using remodelled sol-gel systems and the emulsion method, which are having complex experimental process and also require surfactants (will be discussed in more detail of the section in chapter 5).

#### **2.4 Non-specific protein adsorption onto nanoparticle surfaces:**

Nanomedicine is a promising field which has a very huge potential among the others to improve the human health and to defeat other intractable diseases. In this respect, Proteins occupy a dominant position within biomedical and toxicological studies because they are the most abundant organic molecules found in living systems. The adsorption of proteins on nanoparticle surfaces plays a vital role in biology, biochemical, pharmaceutical and food processing applications [103-106]. For these reasons the subject has drawn more attention from many fields of the natural sciences, and also from the industry sector. There are numerous problems associated with nanomaterials which may come in contact with biological systems. The main significant problem associated with all material surfaces is the undesired adsorption of protein. In medical prosthesis it is important to prevent blood protein adsorption and hence to reduce the risk of unwanted blood clotting [107] and to make the material as biopersistent.

Proteins usually contain both hydrophobic and hydrophilic (charged) segments: a combination of hydrophobic interactions and electrostatic interactions results in the "non-specific adsorption of proteins" onto the surface. Proteins are having large degrees of freedom, where they can change their confirmation with a process called unfolding. During the interaction with surfaces, proteins can change their confirmations in order to minimize or maximize the exposure of hydrophilic and hydrophobic components.

The process of non-specific protein adsorption is mainly governed by the physico-chemical properties of proteins (structure, size, and distribution of charge and polarity), the properties of nanoparticle surface (well-defined size, charge and surface area), environmental conditions (pH, temperature and ionic strength) and the kinetics of adsorption process [108].

The main causes of non-specific adsorption of proteins at the interface are due to two reasons: 1) the surface properties of the nanomaterial and 2) the nature of the proteins present in the biological medium. There are many comprehensive reviews for hypothesis based on experimental measurements <sup>[109, 110]</sup> and theoretical calculations <sup>[111]</sup>, which explains the molecular events taking place during non-specific protein adsorption.

#### **2.4.1 Nanoparticle- protein corona:**

When nanoparticles (NPs) enter a biological fluid, proteins and other biomolecules rapidly compete for binding to the nanoparticle surface, leading to the formation of a so-called "protein corona" that critically defines the biological identity of the particle <sup>[112-115]</sup>, and also shields their original surface properties <sup>[116, 117]</sup> (Figure 11). The biophysical properties of such a particle-protein complex offer significantly from those of the formulated particle <sup>[115]</sup>. Therefore, the further biological responses and particle biodistribution are predominantly influenced by the nanoparticle-protein complex, potentially contributing to unwanted biological effects <sup>[11, 115, 118, 119]</sup>.

In biological media (BSA medium), it is known that the particle surface is covered by a corona of BSA molecules that may be divided into a "soft corona" (short-lived) in which dynamic exchange of biomolecules between BSA medium and particle surface is less (seconds to minutes). Whereas, "hard corona" (long-lived) are having high affinity between BSA medium and particle surface in biological environment (incubated for hours). It is believed that the soft corona forms on short time scales (from seconds to minutes) and evolves to hard corona over the incubation times in hours <sup>[11, 115]</sup>.

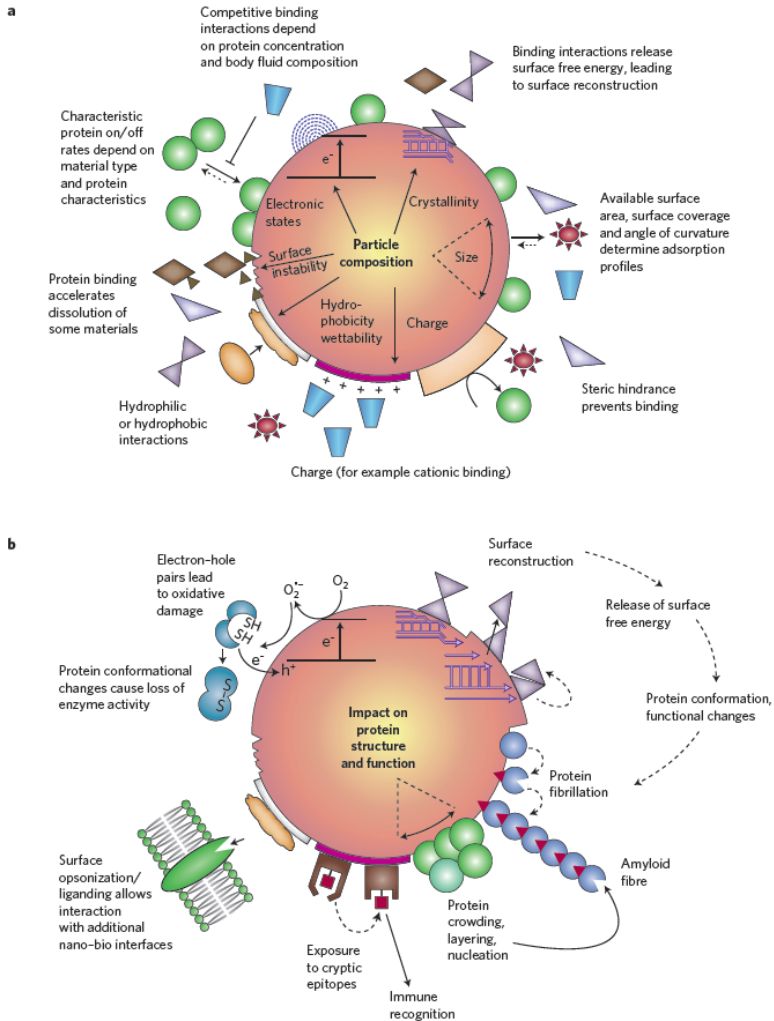


Figure 11: Effects of protein corona surrounding a nanoparticle. The corona constitutes a primary nano-bio interface that determines the fate of the nanoparticle. (a) Pre-existing or initial material characteristics contribute to the formation of the corona in a biological environment. (b) Potential changes in protein structure and function as a result of interacting with the nanoparticle surface can lead to potential molecular mechanisms of injury that could contribute to disease pathogenesis. (Reprinted with permission, from Ref. <sup>[120]</sup> Copyright © 2009, Nature Publishing Group)

## 2.4.2 Nanoparticle-protein interactions:

In biomaterial interface, proteins have a tendency to adsorb onto the nanoparticle surface due to high molecular weight and presence of polar and non-polar regions<sup>[121]</sup>. Several molecular forces/interactions are influenced during the adsorption process can be shown in Figure 12.

The main forces are hydrophobic interactions, electrostatic forces van der Waals forces and hydrogen bonding.

*Hydrophobic interaction* is a strong attraction between non-polar molecules and nanoparticle surfaces in water. The hydrophobic interactions between proteins and nanoparticle surfaces generally lead to unfolding of the proteins, due to an attraction between the hydrophobic parts inside the protein and the particle surface. Many studies have been reported that protein adsorption is more favourable towards hydrophobic surfaces than hydrophilic surfaces<sup>[122-124]</sup>.

*Electrostatic interactions* present in between proteins and surfaces which drives towards protein adsorption. When nanoparticle surfaces are charged (positively or negatively) electrostatic interactions plays a vital role in adsorption because proteins are also charged. Pasche et al.<sup>[125]</sup> reported that on hydrophilic surfaces, structurally stable proteins adsorb only if electrostatic interaction is favourable.

*van der Waals forces* are occurred with interactions of proteins and nanoparticle surface.

*Hydrogen bonding* is mainly present in proteins are between amide and carbonyl groups of the polypeptide chain. Nevertheless, formation of hydrogen bonding is not to be the main driving force for protein adsorption.

The adsorption process mainly depend on the nature of the nanoparticle surface and protein, binding/kinetic energies, orientation/confirmation of protein by which it approaches to the surface of nanoparticle.

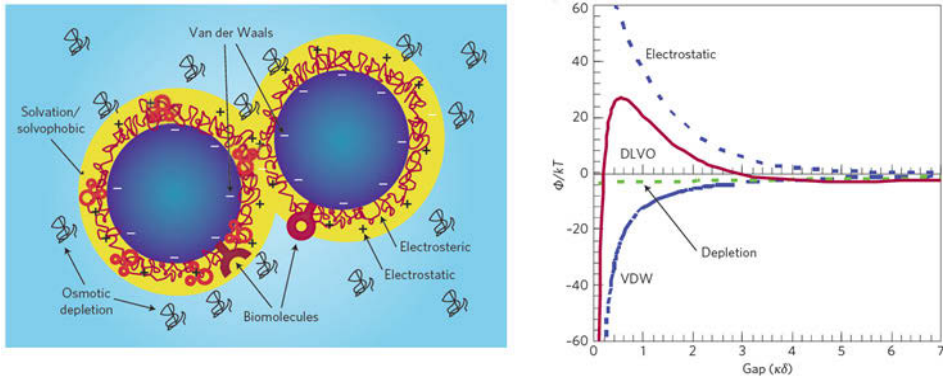


Figure 12: Colloidal interactions between nanoparticle-protein (a) Traditional forces for colloidal fabrication (for example electrostatic, VDW, covalent) and other important interactions (for example solvation, solvophobic, biomolecular, depletion) that occur when particles are suspended in biological media and come into contact with cells. (b) VDW and depletion forces are attractive whereas the electrostatic forces are repulsive over a typical length scale. The DLVO theory in colloid science considers the sum of these forces.  $\Phi$ , interaction potential;  $k$ , Boltzmann constant;  $T$ , absolute temperature;  $\kappa$ , inverse debye length;  $\delta$ , separation distance. (Reprinted with permission, from Ref. <sup>[120]</sup> Copyright © 2009, Nature Publishing Group).

### **2.4.3 Surface modification of nanoparticle surface to reduce non-specific protein adsorption:**

Surface modification is founded as a major factor in determining the biocompatibility of any biomedical device. Numerous studies have been focussed on surface modification to reduce protein resistance. The major studies of surface modifications are surface coating, physical adsorption, incorporation of surface active components and covalent attachment (chemical grafting). In this work, covalent attachment with polymers was pursued for reduction of non-specific protein adsorption. As explained earlier, surface modification with hydrophilic polymers like PEG has been widely used method to reduce non-specific protein adsorption.

Although, the exact reasons for the protein resistance of PEG surfaces have been studied and discussed extensively theoretically and experimentally, some questions remain unanswered [126, 127]. However, several factors have been hypothesized which are responsible for protein resistance properties of PEG modified surfaces. Two mechanisms have been proposed to explain the optimal protein resistance of PEG attached to a surface. The first mechanism involves the flexibility and mobility of PEG chains. Flexibility is due to the conformational freedom of the -C-C-O- backbone of PEG due to unrestricted rotation around the -C-O- bonds. This mechanism is usually referred to as “excluded volume-steric repulsion” (Figure 13-a). When the protein approaches the PEG modified surface, it compresses the flexible PEG chains. This implies an entropy loss generating a repulsive interaction, thus effectively pushing the protein away from the surface. The second mechanism is related to the low interfacial energy at the PEG-water interface and the ability of the PEG chains to bind water tightly (hydrogen bonding) (Figure 13-b). Based on this mechanism the proteins are kept away from the surface by the water barrier. This phenomenon also referred to as “osmotic repulsion” [128].

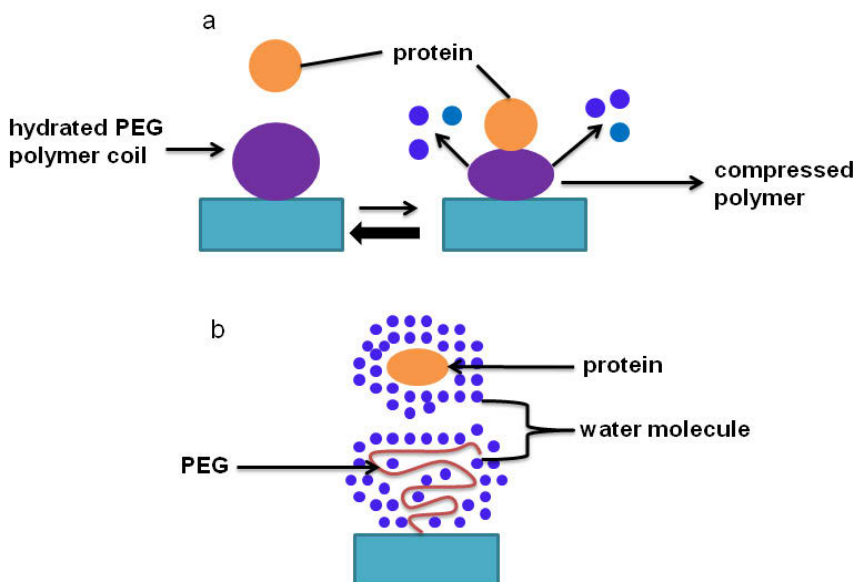


Figure 13: Schematic presentation of a) excluded volume- steric repulsion, b) water molecule as a barrier (adapted and redrawn from ref <sup>[129]</sup>).

It was early reported that the average length of the PEG chains influences the protein adsorption of PEG-coated materials <sup>[71, 130]</sup>. From the published literature point of view, longer PEG chains give grater protein resistance, in particular in demanding biomedical applications <sup>[131]</sup>. However, only two or three units of adsorbed ethylene glycol (EG) have been also reported to be sufficient to obtain protein resistant surfaces under many conditions <sup>[132, 133]</sup>. This effect, could not be due to steric repulsion, but instead appears to relate to the formation of a strongly bound hydration layer on the EG surface <sup>[134]</sup>. Apparently, the idea is that polymer (PEG) chain length is a critical parameter for the protein resistance of PEG. Besides PEG chain length, the other main parameter to consider is the density of grafted PEG chains or spacing between the chains (d).

If the density or surface coverage is low, the PEG will be in a random coil conformation giving the so-called "mushroom regime", where the PEG chains do not overlap and there are empty spaces between them. As the density increases, the PEG chains cannot maintain the random coil state and must stretch to be accommodated. At higher density when the distance between the PEG chains is smaller than the radius of gyration the chains will be more

completely stretched, and the surface is said to be in the “brush regime” confirmation. The illustration of mushroom and brush confirmation is shown in Figure 14.

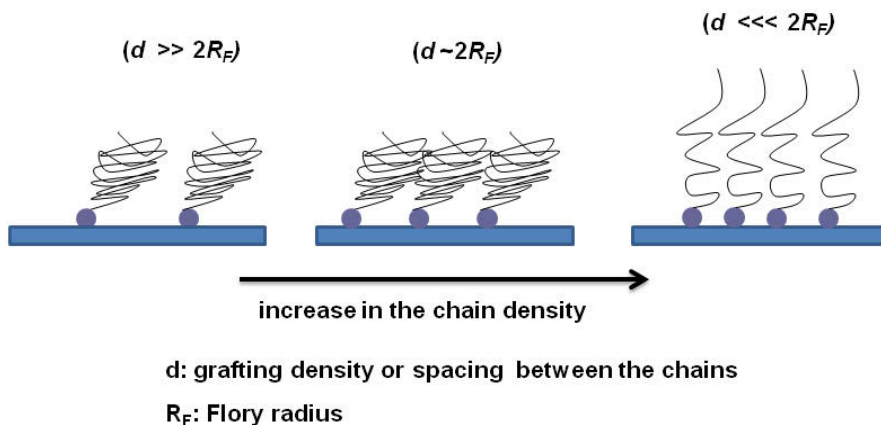


Figure 14: Illustration of PEG regimes upon end grafted PEG chains at the interface, depending on whether the chain is attracted to the surface or repelled (adapted and redrawn from ref. [67]).

Due to the relevance of chemical grafting for the work reported in this thesis, a summary of the literature on surface modification with PEG through chemical grafting is presented now. Carignano et al. [135] reported that a very high surface coverage will modify the chemistry of the surface and may result in an attractive surface to proteins. This indicates that there is a critical value of chain density and chain length to effectively inhibit the adsorption of protein. There are many studies influencing the effect of chain density and chain length of PEG on protein adsorption. Grafting of PEG on TiO<sub>2</sub> showed that when ethylene glycol densities were above 15-20 EG/nm<sup>2</sup>, very little protein is adsorbed to the surfaces (less than 10ng/cm<sup>2</sup>) [136]. Sofia et al. [137, 138] modified silicon surfaces with PEGs of several molecular weights and densities and showed that with increasing grafting density of PEG, fibronectin and albumin adsorption were reduced and reached zero at a PEG density of ~100 ng/cm<sup>2</sup>. Unsworth et al. [67, 139, 140] studies reported the effect of the chain length, chain density and PEG hydration layer and moiety groups (-OH and -O-CH<sub>3</sub>) on protein adsorption using gold as a model substrate. Hydroxy-terminated PEG performed better than methoxy-terminated PEG. Moreover, the PEG chain density was found to play a more important role in reducing protein



(Fibrinogen) adsorption. The main conclusions from their studies are that there was an optimal chain density beyond the increase of protein adsorption. Dong et al. <sup>[141]</sup> reported, PEGs of different molecular weights ranging from 200 to 4600 were immobilized on poly(ethylene terephthalate) (PET). Out of which PEG of molecular weight 2000 was found to be the best surfaces in terms of resisting protein adsorption. Currie et al. <sup>[142]</sup> reported the adsorption of BSA decreased continuously with the increase of PEO grafting density, the main observation is that the long chains can more easily trap the proteins than short chains. From all the above mentioned literature, many questions have been therefore raised regarding the viability of using PEG as a long term protein resistant material and lack the clinical success of PEG-coated biomaterials may be appear to support this idea <sup>[143]</sup>. Overall, surface coverage (grafting density), chain length, chain flexibility and chain conformation are the major factors that contribute to the protein resistance and most importantly, act inherently together (the present section 2.4.3 is modified and rewritten from ref. <sup>[129, 144]</sup>).

## **2.5 Open questions:**

In the last few years, the question of SNPs stability in cell culture media (CCM) has attracted more interest, since the toxicity related to single particle or agglomerates needs to be elucidated. Toxicological investigations of SNPs are hampered by a number of technical difficulties such as the main difficulty is to avoid aggregation of nanoparticles. As discussed in chapter 1, research has shown that non-specific protein adsorption or to avoid aggregation of NPs can be minimized by surface modification. A variety of approaches has been developed to reduce the adsorption of proteins in physiological environment, out of which coating or modification of silica surfaces with neutral hydrophilic polymers is a widely accepted method as a means to reduce non-specific adsorption of proteins. Further, there are only a limited number of materials that are suitable for surface modification aimed at preventing non-specific protein adsorption. In this small arsenal, poly(ethylene glycol) (PEG) is widely explored as a protein resistant material. Nevertheless, PEG shows excellent stabilizing properties on the SNPs surface due to a steric barrier formed by PEG chains <sup>[68]</sup>.

Besides, little is known about time evolution of adsorbed proteins onto pristine and modified NPs, their orientation (side-chain or perpendicular confirmation), about the strength of the NP-protein interactions and the influence on colloidal stability and biocompatibility <sup>[145]</sup>. In addition, the synthesis of small NIR-fluorescent silica particles with sizes  $\leq 100$  nm still presents a challenge and only few successful attempts have been yet reported.

With the above all in the mind, important scientific open questions arising to this thesis are the following,

- Necessity of silica surface modification with dyes and polymers with different molecular weights to achieve suppression of protein adsorption,
- Influence of NPs properties on the colloidal stability and proteins,
- Time evolution of adsorbed proteins onto pristine and modified NPs and their orientation.

The aim of the present thesis was to bring more light into the understanding of fundamental aspects regarding the surface modification of SNPs and their colloidal stability in biological media.

## Chapter 3

### Experimental Methods

---

This chapter describes about the chemicals and experimental techniques (methods) used in this thesis.

#### 3.1 Chemicals

Tetraethoxysilane (TEOS, 99%), 3-aminopropyltriethoxysilane (APTES, 99%), 3-isocyanatepropyltriethoxysilane (IPTES, 99%), poly(ethylene glycol) monomethylether 350, 2000 and 5000 g/mol, dibutyltin dilaurate (DBDU), tetrahydrofuran (THF), bovine serum albumin (BSA), phosphate buffered saline (PBS), anhydrous ethanol (99.9%), Spectra Pore Cellulose ester membranes (MWCO: 100,000) were purchased from Sigma-Aldrich (Berlin, Germany) and Milli-Q-water with a resistance greater than 18 M $\Omega$  was used for all experiments. Ammonium hydroxide (NH<sub>4</sub>OH, 30%), methanol (99.9%), ethanol (99.9%), dimethylformamide (DMF), isopropyl alcohol (IPA, 98%) were purchased from Sigma-Aldrich (Berlin, Germany). Alexa 647 and 754 were purchased from Invitrogen. Milli-Q-water with a resistance greater than 18 M $\Omega$  was used for all experiments. Single-side polished silicon wafers (P-type, orientation [100]) were used as a substrate. Before use the wafers were cut into 1 cm  $\times$  1 cm squares using a special wafer saw.

## **3.2 Methods:**

### **3.2.1 Dynamic Light Scattering (DLS)**

Dynamic light scattering is also known as "photon correlation spectroscopy" or "quasi-elastic light scattering". It is a powerful technique to characterize dilute and transparent dispersions of particles. It also provides size measurements from the nanometer up to a few microns.

In practice, particles suspended in a liquid are never stationary. The particles are constantly moving due to Brownian motion. Brownian motion is the movement of particles due to the random collision with the molecules of the liquid that surrounds the particle. An important feature of Brownian motion for DLS is that small particles move quickly and large particles move more slowly. The relationship between the size of a particle and its speed due to Brownian motion is defined in the Stokes-Einstein law (equation 1). Thereby, the measured hydrodynamic diameter refers to how a particle diffuses within a fluid.

#### *Working principle of DLS*

The principle of this measurement technique is based on a monochromatic laser beam that passes through a cuvette with a colloidal dispersion. Some of the light is uniformly scattered by the particles in all directions via Rayleigh scattering. The changing distances of the particles due to their Brownian motion causes interferences of the light scattered by neighbouring particles. The analysis of these occurred time-dependent fluctuations in the scattering intensity gives information about the speed of the particles in the solution. Using a diffusion coefficient, the hydrodynamic diameter of a nanoparticle could be determined (Figure 15).

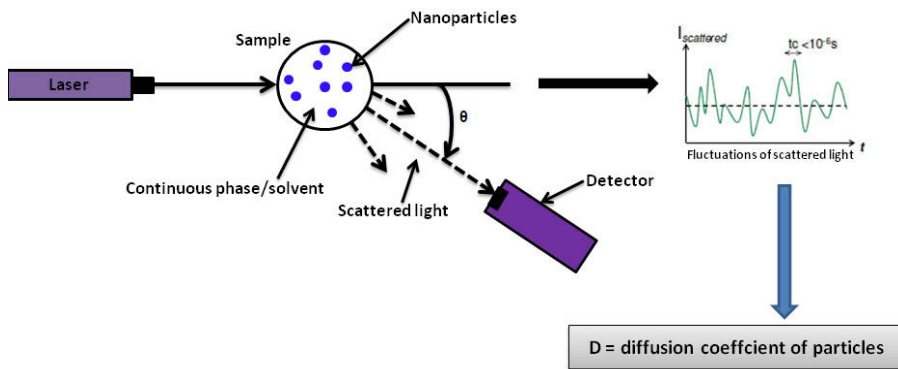


Figure 15: Illustration of dynamic light scattering principle

$$R_h = \frac{k_B T}{6\pi\eta D} \quad (1)$$

Where  $D$  is the diffusion coefficient of particles,  $K_B$  the Boltzmann constant,  $T$  the temperature,  $\eta$  the dynamic viscosity of the continuous phase and  $R_h$  is the hydrodynamic radius.

DLS measurements were carried out by use of a Malvern Zeta Nanosizer. This instrument operates at 4-mW He-Ne laser power, a scattering angle of  $173^\circ$  and a wavelength of 633 nm. The decay of the correlation function was fitted by the cumulants method <sup>[146]</sup>. The first cumulant provides the mean value of the diffusion relaxation rates and the second cumulant the variance of the distribution or polydispersity index (PDI).

### *Zeta potential*

The zeta potential is a physical property which is exhibited by any particle in suspension and is determined via ELS (Electrophoretic Light Scattering). It is the potential difference between the dispersion solution and the stationary layer of fluid attached to the particle, thereby it is measured at the slipping plane of particles. The liquid layer which surrounds a particle consists of two parts: an inner region (Stern layer) where the ions are strongly associated and an outer diffuse region, where ions are loosely bound. Within the diffuse layer there is a fictive boundary inside which the ions and particles form a stable unit. That would mean, if a particle moves, ions within the boundary move it. The potential at this boundary (surface of hydrodynamic shear) is the zeta potential (Figure 16). The zeta potential is a measure for the degree of stability of a colloidal system. If all particles in suspension have a high negative or positive zeta potential, there will be no tendency for the particles to come together and so they repel each other. In contrast, if the particles have a low zeta potential, there will be no forces preventing the agglomeration of particles. The ELS measurement principle is based on the application of an electric field to the dispersed particles. By alternating the charge between the electrodes, the particles move back and forth between the electrodes at a velocity relative to their surface charge and the potential of the electrode (Malvern Technical Note).

Each sample was measured at 25 °C three times with each measurement consisting of about 100 data acquisitions.

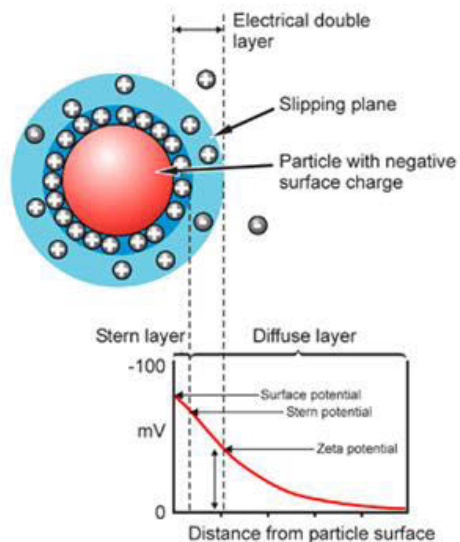


Figure 16: Schematic illustration of the zeta potential (figure taken from Malvern Technical note)

### 3.2.2 Transmission electron microscopy (TEM)

TEM measurements were performed on a Jeol JEM 2200-FS, operating at 200 kV. At high magnification, the in-column  $\Omega$ -Filter was used to improve the contrast. Samples were prepared by immersion of grids type S-160-3 (Cu coated with carbon film, Plano GmbH) in a small volume (0.5 mL) of BSA solutions and solvent evaporation in a dust protected atmosphere. Particle size distributions were obtained by analysing the TEM images using Image software<sup>[147]</sup> by taking into account more than 200 particles.

### 3.2.3 Fourier Transformation Infrared Spectroscopy (FTIR)

ATR-FT-IR spectra were recorded with a Nicolet 8700 Research FT-IR spectrometer using the ATR technique with a diamond cell ('Golden Gate' accessory, single reflection, Nicolet USA). The information depth in this setup is about 2.5  $\mu\text{m}$ . Spectra were recorded over a range of 400–4000  $\text{cm}^{-1}$  at 4  $\text{cm}^{-1}$  resolution, averaging 120 scans. The processing of the spectra was done using the OMNIC 7.3 software.

### **3.2.4 X-ray Photoelectron Spectroscopy (XPS) Measurements**

The spectrometer used was a SAGE 150 (Specs, Berlin, Germany) equipped with a hemispherical analyzer Phoibos 100 MCD-5 and a non-monochromatic MgK $\alpha$  radiation with 11 kV and 220 W settings at a pressure  $10^{-7}$  Pa in the analysis chamber. The angle between the axis of X-ray source and analyzer lenses was  $54.9^\circ$ . The analyzer was mounted at  $18^\circ$  to the surface normal. XPS spectra were acquired in the constant analyser energy (CAE) mode. The analyzed surface area was about 3 mm x 4 mm.

### **3.2.5 Thermogravimetric Analysis**

Thermogravimetric analysis was performed in a thermogravimetric Apparatus TG/DTA 220, Seiko, THASS Germany. The temperature ranged from ambient temperature to 800 °C/min under argon atmosphere at a heating rate of 10 °C/min.

### **3.2.6 Atomic force microscopy (AFM)**

The substrate was a silicon wafer, cleaned with RCA-1 method <sup>[148]</sup> and then thoroughly rinsed with Milli-Q water. The morphology of each and every silicon wafer was measured in AFM tapping mode with an iDrive cantilever BL-TR400PB (Asylum Research, Santa Barbara, CA) in Milli-Q water. The root-mean-square (rms) roughness was calculated from height images in each  $1 \times 1 \mu\text{m}^2$  box of the image so as to be comparable to standard reflectivity measurements using a 1  $\mu\text{m}$  beam coherence length.

### **3.2.7 Absorption and fluorescence spectroscopy**

Prior to each spectroscopic measurement, the washed nanoparticles were suspended in water, yielding a particle concentration of 0.1 wt% that were transferred to optical cells for the absorption and fluorescence measurements.



### 3.2.7.1 Absorption measurements

Absorption measurements were carried out with a Cary 5000 UV-Vis-NIR spectrophotometer from Varian Inc. at r.t. For the determination of the molar absorption coefficients of the fluorophores in 15% DMF/ethanol at pH 8, the absorption spectra of dye solutions of different concentrations were measured that originated from at least two stock solutions. The dye concentration was varied from  $5 \times 10^{-6}$  mol/L to  $1 \times 10^{-5}$  mol/L. In all cases, 1 cm-quartz cuvettes (Hellma) were used.

### 3.2.7.2 Fluorescence measurements

Fluorescence measurements were performed with a calibrated Spectronics Instruments 8100 spectrofluorometer equipped with Glan Thompson polarizers in the excitation and emission channel in a  $0^\circ/90^\circ$  standard measurement geometry. The excitation polarizer was set to  $0^\circ$  and the emission polarizer to  $54.7^\circ$ . The resulting emission spectra were corrected for the spectral responsivity of the fluorometer's emission channel as previously described<sup>[149]</sup>. For all spectroscopic measurements, the temperature was kept constant at r.t., here  $298 \pm 1$  K. To minimise reabsorption effects, the size of which depends on the dye- and matrix-specific Stokes-shift and on dye concentration, only dilute suspensions and short optical path lengths were used for the fluorescence studies. In all cases, 4 mm semi-micro PMMA cuvettes (Brand; non-fluorescent) were employed for the fluorescence measurements.

### 3.2.7.3 Absolute fluorescence quantum yields

The absolute fluorescence quantum yields ( $\Phi_f$ ) of the dye solutions and the suspensions of the dye-labelled PSP that equal the number of emitted photons ( $N_{em}$ ) per number of absorbed photons ( $N_{abs}$ ) were determined with a custom-designed integrating sphere setup. This setup consists of a xenon lamp coupled to a single monochromator and a six inch SpectraReflect-coated integrating sphere (Labsphere GmbH) coupled with a quartz fiber to an imaging spectrograph (Shamrock 303i, Andor Inc.) and a Peltier cooled thinned back side illuminated deep depletion CCD array. A reference detector was implemented into the setup to account for fluctuations of the radiant power reaching the sample. The sample or blank (i.e., the pure solvent) in a conventional 1 cm-quartz cell (Hellma) was mounted into the center of the

integrating sphere and the excitation light was focused into the middle of the sample. The absolute fluorescence quantum yields were calculated from the measured spectrally corrected signals of the blank ( $I_{CB}$ ) and the sample ( $I_{CS}$ ) according to equation 1<sup>[150]</sup>.

$$\Phi_f = \frac{\int_{\lambda_{em1}}^{\lambda_{em2}} \frac{\lambda_{em}}{hc_0} (I_{CS}(\lambda_{em}) - I_{CB}(\lambda_{em})) d\lambda_{em}}{\int_{\lambda_{ex1}}^{\lambda_{ex2}} \frac{\lambda_{ex}}{hc_0} (I_{CB}(\lambda_{ex}) - I_{CS}(\lambda_{ex})) d\lambda_{ex}} = N_{em} / N_{abs} \quad (2)$$

In equation 2,  $\lambda_{ex}$  and  $\lambda_{em}$  represent the excitation and emission wavelength, respectively, and  $hc_0/\lambda_{em}$  and  $hc_0/\lambda_{ex}$  the energy of the emitted and absorbed photons<sup>[151]</sup>.

As the dyes studied display a considerable spectral overlap between absorption and emission, the emission spectra measured with the integrating sphere setup were corrected for reabsorption effects as previously described<sup>[151]</sup>. All data provided were obtained as mean values from three independent measurements after reabsorption correction. The uncertainties of the quantum yield measurements were estimated to  $\pm 0.025$ .

### 3.2.7.4 Determination of the amount of SNP-coupled dye and calculation of particle brightness

For the determination of the amount of SNP-bound dye, the dye-labelled SNPs were centrifuged after the coupling reaction and the absorption spectra of the supernatants were measured after dilution by a factor of 10. The average amount of dye  $N$ , bound per mg silica particles, was calculated from the absorbance measured at the dye's longest wavelength absorption maximum, using the Beer-Lambert law and the molar absorption coefficient of the dye, previously determined in 15% DMF/methanol at pH 8. The relative amount of coupled dye equals the quotient of the applied and the actually bound amount of fluorophore molecules. The amount of dye coupled per  $\text{nm}^2$  was then calculated as the quotient of the number of dye molecules found and the surface of the spherical and non-porous SNPs determined to 80 nm by TEM.

Brightness values  $B$  of the dye labelled SNP were calculated according to equation 3.

$$B = \Phi_f \cdot \varepsilon \cdot N \quad (3)$$

Here,  $\Phi_f$  and  $\varepsilon$  equal the measured absolute fluorescence quantum yields of the dye-labeled SNPs (see Table 4) and the molar absorption coefficients of the Alexa dyes in water ( $239,000 \text{ L} \times (\text{mol} \times \text{cm})^{-1}$  for Alexa 647 and  $240,000 \text{ L} \times (\text{mol} \times \text{cm})^{-1}$  for Alexa 750), according to information from the dye manufacturer). Equation 3 assumes that the molar absorption coefficient of the coupled fluorophore molecules is not affected upon SNP attachment and remains constant regardless of the amount of dye molecules bound. Also, scattering of SNP and resonance effects are neglected in this strongly simplified approach <sup>[152]</sup>.

## Chapter 4

# Synthesis and characterisation of highly fluorescent core-shell nanoparticles based on Alexa dyes

---

\* *This chapter has been accepted for publication in Journal of Nanoparticle Research (2012) 14: 680*

**Kishore Natte**, Thomas Behnke, Guillermo Orts-Gil, Christian Würth, Jörg F. Friedrich, Werner Österle and Ute Resch-Genger.

### 4.1 Introduction

In the last years, many efforts have been dedicated to the rational synthesis of new chemically stable fluorescent nanomaterials in the emerging field of nanobiotechnology. Here, silica nanoparticles (SNPs) are increasingly used, e.g., as fluorescent labels and probes for bioanalysis and medical diagnostics<sup>[153-158]</sup>. Compared to other nanomaterials like quantum dots that suffer from potential toxicity concerns and photobrightening<sup>[159, 160]</sup>, silica is accepted as “Generally Recognized As Safe” (GRAS) by the United States Food and Drug Administration (FDA)<sup>[161]</sup>. Only very recently, first dye-doped silica particles have received approval from the FDA for the first Investigational New Drug (IND) application for targeted molecular imaging of cancer<sup>[162]</sup>.

For *in vitro* and especially *in vivo* studies, particles are desired that absorb and emit in the near infrared (NIR) spectral region where absorption, scattering, and autofluorescence from tissue and blood components is minimum<sup>[163, 164]</sup>. Hence, facile and reliable synthetic pathways to bright and colloidally stable NIR-emissive particles with precise size control are of considerable interest. Here, the synthesis of fluorescent silica particles via encapsulation of dye molecules into the silica network during Stöber like process has been frequently employed<sup>[165, 166]</sup>. However, not all NIR fluorophores are easily incorporated into SNPs using these approaches as the dyes may not survive the alkaline conditions of the Stöber process<sup>[167]</sup>. Alternatively, organic fluorophores can be incorporated into a silica matrix by coupling them to reactive organosilicates<sup>[168]</sup>. However, the sizes of the resulting particles are typically in the region of hundreds of nanometers. The synthesis of small NIR-fluorescent silica particles with sizes  $\leq 100$  nm still presents a challenge and only few successful attempts have been yet reported<sup>[169, 170]</sup>.

In order to overcome the challenges linked to the synthesis of monodisperse, small, and bright NIR-emissive SNPs, a promising alternative synthetic route was developed exploiting grafting and labelling strategies in conjunction with the subsequent preparation of protection of the dye [171-173]. For the synthesis of the latter, we used a comparatively new strategy involving immobilisation of a catalyst onto the surface of the SNPs followed by controlled hydrolysis of a silica precursor [174, 175]. As NIR-emissive amine-reactive dyes, the *N*-hydroxysuccinimidyl esters of Alexa 647 and 750 were chosen due to their high molar absorption coefficients and high fluorescence quantum yield and their chemical and photochemical stability [176, 177]. Moreover, their optical properties are barely affected by pH contrary to, e.g. xanthene dyes. The resulting particles were studied by dynamic light scattering (DLS), transmission electron microscopy (TEM), and fluorescence spectroscopy. The latter included the first-time determination of absolute fluorescence quantum yields of such scattering nanoparticles in suspension. Although knowledge of this fluorometric key parameter is of special interest to evaluate dye and bead performance, the vast majority of spectroscopic studies of the influence of dye encapsulation or dye coupling on the chromophore's optical properties rely on relative measurements of absorption and fluorescence which are strongly affected by scattering. However, only a reliable spectroscopic characterization can eventually provide the basis for the optimisation of signal-relevant spectroscopic properties like particle intensity and the comparison of different beads [152, 178-180].

## **4.2 Preparation of materials**

### **4.2.1 Preparation of silica nanoparticles (SNPs)**

SNPs were synthesised by the Stöber method <sup>[24]</sup>: ethanol (30 ml), ammonium hydroxide (2 ml) and de-ionised water (0.5 ml) were first mixed, and then 1 ml of TEOS was added. The reaction was run at room temperature (r.t.;  $298 \pm 2$  K) for 18 h, and the resulting product was centrifuged at 6000 rpm for 1 h. The silica particles obtained were washed with IPA to remove unreacted traces of TEOS and dried in a vacuum oven at 100 °C.

### **4.2.2 Preparation of amino functionalised silica particles (SNPs-NH<sub>2</sub>)**

The SNPs were amino-functionalised with APTES by quickly adding 1 ml of APTES to 30 ml of a vigorously stirred suspension of SNPs (2 %Wt.) in ethanol at r.t.. The crude product was purified by centrifugation at 6000 rpm and redispersed in methanol. This was repeated five times. The SNPs-NH<sub>2</sub> were stored in methanol and filtered before dye coupling (Whatman syringe disc filter, pore size 200 nm).

### **4.2.3 Covalent attachment of Alexa dyes to aminated SNPs**

The NHS esters of the Alexa dyes were dissolved in DMF at different concentrations ranging from  $2 \times 10^{-3}$  mol/L to  $2 \times 10^{-5}$  mol/L. Dye labelling of the SNPs was performed by addition of 100 µL of a dye solution to 600 µL of a methanolic suspension containing 1 % wt of SNPs. The pH was adjusted to 8 with 1 mol/L NaOH. After a reaction time of 2 h, the occasionally shaken suspension was centrifuged (Eppendorf centrifuge 5415D) at 15,000 g for 45 minutes. The resulting dye-labelled particles were washed twice with ethanol to remove traces of non-reacted dye followed by their redispersion in water in an ultrasonic bath. As control for the labelling studies, the free acids of both Alexa dyes were added to the SNPs under the same reaction conditions as used for the previous labelling studies with NH<sub>2</sub>-reactive fluorophores. The free acids were obtained by hydrolysis of the NHS esters (storage in water for 12 h at pH = 8) and removal of the solvent. Under these conditions, no colored particles were obtained.

#### 4.2.4 Formation of a protective pure silica shell

The fluorescent core-shell SNPs labelled with Alexa 647 and 750 were divided into two portions and subsequently, different amounts of TEOS were added to these SNPs (Table 1). For the first batch, 10  $\mu\text{L}$  of TEOS (2.5  $\mu\text{L/h}$ ) and for the second batch, 40  $\mu\text{L}$  of TEOS (10  $\mu\text{L/h}$ ) were used. To generate a silica shell and hamper the formation of new particles, TEOS was always added very slowly.

Table 1: List of materials used and samples prepared and employed for physico chemical studies. <sup>a</sup> amount of added TEOS for shell formation.

Material	Sample code	Method	TEOS <sup>a</sup> [ $\mu\text{L}$ ]	dye concentration [mmol/L]
Silica	SNPs	Stöber	-	-
Aminated silica	SNPs-NH <sub>2</sub>	Silanisation	-	-
Alexa dye 647/750	A647/A750	-	-	-
Aminated silica-dye	Core-A647-1	Esterification	-	0.2
Aminated silica-dye	Core-A647-2	Esterification	-	2
Aminated silica-dye	Core-A750-1	Esterification	-	0.2
Aminated silica-dye	Core-A750-2	Esterification	-	2
Aminated silica-dye-silica	Core-A647-2@shell-1	Shelling	10	2
Aminated silica-dye-silica	Core-A647-2@shell-2	Shelling	40	2
Aminated silica-dye-silica	Core-A750-2@shell-1	Shelling	10	2
Aminated silica-dye-silica	Core-A750-2@shell-2	Shelling	40	2

## 4.3 Results and Discussion

### 4.3.1 Physicochemical characterisation

Figure 17 illustrates the schematic representation of core-shell fluorescent silica nanoparticles.

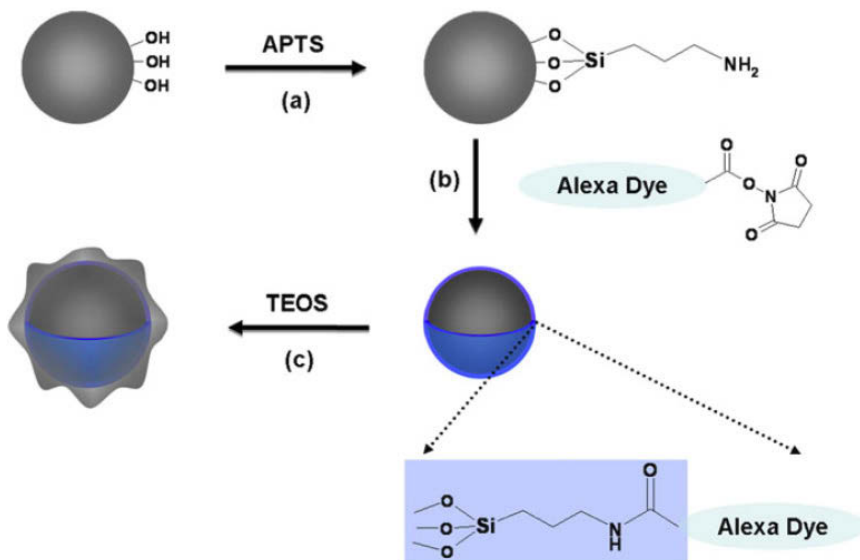


Figure 17: Schematic representation of the synthetic pathway to core-shell fluorescent silica nanoparticles: (a) silanization; (b) covalent attachment of Alexa dyes to surface amino groups; (c) formation of a protective silica shell.

The initially prepared SNPs were highly monodisperse (PDI 6 %) and spherical with a hydrodynamic radius of 90 nm as obtained by DLS. The SNPs surface was negatively charged with a zeta potential of -35 mV in water. Reaction with APTES yielded silica particles with amino surface functionalities (termed SNPs-NH<sub>2</sub>) that were positively charged (zeta potential of +2 mV in water) and strongly agglomerated in aqueous suspension after some hours as has been also observed, e.g., by Schiestel<sup>[181]</sup>. Dispersion of SNPs-NH<sub>2</sub> in methanol showed to be an effective alternative in order to minimise agglomeration (PDI < 20%). Successful amination was further proven by NMR, FTIR, and XPS (see



Appendix 4). Coupling of Alexa 647 and 750 dyes to aminated SNPs transformed these positively charged SNPs into negatively charged particles with a zeta potential of *ca.* -30 mV. The dye-labeled nanoparticles were stable in water suspension for weeks without agglomeration. TEM studies of the different nanoparticles revealed smooth morphologies for both pristine and dye-coupled SNPs (Figure 18, panels A and B). Addition of small amounts of TEOS (10  $\mu$ L) resulted in slight changes in zeta potential and led to the observation of raspberry-like structured surfaces. This points to formation of a silica shell (Figure 18, panel C). After addition of higher amounts of TEOS (40  $\mu$ L), the zeta potential decreased more drastically reaching values of -60 mV. TEM images of these SNPs showed clear raspberry-like surface structures (Figure 18, panel D). The TEOS-induced changes in zeta potential and surface morphology suggest that the fluorescent SNPs are still chemically reactive despite dye labelling, most likely due to the existence of free amino groups. Such remaining amino groups can readily act as *in situ* catalysts for silica hydrolysis followed by condensation and formation of a silica network on the SNP surface as proposed by other groups<sup>[175, 182, 183]</sup>. The active sites may be located in the interstitial space between the dye-labelled functional groups, catalysing the formation of a non-uniform silica shell with a raspberry-type structure. The increased, i.e., more negative zeta potential resulting after TEOS addition could be caused by the enlarged surface area of the raspberry-type structures. A dependence of zeta potential on particle size has been previously reported by other groups<sup>[184, 185]</sup>. Precise determination of the shell thickness formed after TEOS addition was not straight forward. Although DLS results showed an increase in particle size for core-shell NPs with respect to the pristine starting material, the sizes of particles obtained from intensity-averaged DLS data can be strongly affected by sample polydispersity and possibly also by dye fluorescence leading to an overestimation of particle size with respect to sizes determined by TEM<sup>[186]</sup>. Moreover, due to the identical chemical composition of core and shell, a direct estimation of shell thickness by differences in TEM contrast as done for instance for gold@silica hybrids<sup>[172]</sup>, was not possible. Nevertheless, a comparison of TEM mean sizes between the starting material and core@shell samples revealed differences in the order of 5 nm. Despite the uncertainty associated to the comparison of the statistical distribution of sizes for nanoparticles with smooth and rough surfaces<sup>[187]</sup>, this provides a strong hint for the formation of very thin shells after TEOS addition. The shelled dye-labelled nanoparticles were stable in water suspension for at least two months without agglomeration which is a prerequisite for their future application as fluorescent labels.

Table 2: Physico-chemical characterisation of the nanoparticles prepared.  $D_h$  corresponds to the hydrodynamic diameter as computed from the mean value of the DLS intensity curves. PDI is the polydispersity index as computed by the cumulants method. ZP is the zeta potential in pure water.

Sample	Surface morphology	$D_h$ [nm]	PDI[%]	ZP[mV]
SNPs	Smooth	90	6	-35
SNPs-NH <sub>2</sub>	Smooth	-	-	+2
Core-A647-1	Smooth	-	18	-32
Core-A647-2	Smooth	-	-	-
Core-A750-1	Smooth	-	16	-32
Core-A750-2	Smooth	-	-	-
Core-A647-2@shell-1	Smooth + Raspberry	150	19	-30
Core-A647-2@shell-2	Raspberry	169	16	-55
Core-A750-2@shell-1	Smooth+ Raspberry	138	14	-41
Core-A750-2@shell-2	Raspberry	148	21	-60

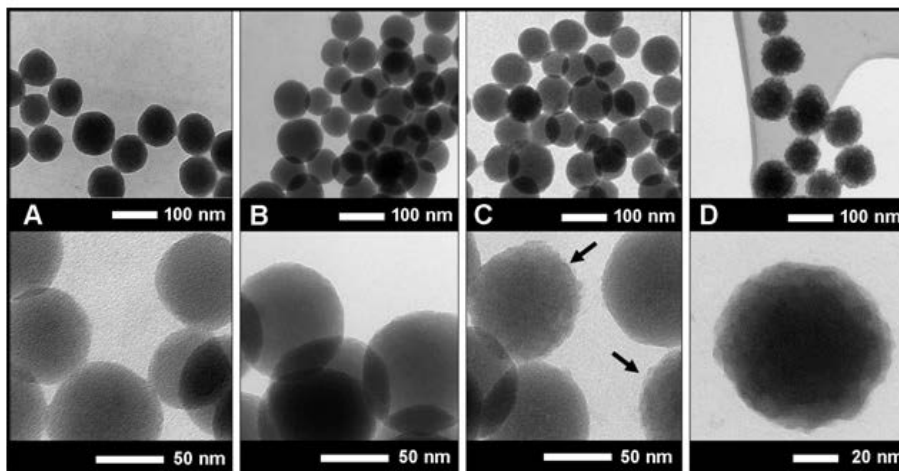


Figure 18: TEM images of the SNPs prepared (Table 1). (A) monodisperse SNPs; (B) labelled silica (core-A647); (C) core-A647@shell-1 and (D) core-A647@shell-2.

#### 4.3.2 Spectroscopic characterisation

The fluorescence emission spectra (Figure 19, left) of the Alexa dyes did not change upon coupling to the surface-grafted SNPs. For the lowest concentration of applied dye, the fluorescence quantum yields of the silica-bound dyes matched the quantum yields of the free dyes that were determined to 0.33 and 0.12 for Alexa 647 and Alexa 750 in water. The fluorescence quantum yields of the dyes were in excellent agreement with the data provided by the manufacturer (Alexa 647:  $\Phi_f = 0.33$  and Alexa 750:  $\Phi_f = 0.12$ , homepage from Invitrogen). Use of a higher dye concentration, however, led to a bathochromic shift of the emission spectra due to re-absorption and a decrease in absolute fluorescence quantum yield of the bound dyes (Table 3). This is ascribed to fluorescence quenching dye-dye interactions [178, 188, 189], the size of which depends on the distance between the attached fluorophores and thus, on dye labelling density. The formation of non-fluorescent aggregates on the SNP surface is indicated by changes in the absorption spectra of the highly labelled SNPs (Figure 19), right, increase in the shorter wavelength peak of the dye's main absorption band). Accordingly, a high amount of coupled dye must not necessarily result in enhanced particle fluorescence intensity. Although constant coupling efficiencies of  $> 80\%$  were found for the dyes studied, the resulting fluorescence intensity increased by factors of 5 (Alexa 647) and

7.5 (Alexa 750), respectively, when increasing the amount of applied dye by a factor of 10. The actual fluorescence intensity of the highly labeled SNPs is most likely lower than stated here as the molar absorption coefficients of the dyes in water provided by the manufacturer was used for the calculation of the fluorescence intensity and not the actual molar absorption coefficients of the SNP-bound monomeric and dimeric dyes that are expected to be lower. These results also suggest that most likely particle fluorescence intensity needs to be optimised for each dye, thereby considering SNP-binding and labelling density-induced changes in its spectroscopic properties.

After formation of a thin silica shell, the fluorescence quantum yields of the particle-bound dyes increased, reaching values resembling the fluorescence quantum yields of the free dye. Whether this can be ascribed to dye rigidisation, which decreases the number of non-radiative deactivation pathways in the case of fluorophores with non-bridged “rotatable” double bonds that can undergo cis-trans isomerisation, or to a reduction of the amount of non-emissive dye aggregates remains to be elucidated <sup>[190]</sup>. Although a hint for dye decomposition during shell formation was not found, this cannot be fully excluded. However, the considerable change in fluorescence quantum yield would imply a high degree of dye degradation which seems not to be very plausible. The high amount of coupled fluorophores per SNP even in the case of SNPs revealing diminished fluorescence quantum yields compared to the free fluorophore reflects the advantages of particle labels with fluorescence intensity values strongly exceeding those of molecular chromophores.

Table 3: Spectroscopic data of free and SNP-coupled Alexa dyes

Sample	Amount of SNP-coupled dye [mmol per mg SNP x 10 <sup>-5</sup> ]	Labeling density (dye molecules per nm <sup>2</sup> )	Molecules per particle	Absolute QY	Fluorescence intensity per particle/ molecule [L×(mol×cm) <sup>-1</sup> ]
A647	-	-	-	0.330	7.9 x 10 <sup>4</sup>
A750	-	-	-	0.123	3.0 x 10 <sup>4</sup>
Core-A647-1	0.57	0.082	1659	0.300	1.2 x 10 <sup>8</sup>
Core-A647-2	5.8	0.838	16841	0.155	6.3 x 10 <sup>8</sup>
Core-A647-2@shell-1	-	-	16841	0.306	1.2 x 10 <sup>9</sup>
Core-A750-1	0.66	0.095	1907	0.090	4.1 x 10 <sup>7</sup>
Core-A750-2	6.6	0.955	19200	0.067	3.1 x 10 <sup>8</sup>
Core-A750-2@shell-1	-	-	19200	0.123	5.7 x 10 <sup>8</sup>

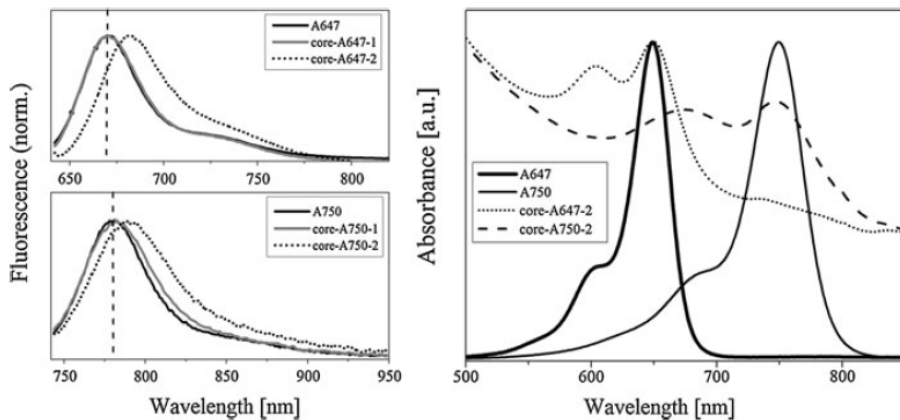


Figure 19: Left: Normalised fluorescence spectra of free and SNP-coupled Alexa dyes 647 (top) and 750 (bottom). Right: Absorption spectra of the free dyes and the SNP-bound Alexa fluorophores (coupling of  $2 \times 10^{-3}$  mol/L Alexa dyes). The red shift in emission resulting for both fluorophores for increased dye labeling densities (see emission spectra of core-A647-2 and core-A750-2) are ascribed to reabsorption effects. The sample description is given in Table 3.

#### 4.4 Conclusions

A facile synthetic route for the preparation of NIR-emissive core-shell particles was developed, yielding colloidally stable, nanometer-sized, bright silica particles. The main advantage of this synthetic route is that fluorescent reporters can be protected from the surrounding medium by formation of a size-tunable silica shell. Moreover, this strategy can be possibly used to produce highly fluorescent SNP of practically any size which can be further functionalised with, e.g., biomolecules or other ligands <sup>[191-193]</sup>. The results of the spectroscopic studies show that coupling of the Alexa dyes 647 and 750 to silica particles does not affect the spectral position of the emission maxima and the size of the fluorescence quantum yields of these fluorophores at low labelling densities. Moreover, the covalently bound charged dyes enhance the colloidal stability of the silica particles in comparison to their aminated precursors by decreasing the negative zeta potential of the initially formed aminated silica particles. Interestingly, fluorescence quenching observed at higher dye labelling densities can be partly overcome by subsequent formation of a thin silica shell, which is indicated by an increase of the quantum yields afterwards <sup>[194]</sup>. The formation of this silica shell also changes the morphology of the particles, depending on the concentration of the silica precursors used. This renders further optimisation of all parameters affecting shell formation mandatory including shell thickness. Although an increase of the dye fluorescence quantum yield compared to the free dyes was not found as reported for silica particles with encapsulated dyes, the high number of silica-bound dye molecules per particle renders these materials interesting for future applications as fluorescent reporters due to their high brightness exceeding that of a typical dye molecule by a factor of several thousand.

# Chapter 5

## Tuning interfacial properties and colloidal behavior of hybrid nanoparticles by controlling the polymer precursor

---

*\*This chapter has been accepted for publication in *Macromolecular Chemistry and Physics* 213 (2012) 2412–2419*

**Kishore Natte**, Werner Österle, Jörg F. Friedrich, Regine von Klitzing and Guillermo Orts-Gil.

### 5.1 Introduction

This chapter introduces a novel chemical strategy to produce two different types of spherical, organic-inorganic hybrid SNPs with a facile and versatile synthetic route.

As discussed earlier (in Chapter 1), the question how to control the protein adsorption onto nanoparticles has been mainly addressed to the modification with polymers <sup>[7, 18-20]</sup>. In this regard, two different methods can be mainly indentified in order to produce silica-polymer hybrid nanoparticles with suppressed non-specific protein adsorption: post-synthesis (grafting) and direct synthesis (co-condensation or copolymerizing the alkoxy-silanes with silica precursors). While grafting of polyethylenglycol (PEG) has been used since the 1980s in order to improve the biocompatibility of different substrates <sup>[195, 196]</sup>, condensation process enables a higher and more homogenous surface coverage of functional groups but has been much less studied <sup>[197-200]</sup>.

Although several publications are available concerning the synthesis of silica-PEG hybrid nanoparticles by using polymers and other reagents <sup>[201, 202]</sup>, to our knowledge, up to date, none of them addresses the tuning of nanoparticles size and charge by using a polymer precursor. In order to overcome the challenges linked to the synthesis of silica-PEG hybrid NPs, a promising alternative synthetic route was developed exploiting condensation and grafting methods. In addition, the influence of silica-PEG hybrid NPs properties on the colloidal stability and BSA adsorption is also well discussed.

To synthesize polymer precursor mPEG-IPTES, poly(ethylene glycol) monomethyl ether (mPEG) was used, which is a simple and representative linear polymer with a molecular weight (MW) of 2000 g/mol. This polymer length was chosen according to the optimal molecular values reported in the literature for the suppression of non-specific protein

adsorption <sup>[203]</sup>. 3-isocyanato propyl (triethoxy silane) (IPTES) was used as a suitable coupling reagent due to high electrophilic nature of the carbon atom in  $-N=C=O$  group, making that isocyanates readily undergo reactivity with a variety of nucleophilic groups such as alcohols, amines and thiols.

Two different types silica-PEG hybrid NPs have been prepared by mPEG-IPTES as a polymer precursor. By grafting the polymer precursor to pristine silica, core-shell nanoparticles (G-SiO<sub>2</sub>@PEG) were obtained, while direct condensation of the polymer precursor with TEOS lead to bulk hybrid nanoparticles (H-SiO<sub>2</sub>-PEG). For polymer-grafted NPs, the density of polymer chains on the surface is strongly affected by the concentration of precursor. Nevertheless, for condensed NPs, the precursor concentration determines the particle size but not the density of polymer chains on the surface or the adsorption of bovine serum albumin (BSA).

Results presented in this chapter are relevant since the size and charge of nanoparticles may govern a wide spectrum of biological processes like cell internalization, radical oxidative species (ROS) production, protein adsorption, biopersistence, cell adhesion, toxicity and diffusion <sup>[204-206]</sup>.

## **5.2 Preparation of materials**

Refer section 4.2.1 for preparation of SNPs.

### **5.2.1 Synthesis of mPEG-IPTES precursor**

The mPEG-IPTES precursor was synthesized by a simple one-step reaction between mPEG and IPTES addition in presence of DBDU catalyst. mPEG polymer of average molecular weight (MW 2000 g/mol) was dissolved in THF. To this solution an excess of IPTES and DBDU were added at room temperature. The reaction solution was stirred for 24 h at r.t. under nitrogen conditions. After the reaction was completed, THF was evaporated by rotary evaporator and isolated by column chromatography on 60-120 silica gel (MeOH: CHCl<sub>3</sub>=1:9). Yield: 55% (see <sup>1</sup>HNMR data in Appendix A.5.1).



### 5.2.2 Synthesis of condensated silica-PEG hybrids (H-SiO<sub>2</sub>-PEG)

Hybrid silica-PEG nanoparticles were prepared by mixing TEOS, ethanol and ammonia hydroxide in a necked flask and stirring for 30 min. mPEG-IPTES was then added dropwise to the mixture under the protection of argon. The reaction mixture was stirred under argon atmosphere at ambient temperature for 24 h. In order to investigate the effect of the concentration of mPEG-IPTES on the final silica nanoparticles, mPEG-IPTES was added at different concentrations (Table 2). After the completion of the reaction, the particles were purified by dialysis to remove unreacted reactants and other byproducts. Dialysis was carried for 3 days with changing of Milli-Q water twice per day. Eventually the samples were filtered with 0.200  $\mu\text{m}$  filters and the dispersions were stored at 20 °C.

Table 4: Prepared nanoparticles suspensions. H-SiO<sub>2</sub>-PEG-X refers to bulk hybrid NPs and G-SiO<sub>2</sub>@PEG-X to grafted NPs, where X denotes the % (mole) of used precursor.

Sample	TEOS [mL]	Silica [g]	mPEG-IPTES [g]	NH <sub>4</sub> OH [mL]	Ethanol [mL]
H-SiO <sub>2</sub> -PEG-0	0.5	-	0	0.83	12.5
H-SiO <sub>2</sub> -PEG-5	0.5	-	0.265	0.83	12.5
H-SiO <sub>2</sub> -PEG-10	0.5	-	0.533	0.83	12.5
H-SiO <sub>2</sub> -PEG-15	0.5	-	0.805	0.83	12.5
H-SiO <sub>2</sub> -PEG-20	0.5	-	1.0	0.83	12.5
G-SiO <sub>2</sub> @PEG-5	-	0.5	0.265	-	13
G-SiO <sub>2</sub> @PEG-10	-	0.5	0.533	-	13
G-SiO <sub>2</sub> @PEG-10	-	0.5	0.805	-	13
G-SiO <sub>2</sub> @PEG-20	-	0.5	1.0	-	13

### 5.2.3 Synthesis of silica-PEG grafted NPs (G-SiO<sub>2</sub>@PEG)

Silica-PEG grafted NPs were prepared by dispersing pristine silica nanoparticles in ethanol by sonication for 20 min at room temperature (see Table 2). The suspension was then magnetically stirred under nitrogen atmosphere and catalytic amount (0.5 ml) of acetic acid was added. After the solution was heated up to 50°C and mPEG-IPTES was added drop by drop and reacted with silica nanoparticles for 48 h. The final compound was purified to

remove unreacted reactants and other by-products by dialysis, filtered and stored as in above mentioned procedure.

#### **5.2.4 BSA adsorption onto nanoparticles**

Here, an assay was designed based on the procedure reported by Roach et al. [123] Mixtures of NPs and BSA were prepared by dilution ( $>1/10$ ) of NPs into buffered solutions (PBS) containing BSA (6 wt%) and were placed at 25°C. Final concentration of SNPs was in all cases around 0.03 wt% Mixtures of nanoparticles and BSA in PBS were centrifuged (Heraeus\* Primo R centrifuge) at 14000 rpm for 90 min at r.t. and the obtained residue was redispersed in the equivalent volume of PBS solution.

### **5.3 Results and Discussion**

#### ***5.3.1 Morphology of prepared nanoparticles and degree of functionalization***

Figure 20 illustrates the chemical strategy of hybrid nanoparticles by co-condensation and grafting. Figure 21 displays TEM images of pristine, grafted and condensated hybrid silica nanoparticles. Although pristine silica shows smooth surfaces, grafted silica nanoparticles show less contrasted outer concentric rings which can be attributed to the PEG attached to the silica surface as also observed by Joubert et al. [207]. EDS elemental line scanning for carbon further corroborates that the resulting mPEG-IPTES grafted silica particles have core-shell morphologies with PEG on the surface and SiO<sub>2</sub> on the core. Oppositely condensated hybrid NPs show slightly rough surfaces and no electron contrast variation in good agreement with a bulk hybrid silica-PEG composition. Moreover, EDS line scanning for carbon indicates the homogeneous distribution of carbon in the nanoparticles. An increase in carbon content measured by XPS confirmed the incorporation of PEG into grafted nanoparticles (4% for pristine silica, 28% and 48% for G-SiO<sub>2</sub>@PEG-5 and 20 respectively) and condensated nanoparticles (21 % and 41 % for H-SiO<sub>2</sub>-PEG-5 and 20 respectively). Thus, both XPS and TGA show similar carbon contents for equivalent grafted and condensated NPs. Nevertheless, while, the carbon content for grafted NPs is mainly attributed to polymer attached to the surface of silica NPs, for condensated NPs, carbon is assumed to be distributed in the bulk of the nanoparticles. Therefore, similar total carbon contents suggest

that grafted nanoparticles possess a larger number of polymeric chains on the surface than condensed ones.

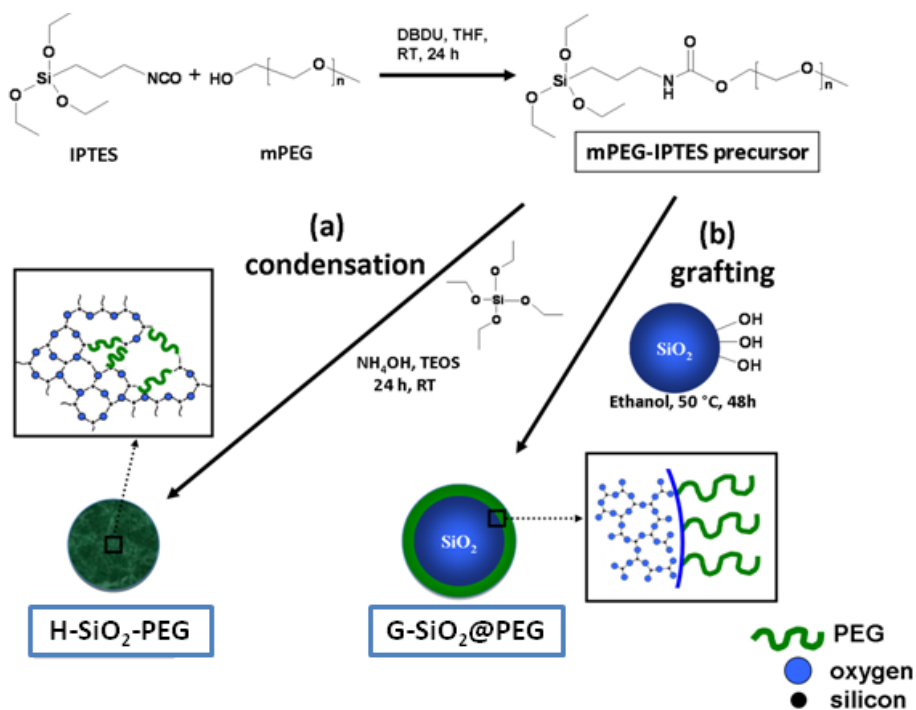


Figure 20: Synthesis of mPEG-IPTES precursor and subsequent use for obtaining hybrid nanoparticles by co-condensation (a) and by grafting (b).

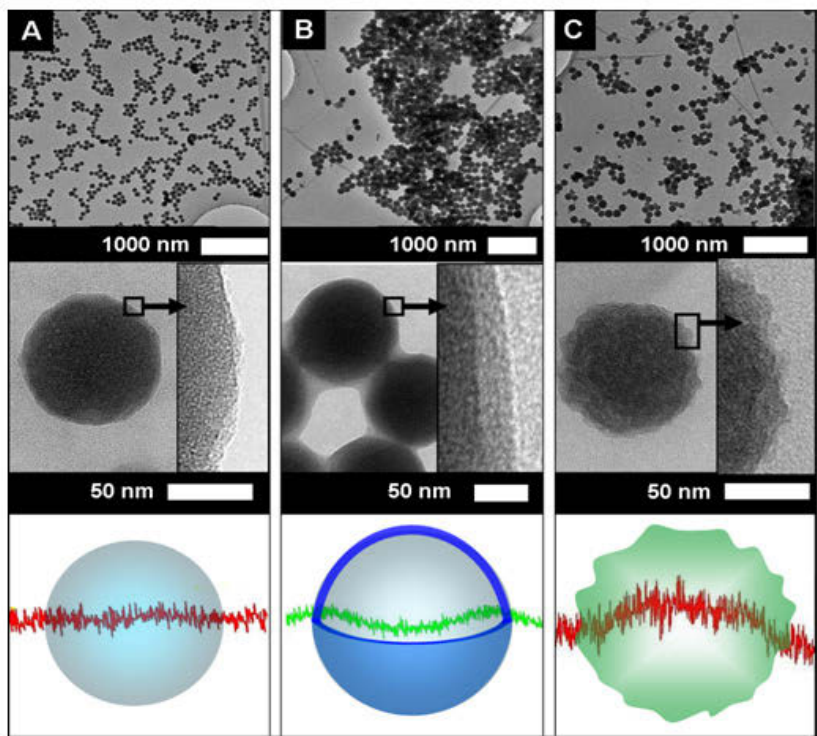


Figure 21: TEM Pictures of pristine silica (A), G-SiO<sub>2</sub>@PEG (B) and H-SiO<sub>2</sub>-PEG nanoparticles (C). In the inset the nanoparticles surfaces are shown at high magnification. In the bottom images the EDX-line scanings for carbon are shown, corroborating the bulk and core-shell structures.

The thermal behavior of pristine silica, hybrid and grafted silica particles was evaluated by TGA (Figure 22). For silica nanoparticles prepared in the absence of mPEG-IPTES, the weight loss below 200 °C was around 5%, which can be mainly attributed to the dehydration of Si-OH groups and decomposition of some residues on the surfaces. Nevertheless, for hybrid nanoparticles a second transition due to the thermal decomposition of mPEG-IPTES blocks can be observed between 350 and 450 °C [208]. Weight loss for hybrid (H-SiO<sub>2</sub>-PEG-10) and grafted (G-SiO<sub>2</sub>@PEG-10) are 17.64 and 23.45 wt% respectively. The temperature range of weight loss was 500-700 °C.

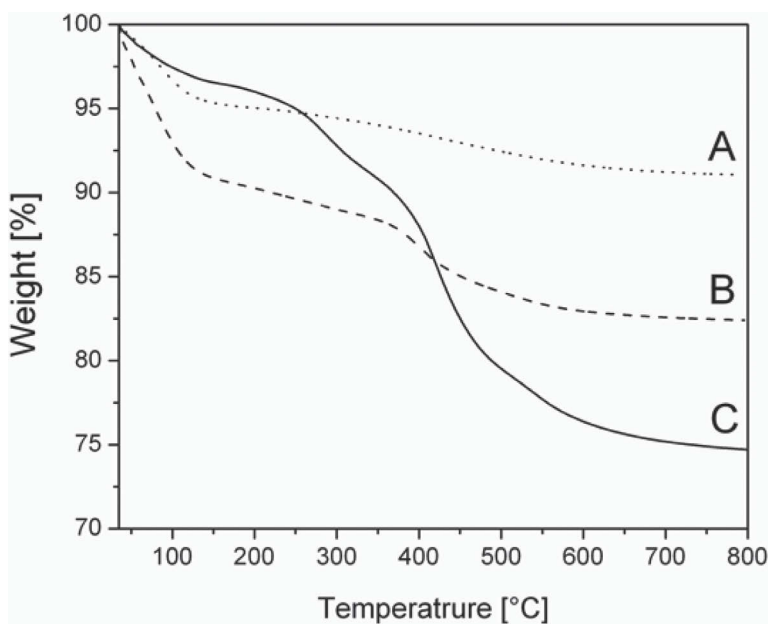


Figure 22: TGA curves of pristine silica (A), H-SiO<sub>2</sub>@PEG (B) and G-SiO<sub>2</sub>@PEG-10 (C).

The chemical structure of pristine silica, grafted and hybrid silica particles were characterized by FTIR spectra as shown in Figure 23. For hybrid (H-SiO<sub>2</sub>-PEG-10) and grafted (G-SiO<sub>2</sub>@PEG-10) silica particles, the characteristic vibration band of carbonyl (-NHCOO-) and amide group (-NHCOO-) appeared at 1700 cm<sup>-1</sup> and 1540 cm<sup>-1</sup> respectively. Moreover, another new band appeared at 2920 cm<sup>-1</sup>, which should be assigned to the asymmetric stretching vibration of an alkyl group (-CH<sub>2</sub>-) of mPEG-IPTES. The peaks at 1380 and 1455 cm<sup>-1</sup> are PEG peaks. All the above peaks, which appeared in grafted and hybrid silica particles, do not exist in pristine silica. This clearly indicates the presence of mPEG in the NPs.

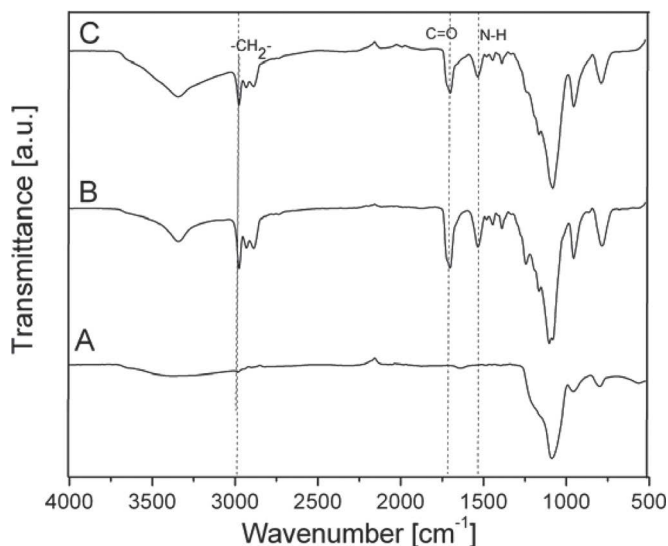


Figure 23: FTIR spectra of pristine silica (A), G-SiO<sub>2</sub>-PEG-10 (B) and H-SiO<sub>2</sub>@PEG-10 (C).

### 5.3.2 Particle size, Colloidal stability and Interfacial properties

#### 5.3.2.1 Condensated hybrid nanoparticles

The concentration of precursor (mPEG-IPTES) was systematically varied in order to evaluate its influence on the size and charge of condensated hybrid nanoparticles. The average size of the silica particles as computed by DLS increases with the concentration of precursor (Figure 24-A). As the concentration of mPEG-IPTES is varied from 0.5 to 1 g, the particle diameter presented significant changes from 120-180 nm, respectively. Particle sizes measured by TEM also corroborated particle growing by increasing the concentration of polymer precursor (Figure 24-B, inset). Nevertheless, mean size values by TEM were significantly lower than those found by DLS. The fact that DLS measures NPs in suspension, with the corresponding solvation sphere, and that TEM is performed in the dry state, with the corresponding NPs shrinking, can partially explain the difference. However, the high polydispersity in sizes computed by DLS (up to 22%) may also play a major role here, since classical DLS is highly affected by larger particles. Therefore, sometimes special set-up like in depolarized dynamic light scattering are used to overcome this problem<sup>[209]</sup>. A possible

explanation for differential NPs growing could be the influence of mPEG-IPTES on the concentration of nuclei particles in the reaction system. When the concentration of mPEG-IPTES increases the rate of hydrolysis and condensation becomes faster<sup>[210]</sup>. After hydrolysis at room temperature the nucleation and formation of silica hybrid particles takes place through ammonium hydroxide. Then, the polycondensation of primary particles results in secondary larger particles. This process continues until all the mPEG-IPTES is consumed or until the reaction system achieves a steady state<sup>[211]</sup>. By using a constant amount of catalyst, the increase in concentration of monomer precursor (mPEG-IPTES) leads to the increase in growth period and longer growth step results in the increase of particle size<sup>[212, 213]</sup>.

ZP measurements on condensed hybrid silica particles were also carried out (Figure 24-A). The ZP of H-SiO<sub>2</sub>-PEG-0 (pure silica) in pure water was around -30 mV, while for H-SiO<sub>2</sub>-PEG-5 and H-SiO<sub>2</sub>-PEG-20 were around -18 mV. These data suggest the existence of some PEG on the surface of the hybrid NPs, in good agreement with He et al.<sup>[214]</sup>. Interestingly, for condensed hybrid NPs the ZP does not change significantly with the precursor concentration, suggesting a similar composition of the particle surface irrespective of the particle size, i.e., precursor concentration.

Modified NPs were also incubated with BSA, and the resulting NP-protein complexes were separated from excess BSA by centrifugation and extensive washing to remove the unbound proteins. In Figure 24-C, the ZP values for mixtures of NPs in PBS and in BSA/PBS after centrifugation are shown. When the ZP is measured in PBS (Figure 24-A), the ZP is decreased in comparison to the values in water, following the effect of higher ionic strength<sup>[215]</sup>. The black bars in Figure 24-B represent the ratio (ZP in PBS)/(ZP in BSA/PBS after centrifugation). For pristine silica this ratio clearly exceeds 1, which indicates the formation of a BSA corona on the non-modified silica<sup>[117]</sup>. However, for hybrid nanoparticles this value decreases until values close to 1, which indicates that PEG on the surface of the NPs effectively reduces the adsorption of BSA.

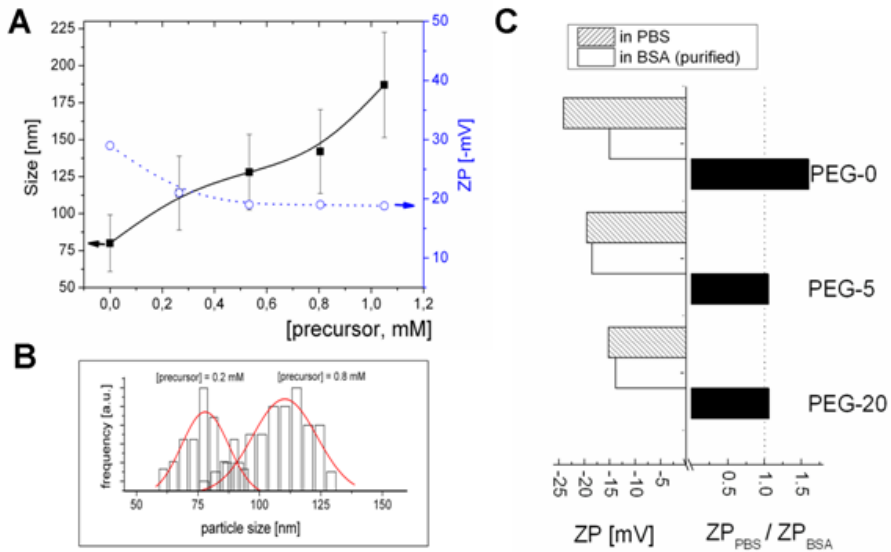


Figure 24: (A) Effect of mPEG-IPTES concentration on the particle size computed by DLS and zeta potential of condensated hybrid nanoparticles in water. (B) Histograms of particles sizes computed by TEM. (C): zeta potential for NPs in PBS and in BSA/PBS. Black bars indicate the ratio  $(ZP \text{ in PBS}) / (ZP \text{ in BSA})$  and shows that hybrid NPs adsorb less BSA than pristine silica.



### 5.3.2.2 Grafted hybrid nanoparticles

For grafted NPs, the increase in precursor concentration was not expected to increase the particle size but the density of polymer chains onto the NPs surface. However, DLS also shows a significant increase in size by increasing polymer concentration (Figure 25-A). Nevertheless, sizes for single particles computed from TEM pictures do not exceed more than 10% the sizes for non-grafted (pristine) silica, which can be attributed to the attached polymer shell (Figure 21 B versus Figure 25 B) <sup>[216]</sup>. Therefore, here it is concluded that, in this case, the increase in particle size found by DLS was due to agglomeration effects by increasing polymer density on the surface of the nanoparticles. Yang et al. <sup>[217]</sup> reported agglomeration of PEG micelles depending on concentration and PEG length. TEM pictures at low magnification show more agglomerated NPs than for pristine silica supporting this idea (Figure 21-A versus B). Agglomeration of PEGylated nanoparticles was also confirmed by the increase in polydispersity computed by DLS (shown in Figure 25-A as error bars) and is also consistent with the decrease in ZP by addition of mPEG-IPTES (Figure 25-A). The ZP of G-SiO<sub>2</sub>@PEG-0, G-SiO<sub>2</sub>@PEG-5 and G-SiO<sub>2</sub>@PEG-20 in PBS are -24, -14 and -2 mV respectively. In other words, the concentration of polymeric precursor increases the PEG density and the hydrophobicity of the NPs surface having a major effect on the agglomeration behavior of grafted silica particles (Figure 25-A) <sup>[218]</sup>.

For grafted NPs a very drastic decline in BSA adsorption was also observed even at low polymer concentrations (Figure 25-C). Unfortunately, for samples with higher polymer content (G-SiO<sub>2</sub>@PEG-20) the interpretation of extension of BSA adsorption is not straightforward by this method due to the low initial ZP.

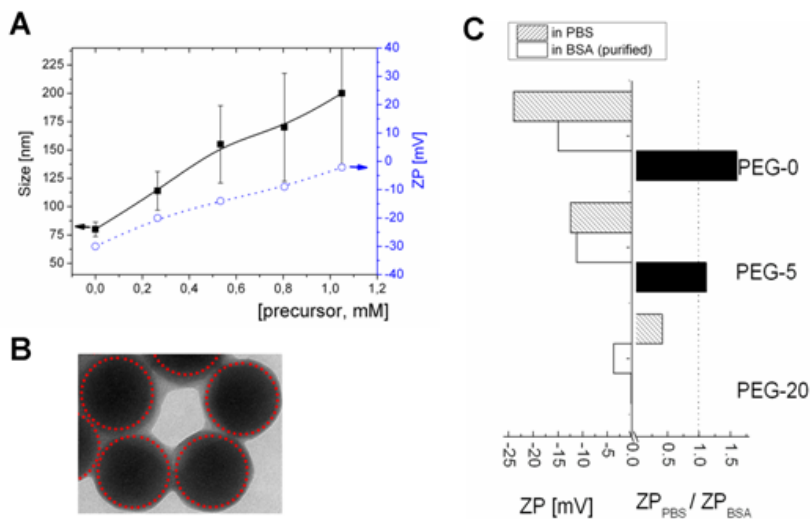


Figure 25: (A) Influence of mPEG-IPTES concentration on the size and zeta potential of and agglomeration of grafted nanoparticles. (B) TEM picture showing grafted nanoparticles with less contrasted shell. Red circles show size of non-grafted nanoparticles. (C) Zeta potential for NPs in PBS and in BSA/PBS. Black bars indicate the ratio  $(ZP \text{ in PBS}) / (ZP \text{ in BSA})$  and shows that hybrid NPs adsorb less BSA than pristine silica

### 5.3.2.3 Discussion of BSA adsorption

Besides environmental conditions like temperature, pH and ionic strength, the main factors affecting the suppression of protein adsorption onto PEGylated silica can be summarised as: (i) polymer length, (ii) polymer density and (iii) NPs specific surface. Factor (i) and (ii) are interrelated<sup>[219]</sup>. Factor (iii) can change with NPs size and agglomeration<sup>[117]</sup>.

In the present study only one polymer length was used. Therefore, it is assumed that the influence of factor polymer length on BSA adsorption was similar for all samples.

Regarding condensed nanoparticles, ZP measurements show no significant differences between all NPs, suggesting a similar density of polymer chains on the surface irrespective of their size. Thus, it was expected that only the NPs size would play a major role leading to different BSA adsorption in the case of condensed NPs. However, no significant differences were found between 75 nm and 110 nm particles (size by TEM). One possible explanation

could be the large size of all prepared condensated NPs when compared with BSA dimensions (prolate ellipsoid with axes 14 x 4 nm). Casals et al. found that protein corona formation onto gold nanoparticles depend on particle size <sup>[117]</sup>. Here, 40 nm Au nanoparticles were less coated with serum than 10 nm Au NPs. However, accommodation-steric effects found by Casals et al. may not play a major role when NPs size largely exceeds protein dimensions.

On the other hand, for grafted NPs the main parameters affecting BSA adsorption were expected to be the grafting density and the specific surface. However, it was experimentally observed that both parameters change simultaneously by increasing precursor concentration. More concretely, grafting density increases while specific surface decreases by agglomeration. Therefore, here it was not straightforward to discriminate between both contributions.

A direct comparison between condensated and grafted NPs in terms of BSA adsorption must be carefully done. For grafted NPs agglomeration takes place, which reduces available surface for BSA adsorption. Moreover, the polymer density may be different for both types of NPs. Thus, grafted hybrid nanoparticles possess higher polymer densities but lower specific surfaces than condensated nanoparticles and a direct comparison is not straightforward. In any case, in the present contribution, for both condensated and grafted NPs the ZP ratios approximate to one for polymer precursor around 5%.

Summarising, the question about which factor mainly determines BSA adsorption was not straightforward as also found by others. For instance, He et al. <sup>[214]</sup> performed systematic studies about HSA adsorption onto mesoporous silica which was PEGylated with different polymer lengths and densities. They concluded that both polymer length and density greatly affect the protein adsorption.

## 5.4 Conclusions

In the present contribution grafting and condensation methods were combined for the first time in order to produce protein resistant silica-polymer hybrids with tunable sizes and surface charges by controlling the polymer silica precursor concentration. It was found that for condensated NPs the precursor concentration determines the particle size but not the density of polymer chains on the surface, i.e. the surface composition. Moreover, condensated nanoparticles adsorb less BSA than pristine silica and show good colloidal stability in water. This aspect is not trivial, since other NPs with PEG functionalities often showed agglomeration <sup>[217]</sup>. On the other hand, although grafted NPs also show suppressed BSA adsorption here, the precursor concentration determines the density of grafted PEG chains at the surface which drastically reduces the surface potential and affects the colloidal stability. Therefore, it can be concluded that grafting strategy could be probably useful only at low grafting densities if well dispersed particles are needed.

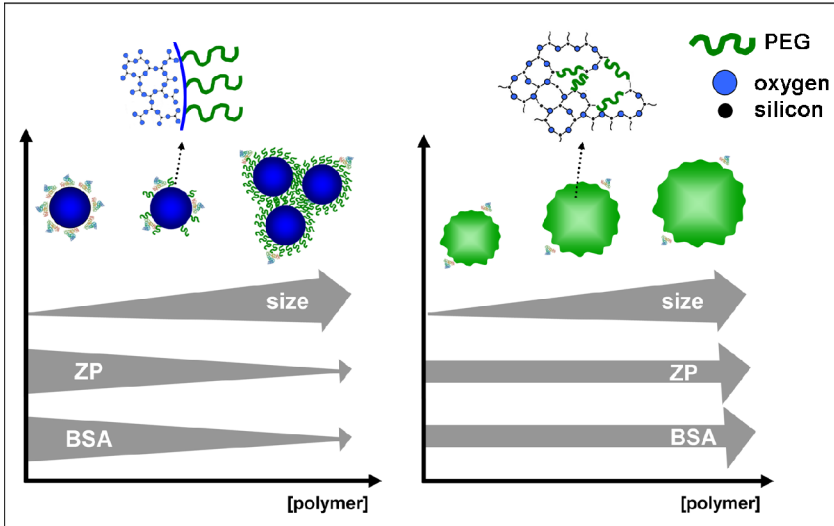
In summary, in the present study both grafting and condensation methods were used to produce silica-PEG hybrids, concluding that condensation may be a more straightforward strategy in order to obtain biopersistent and stable nanoparticles with defined sizes which can be used in biomedical applications like imaging and diagnostics.

This kind of effective approach could be extended to other types of polymers and also organic or inorganic materials for hybrid material synthesis and surface functionalization.

Graphical abstract to chapter 5

Grafted nanoparticles (G-SiO<sub>2</sub>@PEG)

Hybrid nanoparticles (H-SiO<sub>2</sub>-PEG)



## Chapter 6

# Impact of polymer shell on the formation and time evolution of nanoparticle-protein corona

---

*\* This chapter has been accepted for publication in **Colloids and Surfaces B: Biointerfaces**, 104 (2013) 213–220*

**Kishore Natte**, Jörg F. Friedrich, Sebastian Wohlrab, Jana Lutzki, Regine von Klitzing, Werner Österle, Guillermo Orts-Gil.

### 6.1 Introduction

This chapter describes, a systematic study on the adsorption and orientation of BSA onto pristine and PEGylated SNPs, where the emphasis is placed on surface functionalization of SNPs and its related interaction with BSA in physiological media.

Many studies have been performed in the last years in order evaluate the impact of nanoparticles on the environment and human health <sup>[220-222]</sup>. Herein, the importance to elucidate not only the nanoparticles properties but also the basic principles governing nanoparticle-protein interactions has been evidenced <sup>[4]</sup>. More specifically, the formation of NP-protein corona plays a key-role by governing both NPs and protein colloidal stability, stimulating/suppressing immune responses and affecting toxicity<sup>[117]</sup>. Therefore, in the last years many experimental efforts have been done in order to determine the NP-corona composition, shape and properties as well as to model the adsorption phenomena <sup>[112, 223-227]</sup>. The importance of NP-protein corona even led to the postulation of a new classification of nanomaterials depending on the protein corona <sup>[228]</sup>.

Previous studies have shown that the mechanism for protein adsorption onto flat solid surfaces involves different states of adsorbed proteins, i.e., exchangeable perturbed state (P1), the adsorbed protein in the slow exchangeable perturbed state (P2), the exchanged protein (E), and the aggregated proteins <sup>[227]</sup>. The degree and rate of conformational perturbation depend on the specific protein's chemical properties, its stability, and the surface's chemical properties <sup>[228]</sup>. However, little is known about time evolution of adsorbed proteins onto NPs, their orientation, about the strength of the NP-protein interactions and the influence on colloidal stability and biocompatibility <sup>[145]</sup>.

In order to bring more light into the formation and time evolution of protein corona on coated and non-coated NPs, silica is chosen as a fairly spherical monodisperse support and BSA as a model protein. As discussed in chapter 1, surface modification of silica is prerequisite to prevent non-specific protein adsorption and consequent partial agglomeration of SNPs in serum-rich media. In this regard, poly(ethylene glycol) monomethylether (mPEG) is chosen as a polymer, ranging from low to high molecular weights 350, 2000 and 5000 g/mol, corresponding to PEG with 7, 44 and 113 OE (Ethylene oxide) groups <sup>[216]</sup>, from now referred to as PEG-7, PEG-44 and PEG-113 respectively.

Although the mechanisms for protein resisting surfaces have been theoretically and experimentally examined some questions remain unanswered <sup>[126, 127, 229, 230]</sup>. For high molecular weight PEG, the model of steric repulsion gives satisfactory explanation. In this model, the attractive forces between proteins and the surface are balanced by the entropy loss of the conformational constrained PEG chains. Oppositely, only two units of adsorbed ethylene glycol have been also reported to be sufficient to obtain protein adsorption resistants <sup>[130]</sup>. A further method for protein antifouling was reported by plasma functionalisation <sup>[231]</sup>. However, but the mechanisms behind remain unclear. Besides the polymer length, the degree of surface coverage has been postulated as the most important factor for the ability of the polymer layer to prevent protein adsorption <sup>[127]</sup>.

Although the simple mixture of silica and PEG has been previously proposed in order to produce protein resistant NPs, this strategy of physically adsorbed PEG onto silica can be not robust enough if purification and dilution are performed after synthesis <sup>[232]</sup>. Therefore, for the present contribution a novel synthetic route for SNPs@PEG was designed and consistently characterized. Bovine serum albumin (BSA) at different concentrations was used as model protein to study protein corona formation and evolution. For SNPs and SNPs@PEG (MW = 350 g/mol), zeta potential at different incubation times show a dynamical evolution of the nanoparticle-protein corona. Oppositely, for SNPs@PEG with MW  $\geq$  2000 g/mol a significant suppression of corona formation and time evolution was observed. Furthermore, AFM investigations suggest a different orientation (side-chain or perpendicular confirmation) and penetration depth of BSA towards PEGylated surfaces depending on the polymer length which may explain differences in protein corona evolution.

## 6.2 Preparation of materials

Refer section 4.2.1 and 4.2.2 for preparation of SNPs and amino functionalised silica particles (SNPs-NH<sub>2</sub>) respectively.

Also refer Appendix A.6.5 to A.6.5.3 for cleaning of silicon surfaces and their respective surface functionalisation.

### 6.2.1 Tosylation of poly(ethylene glycol) monomethylether (mPEG) (mPEG-OTS)

mPEG-350, 2000 and 5000 (1 g, 0.005 moles) was dissolved in 10 mL of THF/pyridine (1:1) solution. *p*-Toluenesulfonyl chloride (0.426 g, 0.002 moles) and triethylamine (0.077 ml, 0.007 moles) were added and the solution was stirred and heated in an oil bath at 50 °C. Cold water (15 mL) was added and the aqueous phase extracted three times with 20 ml of CH<sub>2</sub>Cl<sub>2</sub>. The combined organic phases were successively washed with 3×20 mL of NH<sub>4</sub>Cl and 3×20 mL of NaCl solution. After drying over Na<sub>2</sub>SO<sub>4</sub> the organic phase was concentrated under reduced pressure and the final resulting product (mPEG-350-OTS, 2000 and 5000) dried under high vacuum. Yield was 700 mg (71 %). (See <sup>1</sup>HNMR data and synthetic route for tosylation in Appendix 6.4).

### 6.2.2 PEGylation of aminated silica particles (SNPs@PEG)

A dispersion of SNPs-NH<sub>2</sub> obtained in methanol (5 ml) was added dropwise to a flask containing 0.1 g of tosylated mPEG-7 (or 44 and 113) in methanol. The mixture was stirred at r.t. for 24 h. For checking the reaction progress with TLC as eluent condition MeOH:CHCl<sub>3</sub> = 1:9 was used. The resulting PEGylated amino silica particles were purified by dialysis (Spectra/Pore cellulose ester (CE) membranes MWCO: 100,000 g/mole) to remove unreacted reactants and other by-products. Dialysis was carried out for 5 days with changing of Milli-Q water thrice per day. Eventually the samples were filtered with 0.200 μm Whatman filters and the dispersions were stored at 20°C. Figure 1 illustrates the various steps involved in the preparation of PEGylated silica particles.



### 6.2.3 Nanoparticles/BSA mixtures and purification

Mixtures of SNPs and BSA were prepared by dilution of nanoparticles into buffered solutions (PBS) containing BSA at different concentrations. Final concentration of SNPs was in all cases 0.02 wt%. To test the efficiency of modified silica against nonspecific proteins adsorption, an *in vitro* assay was designed based on the procedure reported by Roach et al. [123]. Centrifugation has been proposed as an efficient method when performed with adequate control to separate protein incubated nanoparticles from the cell culture media (CCM). In this case, due to high density of silica particles the formation of precipitation takes place in short time. By redispersion of the precipitated SNP in a serum-free media (i.e. PBS) weakly attached nanoparticles may be detached in order to achieve equilibrium conditions [112]. Mixtures of nanoparticles and BSA in PBS were centrifuged (Heraeus\* Primo R centrifuge) at  $12000\text{ min}^{-1}$  for 90 min at r.t. and the obtained residue was dispersed in the equivalent volume of freshly prepared PBS. The free unbound BSA is remained in supernatant. So, only the proteins adsorbed to the surface contribute to the zeta potential after redispersion. Similarly the same procedure was applied before the incubation experiment.

## 6.3 Results and discussion

### 6.3.1 Particles characterization

Table 5, shows the particle sizes, zeta potential and XPS composition of the prepared pristine SNPs and SNPs@PEG hybrid NPs. Nearly monodisperse and spherical pristine SNPs were accounted by DLS (PDI 6%). The electrophoretic mobility studies showed that SNPs are negatively charged (-35 mV) at neutral pH in distilled water, due to deprotonation of surface Si-OH groups. When the ZP was measured in PBS the value decreased to -22 mV, following the effect of higher ionic strength <sup>[9]</sup>.

The surface modifications (Figure 26) of SNPs (amination and PEGylation) could be monitored by successive changes in the zeta potential, going from -35 mV to +2 mV and to -23 mV, respectively. The highly positive surface charge of aminated silica nanoparticles (SNPs-NH<sub>2</sub>) is due to the basicity of primary amino groups. Unfortunately, it was found that SNPs-NH<sub>2</sub> strongly aggregate after short time in water in good agreement with those reported elsewhere <sup>[233]</sup>. Aggregation of aminated silica nanoparticles partially could be avoided by dispersing them (SNPs-NH<sub>2</sub>) in methanol and performing PEGylation in the same solvent. After PEGylation (SNPs@PEG) the NPs show better colloidal stability. Nevertheless, a slight agglomeration was also found for the final SNPs@PEG particles as proved by DLS. This may partially arise from the previously aminated (SNPs-NH<sub>2</sub>) compounds but also from high density of polymer chains on the NPs surface <sup>[234]</sup>. FTIR, UV and solid state NMR analysis of the samples further confirms the success of amination and PEGylation (not shown here). Investigation of chemical composition of the nanoparticle surfaces was carried out by XPS (results in table 2, discussion in Appendix 6). Grafting densities were calculated from XPS results by using silica density (2.0 g/cm<sup>3</sup>) and TEM size according to Zhang et al. <sup>[235]</sup>, being 1.9, 2.4 and 3.6 mg/m<sup>2</sup> for PEG-7, PEG-44 and PEG-113, respectively. Although grafting densities expressed as mass/surface increase with PEG length, in fact grafting densities decrease in terms of number of chains/surface approximately by a factor of ten going from PEG-7 to PEG-113. This may arise from steric hindrance and exclude volumes for large polymer lengths <sup>[236]</sup>. The thermal behavior of SNPs@PEG was evaluated by TGA (see Appendix 6). TGA shows that the carbon content was similar for all samples, in good agreement with XPS.

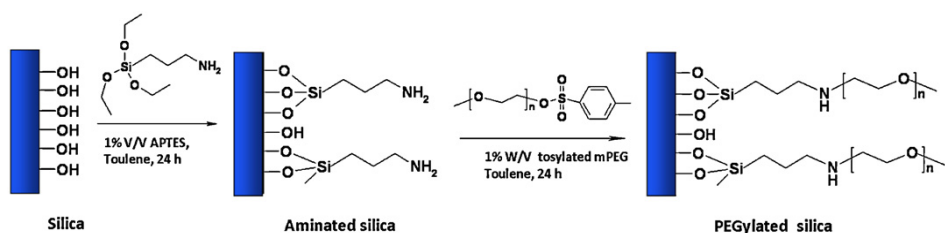


Figure 26: schematic pathway for the synthesis of SNPs@PEG nanoparticles

Table 5: Synthesized silica nanoparticles and properties. <sup>a</sup>D<sub>TEM</sub> is the mean particle diameter computed from TEM; <sup>b</sup>D<sub>DLS</sub> corresponds to the hydrodynamic diameter; <sup>c</sup>PDI in water (from DLS, cumulants analysis); <sup>d</sup>ZP<sub>water</sub> stands for zeta potential in water after dialysis. <sup>e</sup>ZP<sub>PBS</sub> stands for zeta potential in phosphate buffered solution.

Sample	D <sub>TEM</sub> <sup>a</sup>	D <sub>DLS</sub> <sup>b</sup>	PDI <sup>c</sup>	ZP <sub>water</sub> <sup>d</sup>	ZP <sub>PBS</sub> <sup>e</sup>	conc.		XPS Composition			
	[nm]	[nm]	[%]	[mV]	[mV]	[%wt]		[%]			
								Cl1s	N1s	Si2p	O1s
SNPs	80	112	6	-35	-22	1	3	-	37	60	
SNP-NH <sub>2</sub>	-	-	-	2	-	1	18	5	35	62	
SNPs@PEG-7	-	270	24	-25	-17	0.2	25	4	27	44	
SNPs@PEG-44	88	193	16	-24	-18	0.2	28	3	26	44	
SNPs@PEG-113	-	200	17	-22	-19	0.2	31	3	35	51	

Figure 27 displays TEM images of SNPs and SNPs@PEG. While pristine SNPs shows smooth surface, SNPs@PEG shown a outer shell with lower contrast, due to the addition of tosylated mPEG onto the aminated particles which was also observed by Joubert et al.<sup>[207]</sup>. Sizes of the particles as computed by TEM increased to around 8 nm (Table 5) respect to pristine SNPs, further indicating that the particles are modified with polymers. Nevertheless, mean size values by TEM were significantly lower than those found by DLS. The fact that DLS measures NPs in suspension, with the corresponding solvation sphere, and that TEM is performed in the dry state, with the corresponding NPs shrinking, can partially explain the difference. However, the high polydispersity in sizes computed by DLS (up to 24%) may also

play a major role here, since classical DLS is highly affected by larger particles. Therefore, sometimes special set-up like in depolarized dynamic light scattering are used to overcome this problem <sup>[209]</sup>.

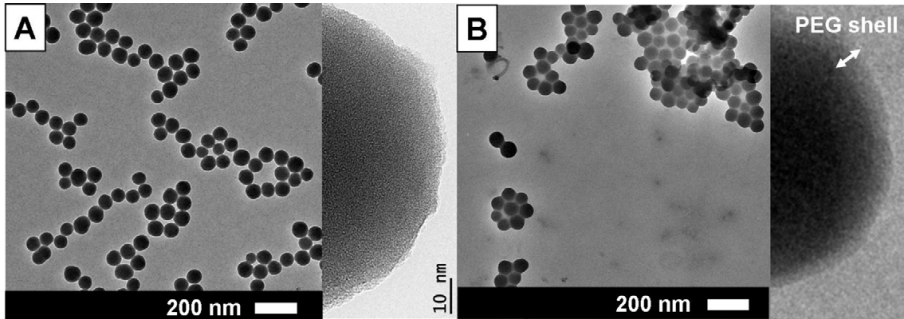


Figure 27: TEM Pictures of pristine SNPs (A) SNPs@PEG-44 (B).

### 6.3.2 Protein corona formation onto pristine SNPs and SNPs@PEG nanoparticles

The surface of amorphous silica presents several different Si-O- chemical groups which are commonly categorized in terms of silanol (hydrophilic) and siloxane (hydrophobic) groups <sup>[237]</sup>. At room temperature and nearly neutral pH conditions dehydroxylated silanol groups predominate on the surface conferring silica a hydrophilic behavior as shown by negatively zeta potential values <sup>[9]</sup>. On the other hand, the surface of BSA is both 345 positively and negatively charged but also possesses non-polar regions <sup>[238]</sup>. Therefore, the SNPs are expected to show a non specific-binding to BSA by ion-ion interactions and hydrogen bonding interactions <sup>[239]</sup>.

The interaction of BSA with a range of metal and metal oxide NPs has been previously assessed by means of zeta potential measurements <sup>[240, 241]</sup>. The amount of adsorbed BSA on pristine SNPs was found to be correlated with the ZP. On the other hand, the adsorbed proteins change the zeta potential and the isoelectric point (IEP) of the oxide particles. Lundqvist et al. <sup>[228]</sup> reported the reversible adsorption of human carbonic anhydrase I (HCA) onto SNPs, where the interaction degree depends on the curvature of the particles. However, little is known about the time evolution or the influence of polymer coating.

Thus, the adsorption of BSA onto pristine SNPs and SNPs@PEG was also studied by means of zeta potential (ZP) measurements. BSA concentration was varied from 0.1 to 6 wt% which represents a large excess of BSA respect to number of nanoparticles ( $\sim 10^4$  to  $\sim 10^6$ ).

Figure 28-A shows zeta potential values for mixtures of pristine silica and different concentrations of BSA in PBS before and after purification and at different incubation times. At lowest BSA concentrations almost undetectable changes in the zeta potential ZP(-21 mV) were found but for concentrated protein mixtures the ZP decreased down to -8 mV, close to ZP values for pure BSA in PBS.

Nevertheless, due to the excess of BSA molecules ZP value would correspond not only to the NP-BSA values but also to the excess of non-bounded BSA. Therefore, more significant are the ZP values after centrifugation. Here, significant differences are found, since loosely bound BSA molecules can be detached during the centrifugation process and excess of protein can be removed (Figure 28-A).

From now, the evolution of the ZP will be analyzed in terms of the ratio (ZP in BSA/ZP in purified PBS), shorted as  $\Delta ZP$ . In other words,  $\Delta ZP$  quantifies the decrease in ZP after protein adsorption (only strongly bound BSA), being 1 for non-detectable BSA corona. The plots of  $\Delta ZP$  for pristine silica-BSA mixtures depending on BSA concentration and incubation time are shown in Figure 29. Both parameters increase with increasing the incubation time and BSA concentrations. Thus, by increasing incubation times larger amounts of proteins are adsorbed on the particles. However, a major part of them have to be weakly attached since most of the BSA can be detached after centrifugation. This indicates a dynamical process on the formation of the corona. A possible explanation could be that a hard (non-reversible) corona is formed after some time and once built only allows the further formation of a loosely attached soft corona as found for gold nanoparticles by Casals et al.<sup>[242]</sup> and for polystyrene nanoparticles by Milani et al.<sup>[243]</sup>

The formation of BSA monolayers onto pristine SNPs has been postulated before<sup>[244]</sup>. However, the progressive decline of the zeta potential values by increasing BSA concentration and incubation times indicate that the BSA corona formation is a dynamic process probably involving more than simply monolayer silica coverage. TEM measurements on SNPs/BSA mixtures at low BSA concentrations (0.1 wt%) seem to confirm this. In Figure 28-B silica nanoparticles with a bright ring are shown. If the lower contrast ring is assumed to belong to adsorbed BSA, a protein corona thickness between 10-15 nm can be derived. TEM pictures of BSA concentrated solutions even show thicker low contrasted rings (not shown here).

Su et al. used neutron reflectivity to study the silica-BSA systems and formulated a model of monolayer of sideways-on BSA molecules onto silica with a maximum thickness of 4 nm. Despite the assumed large error in the estimation of the BSA corona thicknesses, the values

found here clearly exceeded the theoretical value of 4 nm for a BSA monolayer onto silica [245].

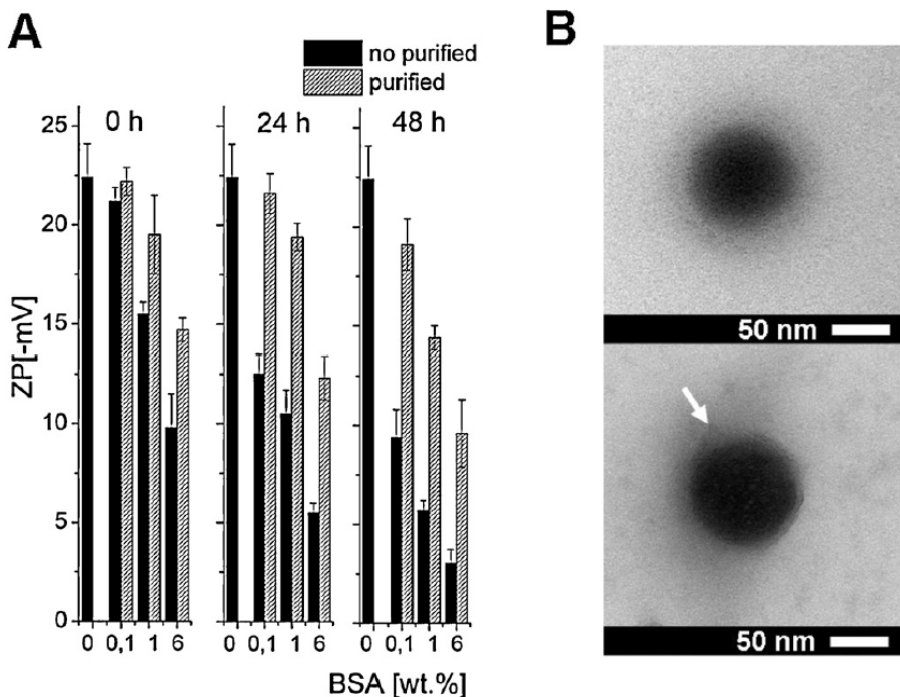


Figure 28: (A) Zeta Potential (ZP) of SNPs/BSA mixtures before and after purification at different incubation times. Error bars represent the standard deviation between 9 independent measurements. (B) TEM pictures of SNPs in a diluted BSA/PBS solution. The formation of BSA corona onto silica can be observed (top picture), while no uniform corona can be observed on SNPs@PEG (MW 2000 g/mol) (bottom picture).

Analogously to pristine SNPs, ZP experiments were also conducted for the SNPs@PEG hybrids in the presence of BSA. Here, the total amount of adsorbed protein depends again on incubation time and BSA concentration but the particular behaviour strongly depends on the PEG polymer length (Figure 29). For short chain polymers (PEG-7) a clear decrease ZP is observed by increasing both incubation times and protein concentrations. Nevertheless,  $\Delta ZP$  values are still higher than for pristine silica, indicating that even short PEG chains can reduce the adsorption of BSA. Interestingly, for PEG-7 the  $\Delta ZP$  changes with the BSA

concentration and incubation time in the same way as for bare silica. For larger polymer lengths  $\Delta ZP$  slightly decreases with BSA concentration but does not vary drastically with incubation times. This suggests that large PEG chains inhibit short and long term formation of BSA corona. TEM picture of SNPs@PEG (MW 2000 g/mol) in a diluted solution of BSA/PBS does not show uniform low contrast rings on the surface of the nanoparticles but some bright dots which may correspond to BSA (arrow in Figure 28-B).

In resume, short PEG-7 chains reduce the total amount of adsorbed protein compared to pristine silica but still show a time evolution. On the other hand, larger PEG reduces the amount of adsorbed BSA more efficiently but interestingly, no significant differences were found between PEG-44 and PEG-113. The differences in ZP evolution found for NPs coated with short and large PEG may be explained by different mechanisms leading to the formation of the protein corona, as we show in the next section.

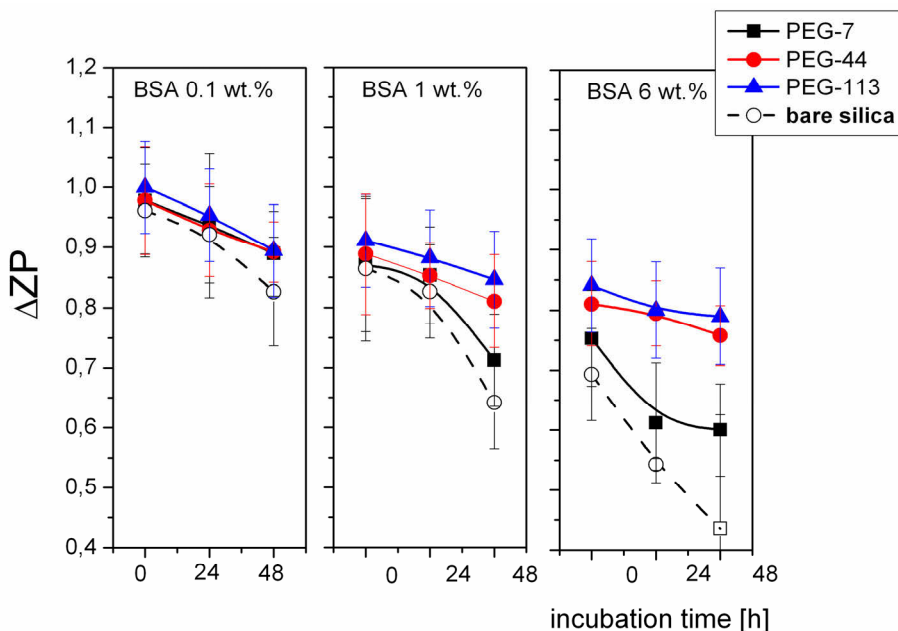


Figure 29: Decrease in ZP ( $\Delta ZP$  in mV) for prepared nanoparticles in the presence of BSA expressed as:  $\Delta ZP = (ZP \text{ in BSA} / ZP \text{ in PBS})$ . Black empty circles correspond to pristine SNPs without polymer coating. Error bars represent the SD associated with the division of ZP values calculated with the general equation of error propagation.

### 6.3.3 AFM study of BSA/polymer surfaces

In order to evaluate the morphological changes on the silicon wafer after successive functionalization (oxidation, amination and PEGylation), a step by step morphological analysis after every surface treatment was performed by AFM (Figure 30-A). Table 6 show RMS (root mean square) values for all prepared surfaces before and after BSA exposure. Since the silicon wafers were previously chemically treated, their surface was expected to consist of amorphous silica <sup>[246]</sup>. This was confirmed by TEM observations of a thin lamella prepared by FIB (see Appendix 6). The RMS of oxidized silicon surface (Si-OH) in dry state is 0.29 nm, in good agreement with the values reported elsewhere <sup>[247]</sup>. The RMS increased to 0.41 nm after silanization process in good agreement with Zengin et al. <sup>[248]</sup>. On the other hand, RMS values for polymer wafers of PEG-7, 44 and 113 were 0.33, 0.34 and 0.73 nm respectively. The increase in surface roughness with increase in molecular weight of polymers is in consistence with Yang et al <sup>[249]</sup>. Nevertheless, RMS values are always below 1 nm. These values are clearly lower than those values for fully extended chains, being 2.32, 16.13 and 41.2 nm for PEG-7, PEG-44 and PEG-113 respectively, as calculated using the length of the monomer OE units of 0.365 nm <sup>[250]</sup>. These values are also lower than those for PEG chains in the wet state as also computed by AFM from McNamee et al. <sup>[216]</sup> (Table 6). However, it is very important to mention here that while surface exposure to BSA was performed in the wet state, all the AFM analysis of each and individual sample were performed in dry state and these values may change after surface wetting due to hydration of functional moieties.

More interestingly, BSA adsorption onto silica significantly increases the RMS up to 1.07 nm. The adsorption of BSA onto silica has been previously described by Rezwan et al <sup>[244]</sup>. This shows that BSA preferently adopts a side-chain conformation onto silica. If a monolayer of BSA coating the silica surface is assumed, the RMS should approach to the thickness of BSA molecule. Short axis of BSA molecule is 4 nm, so a value of 1.07 nm could be consistent with the thickness of BSA molecules in a flat conformation.

BSA adsorption onto SNPs-NH<sub>2</sub> (aminated silica) significantly increases the RMS up to 1.09 nm. This increase is only slightly lower than that observed for silica, suggesting that amination did not critically affect BSA adsorption (Figure 30-B). Nevertheless, detectable change in RMS increase may be due to BSA adsorption between interspatial silane chains as suggested by Bhushan et al. <sup>[247]</sup>.



More interestingly, the increase in RMS after BSA exposing to surfaces functionalized with PEG-7 was significantly lower than for silica and aminated surfaces. This suggests that BSA molecules accommodate between short PEG chains, probably also in a side-chain conformation, thus reducing the surface roughness. For PEG-113 the situation is the opposite and RMS values even increase compared to those for silica, indicating that BSA is not able to penetrate in the large PEG chains and that BSA may orientate perpendicularly to the surface. This may be consistent with the fact that long PEG show more inter-chain interactions than shorter ones as reported by Unsworth et al. <sup>[139]</sup> and also by McNamee et al. <sup>[216]</sup>. Interestingly, RMS values for PEG-7 and 44 after BSA adsorption did not differ significantly, suggesting that BSA is still able to penetrate the polymer shell. Here, it is very important to note that although the adsorption pattern of BSA onto PEG-7 and PEG-44 is similar, the evolution of the BSA corona onto NPs is quite different. A possible explanation would be that although BSA is able to penetrate PEG-44, the degree of silica surface-protein interaction is lower than for PEG-7 (no fully parallel orientation), thus allowing for easily being detached from the surface.

In resume, although, an analysis of the RMS values only provides a partial description of the samples, which may be positive evidence suggesting a different orientation and penetration depth of BSA towards functionalized surfaces depending on polymer length.

Table 6: RMS values of pure silicon dioxide and silicon dioxide coated with PEG calculated from AFM pictures. The thickness of the polymer brush, as well as, the stretching factor according to McNamee<sup>[216]</sup> are also listed. <sup>a</sup>L<sub>s</sub> refers to the approximated thickness of the polymer brushed as determined by McNamee et al.<sup>[216]</sup> in 100 mM NaCl. S<sub>r</sub> is the stretching ratio of the PEG.

Substrate	L <sub>s</sub> <sup>a</sup> [nm]	S <sub>r</sub>	RMS (surface) [nm]	RMS (with BSA) [nm]
Si-OH	-	-	0.29	1.07
Si-O-NH <sub>2</sub>	-	-	0.41	1.09
SiO-NH-PEG-7	4	1.8-1.2	0.33	0.86
SiO-NH-PEG-44	8	0.51	0.34	0.88
SiO-NH-PEG-113	16	0.39	0.73	1.61

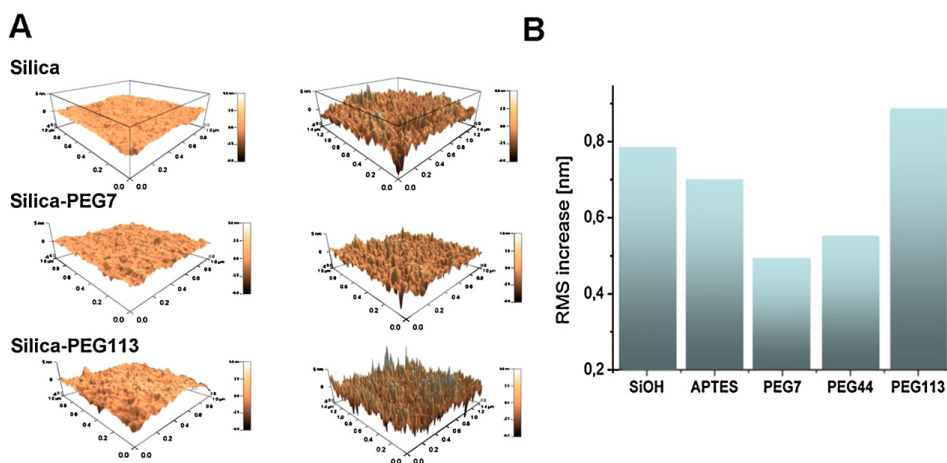


Figure 30: (A) AFM pictures of different substrates before (left) and after (right) BSA adsorption. (B) Increase in rms after BSA adsorption onto different substrates.

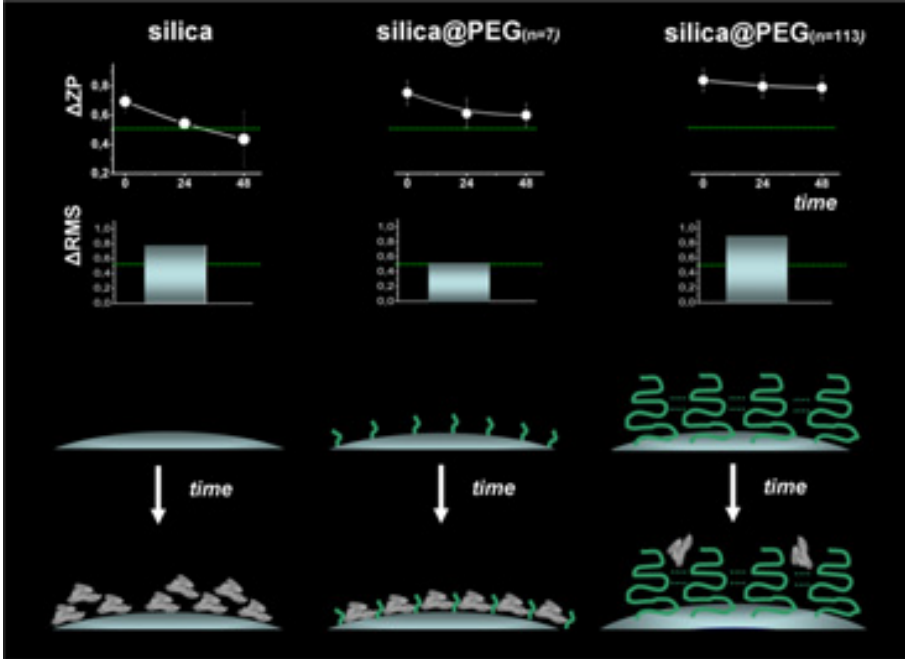
## 6.4. Conclusions

Although some contributions regarding the effect of PEG coating onto silica and the cellular response have been reported, the mechanism of protein adsorption has been not yet fully understood<sup>[251]</sup>. One reason is the fact that dispersions of NPs in cell culture media are highly complex and not easy to understand. Therefore, the study of model systems based on well defined nanoparticles and proteins may be useful to understand some basic processes involving nanoparticles in real systems.

In the present work, silica-poly(ethylene glycol) nanohybrids (SNPs@PEG) or PEGylated surfaces with different polymer molecular weights were successively synthesized and consistently characterized. In addition, the adsorption of the model protein BSA on PEGylated silica surfaces has been systematically investigated. Analysis of zeta potential at different incubation times shows a dynamical evolution of the nanoparticles-protein corona for pristine SNPs and SNPs@PEG with short polymer chains (MW 350 g/mol). This could be a fact that a hard corona is formed after some time and once built only allows the further formation of a loosely attached soft corona as found by Casals et al.<sup>[242]</sup>. Nevertheless, for SNPs@PEG with  $MW \geq 2000$  g/mol (larger PEG molecules) significant suppression of corona formation and time evolution was observed, suggesting larger PEG molecules critically resist the BSA adsorption. AFM investigations suggest a different orientation and penetration depth of BSA towards functionalised flat surfaces (SNPs-NH-PEG) depending on the polymer length.

Similar systematic studies with other relevant proteins like alipoproteins or transferrins may be of interest in order to further scrutinise the mechanisms of proteins corona formation on nanoparticles.

Graphical abstract to chapter 6



## Chapter 7

### Summary and Outlook

---

In the work presented in this thesis, synthesis and surface modification of SNPs with PEGs and dyes was explored in order to avoid non-specific protein adsorption in serum-rich media. The work is divided into three major different sections: Synthesis and characterization of fluorescent silica nanoparticles, tuning the hybrid nanoparticles by controlling the polymer precursor and impact of polymer shell on the formation and time evolution of protein corona.

Firstly, it has proven that the synthetic route is successful in synthesizing fluorescent core-shell and silica shell particles (chapter 4). Moreover, the particles are quite stable in aqueous dispersions, which are useful for many biomedical applications. Addition of TEOS is optimized in order to produce thicker silica shell with well-defined sizes. The advantage of this synthetic route is aminated particles (SNP-NH<sub>2</sub>) can be used as building block material which is possible to couple with other several dyes. The results show that coupling does not alter spectroscopic properties like the emission maxima or quantum yields for low label densities in comparison to the free dye in water. Higher label densities result in an increase of reabsorption and decrease of quantum yield due to self-quenching effects. This strongly affects the resulting brightness and encourages further optimization of applied dye concentration. The high amount of coupled dye molecules per particle even in the case of a decreased quantum yield renders them favourable as label due to the extremely high brightness. One single particle exceeds the brightness of several thousand molecules. Here, in these experiments, dye coupling rate were concentration independent and the covalently coupled dyes promoted the colloidal stability by decreasing the zeta potential.

Secondly, for the first time a simple and effective synthetic method to produce condensated and polymer-grafted NPs with fine control over size and charge by using a versatile polymeric precursor mPEG-IPTES is well executed (chapter 5). The advantage of this method is only a two-stepped synthetic route. It was found that the polymer precursor (mPEG-IPTES) is playing an important role in tuning the size of the silica hybrid particles by condensation and surface charge by grafting. It is also shown how the condensated and polymer-grafted NPs play a crucial role in their respective colloidal stability and in determining the protein surface interactions in terms of hard corona. These particles ensure maximum biocompatibility for potential biological and toxicological applications.

In the final part of this thesis (chapter 6), a novel PEGylated (SNPs@PEG) hybrid particles are synthesized and well characterized. The major experimental findings from this chapter are the adsorption of BSA onto pristine silica and PEGylated surface have been systematically investigated. The PEGylated surfaces were able to inhibit the protein adsorption depending on the molecular weight of the polymers. The effective analysis of zeta potential revealed the dynamic evolution of the nanoparticles protein corona for pristine silica and for short PEGylated silica surfaces. Long PEGylated ( $\geq 2000$  g/mol) silica surfaces have shown significant suppression of the evolution of nanoparticle protein corona. Additionally, orientation and penetration depth of BSA towards flat and PEGylated silica surfaces by using AFM as an analyzing tool is also investigated.

This thesis has merely touched upon the huge and interdisciplinary subject of synthesis and surface modification of SNPs with silanes, polymers and dyes in order to suppress BSA adsorption in serum-rich media: an area of research in which many discoveries and many ideas still remain to be explored.

As a future outlook, the work on PEGs and Alexa dyes should be extended to other polymers like polyglycerols, and dyes (e.g. coumarin, azo, cyanine, nitroso, rhodamine, etc). Thus, the sequential approach should be investigated for the cellular uptake, *in vivo* and *in vitro* studies, encapsulation of drugs.

## Bibliography

---

- [1] S. Milani, F. Baldelli Bombelli, A. S. Pitek, K. A. Dawson, J. Rädler, *ACS Nano***2012**, *6*, 2532.
- [2] R. Landsiedel, L. Ma-Hock, A. Kroll, D. Hahn, J. Schnekenburger, K. Wiench, W. Wohlleben, *Advanced Materials***2010**, *22*, 2601.
- [3] T. Xia, M. Kovoichich, J. Brant, M. Hotze, J. Sempf, T. Oberley, C. Sioutas, J. I. Yeh, M. R. Wiesner, A. E. Nel, *Nano Letters***2006**, *6*, 1794.
- [4] P. Rivera Gil, G. Oberdörster, A. Elder, V. Puentes, W. J. Parak, *ACS Nano***2010**, *4*, 5527.
- [5] D. B. Warheit, *Toxicological Sciences***2008**, *101*, 183.
- [6] C. Barbé, J. Bartlett, L. Kong, K. Finnie, H. Q. Lin, M. Larkin, S. Calleja, A. Bush, G. Calleja, *Advanced Materials***2004**, *16*, 1959.
- [7] Z. Meng, C. Xue, Q. Zhang, X. Yu, K. Xi, X. Jia, *Langmuir***2009**, *25(14)*, 7879.
- [8] R. K. Iler, *Wiley: New York***1979**.
- [9] G. Orts-Gil, K. Natte, D. Drescher, H. Bresch, A. Manton, J. Kneipp, W. Österle, *Journal of Nanoparticle Research***2011**, *13*, 1593.
- [10] D. Drescher, G. Orts-Gil, G. Laube, K. Natte, R. Veh, W. Österle, J. Kneipp, *Analytical and Bioanalytical Chemistry***2011**, *400*, 1367.
- [11] M. P. Monopoli, D. Walczyk, A. Campbell, G. Elia, I. Lynch, F. Baldelli Bombelli, K. A. Dawson, *Journal of the American Chemical Society***2011**, *133*, 2525.
- [12] M. V. D. Z. Park, W. Annema, A. Salvati, A. Lesniak, A. Elsaesser, C. Barnes, G. McKerr, C. V. Howard, I. Lynch, K. A. Dawson, A. H. Piersma, W. H. de Jong, *Toxicology and Applied Pharmacology***2009**, *240*, 108.
- [13] B. Díaz, C. Sánchez-Espinell, M. Arruebo, J. Faro, E. de Miguel, S. Magadán, C. Yagüe, R. Fernández-Pacheco, M. R. Ibarra, J. Santamaría, Á. González-Fernández, *Small***2008**, *4*, 2025.
- [14] K. Natte, T. Behnke, G. Orts-Gil, C. Würth, F. J. Friedrich, W. Österle, U. Resch-Genger, *J Nanopart Res* **2012**, *14*, 680.
- [15] G.-Y. Lee, H.-J. Park, C. Oh, G.-S. Oh, C. Y. Kim, *Langmuir***2007**, *23*, 10875.
- [16] P. He, N. F. Hu, J. F. Hu, J. F. Rusling, *Langmuir***2004**, *20*, 722.
- [17] D. Zhang, Y. Chen, H. Y. Chen, X. H. Xia, *Anal Bioanal Chem***2004**, *379*, 1025.
- [18] X. S. Zhao, G. Q. Lu, *J. Phys. Chem. B***1998**, *102*, 1556.
- [19] S. R. Hall, S. A. Davis, S. Mann, *Langmuir***2000**, *16*, 1454.
- [20] M. H. Lim, A. Stein, *Chem. Mater.***1999**, *11*, 3285.
- [21] H. E. Bergna, W. O. Roberts, *Colloidal Silica: fundamentals and applications CRC Press. Taylor & Francis Group: Boca Raton***2006**.
- [22] L. T. Zhuravlev, *Colloids and Surfaces A: Physicochemical and Engineering Aspects***1993**, *74*, 71.
- [23] F. Orgaz, H. Rawson, *Journal of Non-Crystalline Solids***1986**, *82*, 57.
- [24] W. Stöber, A. Fink, E. Bohn, *Journal of Colloid and Interface Science***1968**, *26*, 62.
- [25] R. M. Pashley, M. E. Karaman, "Surface Tension and Wetting", in *Applied Colloid and Surface Chemistry*, John Wiley & Sons, Ltd, 2005, p. 13.
- [26] K. S. Birdi, "References", in *Surface and Colloid Chemistry*, CRC Press, 2009, p. 229.
- [27] M. Kobayashi, F. d. r. Juillerat, P. Galletto, P. Bowen, M. Borkovec, *Langmuir***2005**, *21*, 5761.
- [28] R. K. Iler, *The Chemistry of Silica: Solubility, Polymerization, Colloid and Surface Properties, and Biochemistry*, Wiley, New York**1979**.
- [29] J. Lindén, *Surface modified silica nanoparticles as emulsifier*,

<http://publications.lib.chalmers.se/records/fulltext/157392.pdf>**2012.**

- [30] J. H. E. Arts, H. Muijser, E. Duistermaat, K. Junker, C. F. Kuper, *Food and Chemical Toxicology***2007**, *45*, 1856.
- [31] L. R. Hirsch, R. J. Stafford, J. A. Bankson, S. R. Sershen, B. Rivera, R. E. Price, J. D. Hazle, N. J. Halas, J. L. West, *Proceedings of the National Academy of Sciences***2003**, *100*, 13549.
- [32] D. J. Bharali, I. Klejbor, E. K. Stachowiak, P. Dutta, I. Roy, N. Kaur, E. J. Bergey, P. N. Prasad, M. K. Stachowiak, *Proceedings of the National Academy of Sciences of the United States of America***2005**, *102*, 11539.
- [33] I. I. Slowing, B. G. Trewyn, V. S. Y. Lin, *Journal of the American Chemical Society***2007**, *129*, 8845.
- [34] J. Wu, C. Wang, J. Sun, Y. Xue, *ACS Nano***2011**, *5*, 4476.
- [35] S. Sharifi, S. Behzadi, S. Laurent, M. Laird Forrest, P. Stroeve, M. Mahmoudi, *Chemical Society Reviews***2012**, *41*, 2323.
- [36] M. Mahmoudi, K. Azadmanesh, M. A. Shokrgozar, W. S. Journeay, S. Laurent, *Chemical Reviews***2011**, *111*, 3407.
- [37] S. Sakka, *Kluwer Acad. Publish., Boston /Dordrecht/London***2005**.
- [38] T. Okubo, T. Miyamoto, K. Umemura, K. Kobayashi, *Colloid & Polymer Science***2001**, *279*, 1236.
- [39] D. Pontoni, T. Narayanan, A. R. Rennie, *Langmuir***2002**, *18*, 56.
- [40] N. Atchison, W. Fan, D. D. Brewer, M. A. Arunagirinathan, B. J. Hering, S. Kumar, K. K. Papas, E. Kokkoli, M. Tsapatsis, *Angewandte Chemie International Edition***2011**, *50*, 1617.
- [41] M. A. Snyder, J. A. Lee, T. M. Davis, L. E. Scriven, M. Tsapatsis, *Langmuir***2007**, *23*, 9924.
- [42] W. Fan, M. A. Snyder, S. Kumar, P.-S. Lee, W. C. Yoo, A. V. McCormick, R. Lee Penn, A. Stein, M. Tsapatsis, *Nat Mater***2008**, *7*, 984.
- [43] K. D. Hartlen, A. P. T. Athanasopoulos, V. Kitaev, *Langmuir***2008**, *24*, 1714.
- [44] T. Yokoi, Y. Sakamoto, O. Terasaki, Y. Kubota, T. Okubo, T. Tatsumi, *Journal of the American Chemical Society***2006**, *128*, 13664.
- [45] T. M. Davis, M. A. Snyder, J. E. Krohn, M. Tsapatsis, *Chemistry of Materials***2006**, *18*, 5814.
- [46] L. G. Britcher, D. C. Kehoe, J. G. Matison, A. G. Swincer, *Macromolecules***1995**, *28*, 3110.
- [47] G. Y. Choi, J. F. Kang, A. Ulman, W. Zurawsky, C. Fleischer, *Langmuir***1999**, *15*, 8783.
- [48] J. D. Le Grange, J. L. Markham, C. R. Kurkjian, *Langmuir***1993**, *9*, 1749.
- [49] F. Faverolle, A. J. Attias, B. Bloch, P. Audebert, C. P. Andrieux, *Chemistry of Materials***1998**, *10*, 740.
- [50] G. Mao, D. G. Castner, D. W. Grainger, *Chemistry of Materials***1997**, *9*, 1741.
- [51] A. N. Parikh, J. D. Beers, A. P. Shreve, B. I. Swanson, *Langmuir***1999**, *15*, 5369.
- [52] A. Arkhireeva, J. N. Hay, W. Oware, *Journal of Non-Crystalline Solids***2005**, *351*, 1688.
- [53] Z. Wu, H. Xiang, T. Kim, M.-S. Chun, K. Lee, *Journal of Colloid and Interface Science***2006**, *304*, 119.
- [54] E. Asenath Smith, W. Chen, *Langmuir***2008**, *24*, 12405.
- [55] Y.-P. Wang, K. Yuan, Q.-L. Li, L.-P. Wang, S.-J. Gu, X.-W. Pei, *Materials Letters***2005**, *59*, 1736.
- [56] H. Tang, W. Zhang, P. Geng, Q. Wang, L. Jin, Z. Wu, M. Lou, *Analytica Chimica Acta***2006**, *562*, 190.
- [57] S. Martwiset, A. E. Koh, W. Chen, *Langmuir***2006**, *22*, 8192.



- [58] P. T. Charles, G. J. Vora, J. D. Andreadis, A. J. Fortney, C. E. Meador, C. S. Dulcey, D. A. Stenger, *Langmuir***2002**, *19*, 1586.
- [59] A. Hreniak, J. Rybka, A. Gamian, K. Hermanowicz, J. Hanuza, K. Maruszewski, *Journal of Luminescence***2007**, *122-123*, 987.
- [60] L. Kind, F. A. Plamper, R. Golbel, A. Manton, A. H. E. Müller, U. Pieleś, A. Taubert, W. Meier, *Langmuir***2009**, *25*, 7109.
- [61] K. Natta, T. Behnke, G. Orts-Gil, C. Würth, J. Friedrich, W. Österle, U. Resch-Genger, *Journal of Nanoparticle Research***2012**, *14*, 1.
- [62] I. Rahman, M. Jafarzadeh, C. Sipaut, *Journal of Sol-Gel Science and Technology***2011**, *59*, 63.
- [63] F. Hoffmann, M. Cornelius, J. Morell, M. Fröba, *Angewandte Chemie International Edition***2006**, *45*, 3216.
- [64] A. Van Blaaderen, A. Vrij, *Langmuir***1992**, *8*, 2921.
- [65] R. P. Bagwe, L. R. Hilliard, W. Tan, *Langmuir***2006**, *22*, 4357.
- [66] K.-J. Liu, J. L. Parsons, *Macromolecules***1969**, *2*, 529.
- [67] L. D. Unsworth, Z. Tun, H. Sheardown, J. L. Brash, *Journal of Colloid and Interface Science***2006**, *296*, 520.
- [68] J. M. e. Harris, *Plenum Press: New York*,**1992**, 485.
- [69] O. Kinstler, G. Molineux, M. Treuheit, D. Ladd, C. Gegg, *Advanced Drug Delivery Reviews***2002**, *54*, 477.
- [70] A. P. Chapman, P. Antoniw, M. Spitali, S. West, S. Stephens, D. J. King, *Nat Biotech***1999**, *17*, 780.
- [71] E. Ostuni, R. G. Chapman, R. E. Holmlin, S. Takayama, G. M. Whitesides, *Langmuir***2001**, *17*, 5605.
- [72] A. Polson, G. M. Potgieter, J. F. Largier, G. E. F. Mears, F. J. Joubert, *Biochimica et Biophysica Acta (BBA) - General Subjects***1964**, *82*, 463.
- [73] P. W. Chun, M. Fried, E. F. Ellis, *Analytical Biochemistry***1967**, *19*, 481.
- [74] P. A. Albertsson, *3rd ed, Wiley: New York*, **1986**, 324.
- [75] A. Abuchowski, T. van Es, N. C. Palczuk, F. F. Davis, *Journal of Biological Chemistry***1977**, *252*, 3578.
- [76] Y. Mori, S. Nagaoka, H. Takiuchi, T. Kikuchi, N. Noguchi, H. Tanzawa, Y. Noishiki, *Trans. Am. Soc. Artificial Internal Organs***1982**, *28*, 459.
- [77] D. C. Carter, J. X. Ho, J. T. E. F. M. R. C. B. Anfinsen, S. E. David, "Structure of Serum Albumin", in *Advances in Protein Chemistry*, Academic Press, 1994, p. 153.
- [78] M. Akgül, N. Burcu Savak, M. Özmak, A. Gümrah Dumanlı, Y. Yürüm, A. Karabakan, *Hacettepe J. Biol. & Chem.***2008**, *36*, 21.
- [79] T. Coradin, A. I. Coupe', J. Livage, *Colloids and Surfaces B: Biointerfaces***2003**, *29*, 189.
- [80] K. Rezwan, L. P. Meier, M. Rezwan, J. Vörös, M. Textor, L. J. Gauckler, *Langmuir***2004**, *20*, 10055.
- [81] F. Zhang, E. T. Kang, K. G. Neoh, P. Wang, K. L. Tan, *Biomaterials***2001**, *22*, 1541.
- [82] P. Kingshott, J. Wei, D. Bagge-Ravn, N. Gadegaard, L. Gram, *Langmuir***2003**, *19*, 6912.
- [83] M. Ochi, R. Takahashi, *Journal of Polymer Science Part B: Polymer Physics***2001**, *39*, 1071.
- [84] M. Vezir Kahraman, M. Kuşçu, Y. Menceloğlu, N. Kayaman-Apohan, A. Güngör, *Journal of Non-Crystalline Solids***2006**, *352*, 2143.
- [85] C. J. T. Landry, B. K. Coltrain, D. M. Teegarden, T. E. Long, V. K. Long, *Macromolecules***1996**, *29*, 4712.
- [86] S. K. Young, G. C. Gemeinhardt, J. W. Sherman, R. F. Storey, K. A. Mauritz, D. A. Schiraldi, A. Polyakova, A. Hiltner, E. Baer, *Polymer***2002**, *43*, 6101.

- [87] M. Vezir Kahraman, M. KuÅu, Y. MenceloÅlu, N. Kayaman-Apohan, A. Gngr, *Journal of Non-Crystalline Solids***2006**, 352, 2143.
- [88] Z. Meng, C. Xue, Q. Zhang, X. Yu, K. Xi, X. Jia, *Langmuir***2009**, 25, 7879.
- [89] X. S. Zhao, G. Q. Lu, *The Journal of Physical Chemistry B***1998**, 102, 1556.
- [90] S. R. Hall, S. A. Davis, S. Mann, *Langmuir***1999**, 16, 1454.
- [91] M. H. Lim, A. Stein, *Chemistry of Materials***1999**, 11, 3285.
- [92] C. Oh, J.-H. Lee, Y.-G. Lee, Y.-H. Lee, J.-W. Kim, H.-H. Kang, S.-G. Oh, *Colloids and Surfaces B: Biointerfaces***2006**, 53, 225.
- [93] R. Richer, *Chemical Communications***1998**, 1775.
- [94] H. Xu, F. Yan, E. E. Monson, R. Kopelman, *Journal of Biomedical Materials Research Part A***2003**, 66A, 870.
- [95] C. A. Bradley, B. D. Yuhas, M. J. McMurdo, T. D. Tilley, *Chemistry of Materials***2008**, 21, 174.
- [96] F. Branda, B. Silvestri, G. Luciani, A. Costantini, F. Tescione, *Colloids and Surfaces A: Physicochemical and Engineering Aspects***2010**, 367, 12.
- [97] H. C. Kolb, M. G. Finn, K. B. Sharpless, *Angewandte Chemie International Edition***2001**, 40, 2004.
- [98] X. Lu, F. Sun, J. Wang, J. Zhong, Q. Dong, *Macromol. Rapid Commun.***2009**, 30, 2116.
- [99] B. Radhakrishnan, A. N. Constable, W. J. Brittain, *Macromolecular Rapid Communications***2008**, 29, 1828.
- [100] C. Oh, Y.-G. Lee, T.-S. Choi, C.-U. Jon, S.-G. Oh, *Colloids and Surfaces A: Physicochemical and Engineering Aspects***2009**, 349, 145.
- [101] C. Oh, C. Do Ki, J. Young Chang, S.-G. Oh, *Materials Letters***2005**, 59, 929.
- [102] J.-Y. Hwang, H.-Y. Lee, C. Oh, D.-Y. Jun, G.-S. Oh, *J. Ind. Eng. Chem***2006**, 12, 380.
- [103] V. Hlady, J. Buijs, *Current Opinion in Biotechnology***1996**, 7, 72.
- [104] D. G. Castner, B. D. Ratner, *Surface Science***2002**, 500, 28.
- [105] B. Kasemo, *Surface Science***2002**, 500, 656.
- [106] J. J. Gray, *Current Opinion in Structural Biology***2004**, 14, 110.
- [107] J. J. Valle-Delgado, J. A. Molina-BolÅvar, F. Galisteo-GonzÅlez, M. a. J. GÅlvez-Ruiz, A. Feiler, M. W. Rutland, *The Journal of Physical Chemistry B***2004**, 108, 5365.
- [108] J. Andrade, V. Hlady, "Protein adsorption and materials biocompatibility: A tutorial review and suggested hypotheses  
Biopolymers/Non-Exclusion HPLC", Springer Berlin / Heidelberg, 1986, p. 1.
- [109] S. Vidyasankar, M. Ru, F. H. Arnold, *Journal of Chromatography A***1997**, 775, 51.
- [110] M. E. Davis, A. Katz, W. R. Ahmad, *Chemistry of Materials***1996**, 8, 1820.
- [111] L. Ye, K. Haupt, *Analytical and Bioanalytical Chemistry***2004**, 378, 1887.
- [112] T. Cedervall, I. Lynch, M. Foy, T. BerggÅrd, S. C. Donnelly, G. Cagney, S. Linse, K. A. Dawson, *Angewandte Chemie***2007**, 119, 5856.
- [113] C. Giulio, P. Daniela, S. Sofia Candeloro De, C. Anna Laura, C. Giuseppe, S. Roberto, L. Aldo, *Applied Physics Letters***2011**, 99, 033702.
- [114] S. Lindman, I. Lynch, E. Thulin, H. Nilsson, K. A. Dawson, S. Linse, *Nano Letters***2007**, 7, 914.
- [115] J. S. Gebauer, M. Malissek, S. Simon, S. K. Knauer, M. Maskos, R. H. Stauber, W. Peukert, L. Treuel, *Langmuir***2012**, 28, 9673.
- [116] C. Rucker, M. Potzl, F. Zhang, W. J. Parak, G. U. Nienhaus, *Nat Nano***2009**, 4, 577.
- [117] E. Casals, T. Pfaller, A. Duschl, G. J. Oostingh, V. Punttes, *ACS Nano***2010**, 4, 3623.
- [118] J. Leszczynski, *Nat Nano***2010**, 5, 633.
- [119] I. Lynch, A. Salvati, K. A. Dawson, *Nat Nano***2009**, 4, 546.
- [120] A. E. Nel, L. Madler, D. Velegol, T. Xia, E. M. V. Hoek, P. Somasundaran, F. Klaessig, V. Castranova, M. Thompson, *Nat Mater***2009**, 8, 543.

- [121] M. Malmsten, *New York : Marcel Dekker***2003**, 2nd Ed. .
- [122] A. R. Denes, E. B. Somers, A. C. L. Wong, F. Denes, *Journal of Applied Polymer Science***2001**, 81, 3425.
- [123] P. Roach, D. Farrar, C. C. Perry, *Journal of the American Chemical Society***2005**, 127, 8168.
- [124] M. Jonsson, H.-O. Johansson, *Colloids and Surfaces B: Biointerfaces***2004**, 37, 71.
- [125] S. Pasche, J. Vörös, H. J. Griesser, N. D. Spencer, M. Textor, *The Journal of Physical Chemistry B***2005**, 109, 17545.
- [126] S. Herrwerth, W. Eck, S. Reinhardt, M. Grunze, *Journal of the American Chemical Society***2003**, 125, 9359.
- [127] I. Szleifer, M. A. Carignano, *Macromolecular Rapid Communications***2000**, 21, 423.
- [128] J. Lee, H. Lee, J. Andrade, *Prog Polym Sci* **1995**, 20, 1043.
- [129] N. Ngadi, *Mechanisms of Molecular Brush Inhibition of Protein Adsorption onto Stainless Steel Surface*, <http://hdl.handle.net/10092/4454>**2009**.
- [130] K. L. Prime, G. M. Whitesides, *Journal of the American Chemical Society***1993**, 115, 10714.
- [131] B. Zhu, T. Eurell, R. Gunawan, D. Leckband, *Journal of Biomedical Materials Research***2001**, 56, 406.
- [132] S. Schilp, A. Rosenhahn, M. E. Pettitt, J. Bowen, M. E. Callow, J. A. Callow, M. Grunze, *Langmuir***2009**, 25, 10077.
- [133] S.-W. Lee, P. E. Laibinis, *Biomaterials***1998**, 19, 1669.
- [134] R. L. C. Wang, H. J. Kreuzer, M. Grunze, *The Journal of Physical Chemistry B***1997**, 101, 9767.
- [135] M. A. Carignano, I. Szleifer, *Colloids and Surfaces B: Biointerfaces***2000**, 18, 169.
- [136] J. L. Dalsin, L. Lin, S. Tosatti, J. Vörös, M. Textor, P. B. Messersmith, *Langmuir***2004**, 21, 640.
- [137] M. J. Harris, S. Zalipsky, "Poly(ethylene glycol)", American Chemical Society, 1997, p. 508.
- [138] J. Sofia Susan, W. Merrill Edward, "Protein Adsorption on Poly(ethylene oxide)-Grafted Silicon Surfaces", in *Poly(ethylene glycol)*, American Chemical Society, 1997, p. 342.
- [139] L. D. Unsworth, H. Sheardown, J. L. Brash, *Langmuir***2005**, 21, 1036.
- [140] L. D. Unsworth, H. Sheardown, J. L. Brash, *Biomaterials***2005**, 26, 5927.
- [141] B. Dong, S. Manolache, A. Wong, F. Denes, *Polymer Bulletin***2011**, 66, 517.
- [142] E. P. K. Currie, W. Norde, M. A. Cohen Stuart, *Advances in Colloid and Interface Science***2003**, 100-102, 205.
- [143] B. D. Ratner, *Biomaterials***2007**, 28, 5144.
- [144] S. Aliebeik, *Surface Modification with Polyethylene Glycol-Protein Conjugates for Improved Blood Compatibility. Open Access Dissertations and Theses. Paper 6244*, <http://digitalcommons.mcmaster.ca/opensdissertations/6244>**2011**.
- [145] A. A. Shemetov, I. Nabiev, A. Sukhanova, *ACS Nano***2012**.
- [146] D. E. Koppel, *J. Chem. Phys.***1972**, 57, 4814.
- [147] G. H. Woehrle, J. E. Hutchison, z. S. O, R. G. Finke, *Turk J Chem***2006**, 30, 1.
- [148] H. Riegler, M. Engel, *Berichte der Bunsen-Gesellschaft-Phys.Chem. Chem. Phys.***1991**, 95, 1424.
- [149] U. Resch-Genger, D. Pfeifer, C. Monte, W. Pilz, A. Hoffmann, M. Spieles, K. Rurack, J. Hollandt, D. Taubert, B. Schonenberger, P. Nording, *Journal of Fluorescence***2005**, 15, 315.
- [150] C. Würth, C. Lochmann, M. Spieles, J. Pauli, K. Hoffmann, T. Schuttrigkeit, T. Franzl, U. Resch-Genger, *Applied Spectroscopy***2009**, 64, 733.

- [151] C. Würth, M. Grabolle, J. Pauli, M. Spieles, U. Resch-Genger, *Analytical Chemistry***2011**, *83*, 3431.
- [152] J. T. Russin, I. E. Altinoglu, H. J. Adair, C. P. Eklund, *J. Phys.: Condens. Matter***2010**, *22*, 334217.
- [153] S. B. Edwards, O. Tudor, R. E. Prossnitz, A. L. Sklar, *Current Opinion in Chemical Biology***2004**, *8*, 392.
- [154] M. Meldal, *Biopolymers***2002**, *66*, 93.
- [155] I. Miletto, A. Gilardino, P. Zamburlin, S. Dalmazzo, D. Lovisolò, G. Caputo, G. Viscard, G. Martra, *Dyes and Pigments***2010**, *84*, 121.
- [156] I. Sokolov, S. Naik, *Small***2008**, *4*, 934.
- [157] H. Härmä, *Technology Review, TEKES, National Technology Agency***2002**, 126.
- [158] G. Schulz-Ekloff, D. Wöhrle, V. B. Duffel, A. R. Schoonheydt, *Microporous and Mesoporous Materials***2002**, *51*, 91.
- [159] U. Resch-Genger, M. Grabolle, S. Cavaliere-Jaricot, R. Nitschke, T. Nann, *Nature Methods***2008**, *5*, 763.
- [160] M. Grabolle, M. Spieles, V. Lesnyak, N. Gaponik, A. Eychmüller, U. Resch-Genger, *Anal. Chem.* **2009**, *81*, 6285.
- [161] J. E. Lee, N. Lee, T. Kim, J. Kim, T. Hyeon, *Accounts of Chemical Research***2011**, *44*, 893.
- [162] M. Benezra, O. Penate-Medina, B. P. Zanzonico, D. Schaer, H. Ow, A. Burns, E. DeStanchina, V. Longo, E. Herz, S. Iyer, J. Wolchok, M. S. Larson, U. Wiesner, S. M. Bradbury, *J Clin Invest.***2011**, *121*, 2768.
- [163] N. Vasilis, B. Christoph, W. Ralph, *European Radiology* **2003**, *13*, 195.
- [164] R. Weissleder, *Nature Biotechnology***2001**, *19*, 316.
- [165] S. A. Ethiraj, S. Kharrazi, N. Hebalkar, J. Urban, R. S. Sainkar, K. S. Kulkarni, *Materials Letters***2007**, *61*, 4738.
- [166] W. Changfeng, S. Craig, M. Jason, *Langmuir***2006**, *22*, 2956.
- [167] F. B. Bringley, L. P. Penner, R. Wang, F. J. Harder, J. W. Harrison, L. Buonemani, *Journal of Colloid and Interface Sci***2008**, *320*, 132.
- [168] A. V. Blaaderen, A. Vrij, *Journal of Colloid and Interface Sci***1993**, *156*, 1.
- [169] L. Wang, Y. Chaoyong, T. Weihong, *Nano Letters***2005**, *5*, 37.
- [170] A. Burns, H. Ow, U. Wiesner, *Chem. Soc. Rev.***2006**, *35*, 1028.
- [171] H. Langhals, J. A. Esterbauer, *Chem. Eur. J.***2009**, *15*, 4793.
- [172] L. Liz-Marzan, G. Michael, M. Paul, *Langmuir***1996**, *12*, 4329.
- [173] K. Aslan, M. Wu, R. J. Lakowicz, D. C. Geddes, *J. Am. Chem. Soc***2007**, *129*, 1524.
- [174] P. Graf, A. Manton, A. Haase, F. A. Thünemann, A. Masic, W. Meier, A. Luch, A. Taubert, *ACS NANO***2011**, *5*, 820.
- [175] L. Kind, F. A. Plamper, R. Göbel, A. Manton, E. H. A. Müller, U. Piesles, A. Taubert, W. Meier, *Langmuir***2009**, *25*, 7109.
- [176] J. E. Berlier, A. Rothe, G. Buller, J. Bradford, D. R. Gray, B. J. Filanosk, W. G. Telford, S. Yue, J. Liu, C.-Y. Cheung, W. Chang, J. D. Hirsch, J. M. Beechem, R. P. Haugland, R. P. Haugland, *The Journal of Histochemistry & Cytochemistry***2003**, *51* (12), 1179.
- [177] P.-V. Nataliya, P. H. Rosaria, B.-S. Janell, K. B. Mahesh, J. M. Paul, M. Fei, L. Wai-Y, P. H. Richard, *The Journal of Histochemistry & Cytochemistry***1999**, *47* 1179.
- [178] U. Schobel, H.-J. Egelhaaf, A. Brecht, D. Oelkrug, G. Gauglitz., *Bioconjugate Chemistry***1999**, *10*, 1107.
- [179] G. Sun, M. Y. Berezin, J. Fan, H. Lee, J. Ma, K. Zhang, K. L. Wooley, S. Achilefu, *Nanoscale***2010**, *2*, 548.

- [180] M. Martini, M. Montagna, M. Ou, O. Tillement, S. Roux, P. Perriat, *J. Appl. Phys***2009**, *106*, 094304.
- [181] S. Thomas, B. Herwig, E. M. T. nter, *Journal of Nanoscience and Nanotechnology***2004**, *4*, 504.
- [182] H. E. Bergna, O. W. Roberts, *CRC Press, Taylor & Francis Group: Boca Raton***2006**, *131*, 895.
- [183] G. Z. Estephan, A. J. Jaber, B. J. Schlenoff, *Langmuir***2010**, *26* 16884.
- [184] J. C. L. Thomassen, A. Aerts, V. Rabolli, D. Lison, L. Gonzalez, M. Kirsch-Volders, D. Napierska, H. P. Hoet, A. E. C. Kirschhock, A. J. Martens, *Langmuir***2010**, *26*, 328.
- [185] C. R. Murdock, L. Braydich-Stolle, M. A. Schrand, J. J. Schlager, M. S. M. Hussain, *Toxicological Sciences***2008**, *101*, 239.
- [186] G. Orts-Gil, M. Losik, H. Schlaad, M. Drechsler, T. Hellweg, *Langmuir***2008**, *24*, 12823.
- [187] D. W. Pyrz, J. D. Buttrey, *Langmuir***2008**, *24*, 11350.
- [188] M. K. Johansson, R. M. Cook, *Chem. Eur. J***2003**, *9*, 3466.
- [189] I. R. Nooney, N. M. C. McCahey, O. Stranik, L. X. Guevel, C. McDonagh, D. B. MacCraith, *Anal Bioanal Chem***2009**, *393*, 1143.
- [190] E. Herz, T. Marchincin, L. Connelly, D. Bonner, A. Burns, S. Switalski, U. Wiesner, *J Fluoresc***2010**, *20*, 67.
- [191] E. Herz, H. Ow, D. Bonner, A. Burns, U. Wiesner, *J. Mater. Chem***2009**, *19*, 6341.
- [192] D. R. Larson, H. Ow, H. D. Vishwasrao, A. A. Heikal, U. Wiesner, W. W. Webb, *Chem. Mater.***2008**, *20*, 2677.
- [193] H. Ow, R. D. Larson, M. Srivastava, A. B. Baird, W. W. Webb, U. Weisner, *Nano Letters***2005**, *5*, 113.
- [194] E. Herz, H. Ow, D. Bonner, A. Burns, U. Wiesner, *Journal of Materials Chemistry***2009**, *19*, 6341.
- [195] K. Yoshimoto, M. Ichino, Y. Nagasaki, *Lab Chip***1286–1289**, *9*, 1286.
- [196] S. A. Sawhney, P. C. Pathak, A. J. Hubbell, *Biomaterials***2003**, *14*, 1008.
- [197] C. Oh, J. H. Lee, Y. G. Lee, Y. H. Lee, J. W. Kim, H. H. Kang, S. G. Oh, *Colloids Surf. B***2006**, *53*, 225.
- [198] S. L. Burkett, S. D. Sims, S. Mann, *Chem. Commun.***1996**, 1367.
- [199] R. Richer, L. Mercier, *Chem. Commun.* **1998**, 1775.
- [200] M. C. Burleigh, M. A. Markowitz, M. S. Spector, B. P. Garber, *J. Phys.Chem. B***2001**, *105*, 9935.
- [201] H. Xu, F. Yan, E. C. Monson, R. Kopelman, *J. Biomed. Mater. Res.***2003**, *66*, 870.
- [202] C. H. Kolb, G. M. Finn, B. K. Sharpless, *Angew. Chem. Int. Ed.* **2001**, *40*, 2004.
- [203] T. M. Peracchia, S. Harnisch, H. Pinto-Alphandary, A. Gulik, D. C. J., D. DesmaeKle, J. d' Angelo, H. R. Müller, P. Couvreur, *Biomaterials***1999**, *20*, 1269.
- [204] L. C. J. Thomassen, A. Aerts, V. Rabolli, D. Lison, L. Gonzalez, M. Kirsch-Volders, D. Napierska, P. H. Hoet, C. E. A. Kirschhock, J. A. Martens, *Langmuir***2010**, *26(1)*, 328.
- [205] W. J. Kim, U. L. Kim, K. C. Kim, *Biomacromolecules* **2007**, *8*, 215.
- [206] F. Turci, E. Ghibaudi, M. Colonna, B. Boscolo, I. Fenoglio, B. Fubini, *Langmuir***2010**, 8336.
- [207] M. Joubert, C. Delaite, E. Bourgeat-Lami, P. Dumas, *Macromolecular Rapid Communications***2005**, *26*, 602.
- [208] F. Zeng-guo, Z. Sanping, *Polymer***2003**, *44*, 5177.
- [209] G. Orts-Gil, M. Losik, H. Schlaad, M. Drechsler, T. Hellweg, *Langmuir***2008**, *24*, 12823.
- [210] G. H. Bogush, C. F. Zukoski, *Journal of Colloid and Interface Sci***1991**, *142*, 1.

- [211] C. Oh, G.-Y. Lee, S.-T. Choi, U.-C. Jons, O. G-S, *Colloids and Surfaces A: Physicochemical and Engineering Aspects***2009**, 349, 145.
- [212] G. H. Bogush, M. A. Tracy, C. F. Zukoski, *J. Non-Cryst. Solids***1998**, 104, 95.
- [213] G. H. Bogush, C. F. Zukoski, *Journal of Colloid and Interface Sci***1991**, 142, 19.
- [214] Q. He, J. Zhang, J. Shi, Z. Zhu, L. Zhang, W. Bu, L. Guo, Y. Chen, *Biomaterials* **2010**, 31, 1085.
- [215] G. Orts-Gil, K. Natte, D. Drescher, H. Bresch, A. Manton, J. Kneipp, W. Österle, *J Nanopart Res* **2011**, 13, 1593.
- [216] C. E. McNamee, S. Yamamoto, K. Higashitani, *Langmuir***2007**, 23, 4389.
- [217] H. Yang, J. J. Morris, T. S. Lopina, *Journal of Colloid and Interface Science***2004**, 273, 148.
- [218] H. Wang, M. Peng, J. Zheng, P. Li, *Journal of Colloid and Interface Science* **2008**, 326, 151.
- [219] Y. Nagasaki, *Polym J***2011**, 43, 949.
- [220] G. Oberdörster, V. Stone, K. Donaldson, *Nanotoxicology***2007**, 1, 2.
- [221] T. J. Brunner, P. Wick, P. Manser, P. Spohn, R. N. Grass, L. K. Limbach, A. Bruinink, W. J. Stark, *Environmental Science & Technology***2006**, 40, 4374.
- [222] W. Lin, Y.-w. Huang, X.-D. Zhou, Y. Ma, *Toxicology and Applied Pharmacology***2006**, 217, 252.
- [223] R. A. Hartvig, M. van de Weert, J. Østergaard, L. Jorgensen, H. Jensen, *Langmuir***2011**, 27, 2634.
- [224] I. Lynch, K. A. Dawson, *Nano Today***2008**, 3, 40.
- [225] D. Walczyk, F. B. Bombelli, M. P. Monopoli, I. Lynch, K. A. Dawson, *Journal of the American Chemical Society***2010**, 132, 5761.
- [226] M. Lundqvist, J. Stigler, G. Elia, I. Lynch, T. Cedervall, K. A. Dawson, *Proceedings of the National Academy of Sciences***2008**, 105, 14265.
- [227] A. A. Vertegel, R. W. Siegel, J. S. Dordick, *Langmuir***2004**, 20, 6800.
- [228] M. Lundqvist, I. Sethson, B.-H. Jonsson, *Langmuir***2004**, 20, 10639.
- [229] M. A. Carignano, I. Szleifer, *Colloids and Surfaces B: Biointerfaces***2000**, 18, 169.
- [230] J. Satulovsky, M. A. Carignano, I. Szleifer, *Proceedings of the National Academy of Sciences***2000**, 97, 9037.
- [231] Y. J. Wu, R. B. Timmons, J. S. Jen, F. E. Molock, *Colloids and Surfaces B: Biointerfaces***2000**, 18, 235.
- [232] N. Derkaoui, S. r. Said, Y. Grohens, R. Olier, M. Privat, *Langmuir***2007**, 23, 6631.
- [233] S. Thomas, B. Herwig, E. M. T. Günter, *Journal of Nanoscience and Nanotechnology***2004**, 4, 504.
- [234] K. Natte, W. Österle, J.F. Friedrich, R.v. Klitzing, G. Orts-Gil, *macromolecular chemistry and physics***2012**, DOI = 10.1002/macp.201200148.
- [235] Z. Zhang, A. E. Berns, S. Willbold, J. Buitenhuis, *Journal of Colloid and Interface Science***2007**, 310, 446.
- [236] S. J. Sofia, V. Premnath, E. W. Merrill, *Macromolecules***1998**, 31, 5059.
- [237] E. Bergna Horacio, "Colloid Chemistry of Silica", in *The Colloid Chemistry of Silica*, American Chemical Society, 1994, p. 1.
- [238] A. Vonarbourg, C. Passirani, P. Saulnier, J.-P. Benoit, *Biomaterials***2006**, 27, 4356.
- [239] Q. He, J. Zhang, J. Shi, Z. Zhu, L. Zhang, W. Bu, L. Guo, Y. Chen, *Biomaterials***2010**, 31, 1085.
- [240] S. H. Brewer, W. R. Glomm, M. C. Johnson, M. K. Knag, S. Franzen, *Langmuir***2005**, 21, 9303.
- [241] P. M. Tessier, J. Jinkoji, Y.-C. Cheng, J. L. Prentice, A. M. Lenhoff, *Journal of the American Chemical Society***2008**, 130, 3106.

- [242] T. P. Eudald Casals, Albert Duschl, Gertie Janneke Oostingh and Victor Puentes, *ACS Nano***2010**, 7, 3623.
- [243] S. Milani, F. Baldelli Bombelli, A. S. Pitek, K. A. Dawson, J. Rädler, *ACS Nano***2012**, 6, 2532.
- [244] K. Rezwan, A. R. Studart, J. Vörös, L. J. Gauckler, *The Journal of Physical Chemistry B***2005**, 109, 14469.
- [245] T. J. Su, J. R. Lu, R. K. Thomas, Z. F. Cui, J. Penfold, *Langmuir***1998**, 14, 438.
- [246] P. Lu, Y.-L. Hsieh, *Powder Technology***2012**, 225, 149.
- [247] B. Bhushan, D. R. Tokachichu, M. T. Keener, S. C. Lee, *Acta Biomaterialia***2005**, 1, 327.
- [248] A. Zengin, T. Caykara, *Materials Science and Engineering: C***2012**, 32, 1107.
- [249] Z. Yang, J. A. Galloway, H. Yu, *Langmuir***1999**, 15, 8405.
- [250] P. J. Flory, *John Wiley & Sons: New York***1969**.
- [251] M. Lord, B. Cousins, P. Doherty, J. Whitelock, A. Simmons, R. L. Williams, B. K. Milthorpe, *Biomaterials***2006**, 27, 4856.
- [252] A. J. Howarter, P. J. Youngblood, *Langmuir***2006**, 22, 11142.
- [253] L. Feng, Y. Wang, N. Wang, Y. Ma, *Polymer Bulletin***2009**, 63, 313.

## Appendix

---

### Appendix to chapter 4:

#### A.4.1 Solid-state $^{13}\text{C}$ NMR of Amino-Functionalized silica particles (SNPs-NH<sub>2</sub>)

$\delta$ 11.1 ppm (SiCH<sub>2</sub>CH<sub>2</sub>CH<sub>2</sub>NH<sub>2</sub>), 25.6 ppm (SiCH<sub>2</sub>CH<sub>2</sub>CH<sub>2</sub>NH<sub>2</sub>), 44.1 ppm (SiCH<sub>2</sub>CH<sub>2</sub>CH<sub>2</sub>NH<sub>2</sub>), 60.6 ppm (CH<sub>3</sub>CH<sub>2</sub>OSi≡), 17.3 ppm (CH<sub>3</sub>CH<sub>2</sub>OSi≡), 51.7 ppm (entrapped CH<sub>3</sub>OH).

#### A.4.2 Fourier transform infrared spectroscopy (FTIR) of SNPs and SNPs-NH<sub>2</sub>

The spectrum of pristine silica nanoparticles shows a prominent resonance band at 1081 cm<sup>-1</sup> attributed to excitation of Si-O-Si stretching mode of vibration (see Figure S1). During the reaction of TEOS and water in alcoholic medium, IR bands appear 952-1097 cm<sup>-1</sup> due to vibration of Si-OH and Si-O-Si bands, indicating the formation of the SiO<sub>2</sub> network. The peak observed at 3419 and 3438 cm<sup>-1</sup> indicated the presence of free Si-OH groups. On the low frequency side of this broad band, there appeared a weak shoulder, near 2891 cm<sup>-1</sup>, which indicated the presence of ethanol. For aminated silica, the characteristic band of amino group (-NH<sub>2</sub>) at 3295 cm<sup>-1</sup> and the absorption band 2920 cm<sup>-1</sup> of the methylene group (-CH<sub>2</sub>-) appears in contrast to that of the pure silica. Besides, a new absorption band at about 1550 cm<sup>-1</sup> was attributed to primary amino groups (-NH<sub>2</sub>) introduced by the addition of APTES.



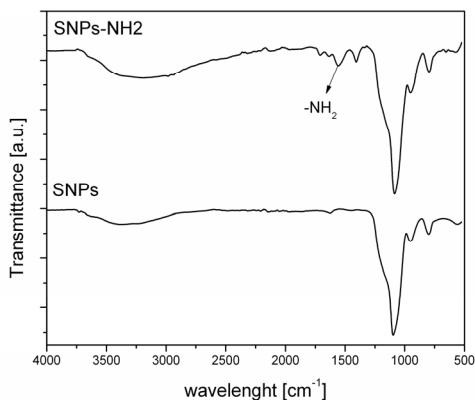


Figure A.4.2: FTIR spectra of pristine silica nanoparticles (SNPs) and aminated silica nanoparticles (SNPs-NH<sub>2</sub>)

#### A.4.3 X-ray photoelectron spectroscopy (XPS) of SNPs and SNPs-NH<sub>2</sub>

Investigation of chemical composition of the nanoparticle surfaces were carried out by XPS (Table S.1). The ratio Si2p:O1s is in both cases close to 2, in good agreement with silica stoichiometry. For aminated silica the atom percentage of N is 4% and the ratio N1s:C1s is 3 indicating a complete hydrolysis of APTES molecules in which all three ethoxy groups have been replaced by siloxane linkages <sup>[252]</sup>.

**Table A.4.1:** XPS of pristine and aminated silica nanoparticles

Sample	XPS composition[%]			
	C1s	N1s	Si2p	O1s
SNPs	3	-	35	62
SNPs-NH <sub>2</sub>	13	4	30	53

## Appendix to chapter 5

### A.5.1 <sup>1</sup>HNMR of mPEG-IPTES precursor

<sup>1</sup>HNMR (Bruker 400 MHz CDCl<sub>3</sub>): δ (ppm) 5.26 (t, 1H NH), 4.2 (q, 6H), 3.73-3.64 (polymer protons, m, 67H), 3.5 (s, 3H), 2.96 (q, 2H), 1.78 (m, 2H), 1.3 (t, 9H), 0.7 (t, 2H).

## Appendix to chapter 6

### A.6.1 XPS

The presence of C1s in SNPs may be due to contamination of bare silica during the XPS spectrometer operation, while Si2p and O1s atom percent is 37 and 60% respectively. In aminated silica particles the atom percent of N is 5% and indicates the modification of APTES on to the pristine surface. As compared with aminated silica, the chemical composition of N1s at PEG-grafted silica surface decreases to 3%, while C1s increases around 30%, further indicating the PEG chains are grafted on to the silica nanoparticles surfaces successfully and part of Si, N and O atoms in centre silica particles are shielded by the outside bonded PEG layer <sup>[253]</sup>.

### A.6.2 TGA

TGA shows that pristine silica has a weight loss of around 5% due to loss of water molecules adsorbed on to the surface and the release of structural water resulting from the bonded hydroxyl groups. The weight loss of aminated silica is higher than that of pristine silica which indicates the modification of APTES modified on to the pristine silica particles and the pyrolysis of organic compounds. The weight loss of PEG-grafted silica increase with increase in temperature, reaching a maxima at about 400-500 °C and then gradually decreases. The residual weight loss at 400-500°C of SNP@PEG7, 44 and 113 are 11, 12, and 10 wt% respectively and they almost kept invariant at high temperatures.

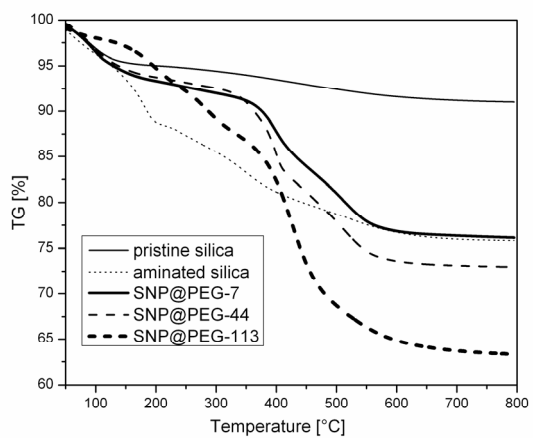


Figure A.6.2: TGA curves of (a) Pristine silica, (b) Aminated silica, (c) SNP@PEG7, (d) SNP@PEG44, (e) SNP@PEG113

### A.6.3 Focused ion beam (FIB)

At the surface of the PEGylated wafer, a cross-sectional lamella for TEM investigation was prepared with a Quanta 3D Dual Beam from FEI. Gallium ion beam working at 30 kV and 20 pA. The SEM column is equipped with a field emission gun. The TEM specimens were prepared by milling an electron-transparent sample, 20  $\mu\text{m}$  long, 5  $\mu\text{m}$  wide and 100 nm thick.

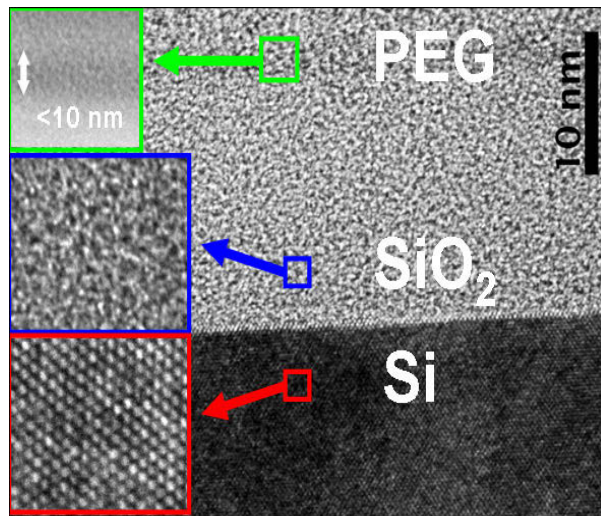


Figure A.6.3: Cross-section TEM of a functionalized (PEGylated) silicon wafer used for AFM analysis. Oxidation of wafer led to formation of an oxide layer which was further functionalized with PEG. Inset on the left side show high magnification TEM pictures of the different phases. Inset on the right side shows elemental EDX line scanning.

#### A.6.4 Reaction scheme and $^1\text{H}$ NMR for tosylation of poly (ethylene glycol) monomethylether (mPEG-OPTS)

$^1\text{H}$  NMR (DMSO-*d*<sub>6</sub>): 7.80 ppm (d, ArH); 7.35 ppm (d, ArH); 4.16 ppm (t, CH<sub>2</sub>CH<sub>2</sub>O-Ts); 3.72-3.61 ppm (m, (-CH<sub>2</sub>CH<sub>2</sub>-O)<sub>n</sub>); 3.38 ppm (s, OCH<sub>3</sub>); 2.45 ppm (s, ArCH<sub>3</sub>).

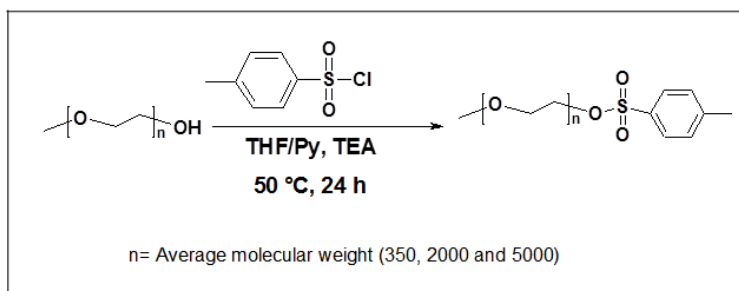


Figure A.6.4: reaction scheme for (mPEG-OTS).

#### A.6.5 Cleaning of silicon surfaces

The cut wafers were sonicated consecutively with freshly prepared "piranha" solution (H<sub>2</sub>SO<sub>4</sub> and 30% H<sub>2</sub>O<sub>2</sub>, v/v = 7/3) for 1 h to get rid of all foreign matter from the surface of the silicon wafers followed by extensive rinsing with plenty of Milli-Q water and acetone. Afterwards the etched silicon wafers were stored under Milli-Q water in a glass container. This procedure yielded a fully hydrophilic surface (Si-OH). Just before experiment, the wafers were taken out of water and dried in a nitrogen flux.

##### A.6.5.1 Preparation of amino functionalized silicon wafer (SNPs-NH<sub>2</sub>)

The pretreated hydrophilic Si-OH wafers were placed into 1% APTES/anhydrous toluene solution and allowed to stand in the solution for 24 h under nitrogen atmosphere at room temperature. The resulting initiator-coated silicon wafers (Si-APTES) were rinsed in acetone 3 times and were immediately used for PEGylation after being dried with a nitrogen stream.

### **A.6.5.2 PEGylation of aminated silica wafers (SNPs-NH-PEG)**

The Si-APTES wafers further functionalized with 1% tosylated m-PEG7 (or 44 and 113)/anhydrous toluene solution and allowed to stand in the solution for 24 h under nitrogen atmosphere at room temperature. The resulting initiator-coated silicon wafers (SNPs-NH-PEG) were rinsed in acetone 3 times to remove unreacted tosylated mPEG and were immediately used PEGylated silicon wafer/BSA mixture after being dried with a nitrogen stream.

### **A.6.5.3 PEGylated silicon wafer /BSA mixtures and purification**

The above functionalized PEGylated samples were immersed in 6% BSA/PBS solution for 10min at r.t. After incubation, the samples were washed with PBS solution for 5 times to remove excess BSA. Then the samples were dried under nitrogen stream. Eventually the samples were stored at r. t. to measure AFM.

## List of symbols

---

A	Absorbance
$R_h$	Hydrodynamic radius
$R_g$	Radius of gyration
$K_b$	Boltzmann constant
D	Diffusion coefficient of particles
$\eta$	dynamic viscosity
T	Temperature
N	Degree of polymerization
wt %	Percentage in weight
$\Phi$	Quantum yields
$\Phi_f$	Fluorescence quantum yields
$N_{em}$	Number of emitted photons
$N_{abs}$	Number of absorbed photons
$\lambda_{ex}$	Excitation wavelength
$\lambda_{em}$	Emission of wave length
$hc_0/em$	Energy of the emitted photons
$hc_0/ex$	Energy of the absorbed photons
nm	nanometer
$\mu\text{m}$	Micrometer

## List of Abbreviations

---

BSA	Bovine Serum Albumin
FCS	Fetal Calf Serum
CCM	Cell Culture Media
DMEM	Dulbecco's Modified Eagle Media
DLS	Dynamic light scattering
ZP	Zeta Potential
PDI	Polydispersity Index
TEM	Transmission Electron Microscopy
SEM	Scanning Electron Microscopy
FIB	Focused ion beam
EDS	Energy Dispersive Scanning
TGA	Thermogravimetric analysis
NIR	Near infrared
FTIR	Fourier Transform Infrared Spectroscopy
ATR	Attenuated total reflectance
NMR	Nuclear magnetic resonance
XPS	X-ray Photoelectron Spectroscopy
AFM	Atomic Force Microscopy
PEG	Poly(ethyleneglycol)
mPEG	Poly(ethylene glycol) monomethyl ether
IPTES	3-(triethoxysilyl) propyl isocyanate
DBTDL	Dibutyl Tin Dilaurate
APTES	3-(triethoxysilyl) propyl amine
IPA	Isopropyl alcohol
NPs	Nanoparticles
SNPs	Silica Nanoparticles
DLVO	Derjaguin, Landau, Verwey and Overbeek
TMOS	Tetramethyl orthosilicate
TEOS	Tetraethyl orthosilicate
FDA	Food and Drug Administration
GRAS	Generally Recognized As Safe



## List of scientific publications

---

Peer reviewed scientific publications, fully related to the work reported in this thesis, are listed below.

1) **Kishore Natte**, Guillermo Orts-Gil, Jörg Friedrich, Regina Von Klitzing, Werner Österle, *Tuning interfacial properties and colloidal behavior of hybrid nanoparticles by controlling the polymer precursor*, Macromol. Chem. Phys. 213 (2012) 2412–2419

2) **Kishore Natte**, Guillermo Orts-Gil, Thomas Bhenke, Christian Würth, Ute Resch Genger, Jörg Friedrich, Werner Österle, *Synthesis and characterization of highly fluorescent core-shell nanoparticles based on Alexa-Dyes*, J Nanopart Res (2012) 14: 680

3) **Kishore Natte**, Jörg F. Friedrich, Sebastian Wohlrab, Jana Lutzki, Regine von Klitzing, Werner Österle and Guillermo Orts-Gil, *Impact of polymer shell on the formation and time evolution of nanoparticle-protein corona*, Colloids and Surfaces B: Biointerfaces, 104 (2013) 213-220

4) Guillermo Orts-Gil, **Kishore Natte**, Daniela Drescher, Harald Bresch, Alexander Manton, Janina Kneipp, Werner Österle, *Characterization of silica nanoparticles prior to in vitro studies: from primary particles to agglomerate*, J Nanopart Res (2011) 13:1593

5) Daniela Drescher, Guillermo Orts-Gil, Gregor Laube, **Kishore Natte**, Rüdiger W. Veh, Werner Österle, Janina Kneipp, *Toxicity of amorphous silica nanoparticles on eukaryotic cell model is determined by particle agglomeration and serum protein adsorption effects*, Anal Bioanal Chem (2011) 400: 1367

6) Guillermo Orts-Gil, **Kishore Natte**, Raphael Thiermann, Matthias Girod, Andreas Thünemann, Michael Maskos and Werner Österle, *On the role of surface composition and curvature on biointerface formation and colloidal stability of nanoparticles in a protein-rich model media* (Colloids and Surfaces B: Biointerfaces (2013), in press, Accepted manuscript) <http://dx.doi.org/10.1016/j.colsurfb.2013.02.027>

## List of contribution in conferences

---

- 1) **Kishore Natte**, Werner Österle, Jörg Friedrich, Regine von Klitzing and Guillermo Orts-Gil, *Functionalization of silica nanoparticles (SNPs) for biomedical studies*. Macro 2012, July 24-29, Virginia Tech Campus, Blacksburg, United States of America (Poster presentation)
  
- 2) **Kishore Natte**, Guillermo Orts-Gil, Jörg Friedrich and Werner Österle, *Novel synthesis for PEGylated SNPs for Biomedical and Toxicological studies*. ISOS-XV1 2011, August 14-18, Hamilton, Canada (Poster presentation)
  
- 3) **Kishore Natte**, Guillermo Orts-Gil, Jörg Friedrich and Werner Österle. *Versatility of aminated silica nanoparticles: from biocompatible nanohybrids to heterogeneous catalysts for Heck-type Reactions*, 2<sup>nd</sup> Indo German conference 2011, June 19-22, Rostock, Germany (Poster presentation)
  
- 4) **Kishore Natte**, Guillermo Orts-Gil, Sebastian Wohlrab, Jörg Friedrich and Werner Österle. *Surface modification of silica particles with PEG for biomedical application*, Macro 2010, July 11-16, Glasgow, United Kingdom (Poster presentation)
  
- 5) **Kishore Natte**, Guillermo Orts-Gil, Daniela Drescher, Janina Kneipp and Werner Österle, *Modification of silica nanoparticles surface for toxicological studies*, Nanotoxicology 2010, June 2-4, Edinburgh, United Kingdom. (Poster presentation)
  
- 6) Guillermo Orts-Gil, **Kishore Natte**, Werner Österle, *Tuning the surface properties of Metal@Polylysine hybrid nanoparticles: equilibrium and metastable conformational states*, Hybrid Materials 2011, March 6-10, Strasbourg, France (Poster presentation)
  
- 7) Daniela Drescher, Guillermo Orts-Gil, Gregor Laube, **Kishore Natte**, Rüdiger W. Veh, Werner Österle, J. Kneipp, *Combining SERS and viability tests for the investigation of nanotoxicity*. ECSBM, Coimbra, August 2011. (Poster presentation)

# Curriculum Vitae

---

## Personal

Name	Kishore Natte
Date of Birth	18.07.1984
Place of Birth	Warangal, Andhra Pradesh
Nationality	Indian
Marital Status	Single
Languages known	English, German (Mittlstufe), Hindi (Intermediate), Telugu (Native)

## Educational qualification

1998 – 1999	Matriculation X standard, Scholars High School, Warangal, India
1999 – 2001	Board of Intermediate Education, SN Junior college, Hanamkonda, India
4/2001 – 4/2004	CKM Arts and Science college, Kakatiya University, Warangal, India Bachelors of Science in Chemistry
4/2005 – 4/2007	Kakatiya University, Warangal, India Master of Science in Organic Chemistry
3/2009 – 10/2012	Technical University of Berlin PhD in Chemistry

## Work experience

5/2007 – /22009	GVK Bio Sciences, Hyderabad, India Research Associate (R&D, Medicinal Chemistry Division)
3/2009 - 3/2012	BAM Federal Institute for Materials Research and Testing, Berlin, Germany Scientific Co-Worker
From 3/2012 – till date	BAM Federal Institute for Materials Research and Testing, Berlin, Germany Research Scientist